



T.C.  
TEKİRDAĞ NAMIK KEMAL ÜNİVERSİTESİ REKTÖRLÜĞÜ  
Genel Sekreterlik  
Basın ve Halkla İlişkiler Birimi

Sayı : E-79746631-824.02.03-304761  
Konu : JBST Dergisi Makale Çağrısı

DAĞITIM YERLERİNE

İlgi : 26.05.2023 tarihli, 96396750-824.02.03-304310 sayılı yazı.

Üniversitemiz Fen Bilimleri Enstitüsü tarafından 2023 yılı Nisan ayı itibariyle 2. Cilt 1. Sayısı yayımlanan Journal of Balkan Science and Technology (The Journal of Tekirdağ Namık Kemal University Institute of Natural & Applied Sciences - JBST), çok disiplinli uluslararası hakemli dergi niteliğinde bir dergi olup, Part A: Natural Sciences, Part B:Engineering Sciences, Part C: Agricultural and Food Sciences ve Part D: Architectural Sciences olmak üzere dört kısımdan oluşmaktadır ve yazım dili İngilizce'dir. JBST doğa bilimleri, mühendislik bilimleri, ziraat ve gıda bilimleri, mimarlık bilimleri alanlarında ulusal ve uluslararası düzeyde akademik bilgi birikimine katkı sağlayacak makaleleri kabul etmektedir.

Söz konusu dergimiz için Üniversitemiz Fen Bilimleri Enstitüsünün makale çağrısını içeren yazısı ve derginin 2. Cilt 1. Sayısı ekte sunulmuş olup, akademik personelinize duyurulması hususunda gereğini rica ederim.

Prof. Dr. Gülsüm ÖZKAN  
Rektör a.  
Rektör Yardımcısı

Ek:

- 1- 2. Cilt 1. Sayı (54 sayfa)
- 2- Fen Bilimleri Enstitüsü JBST -Makale Çağrısı Yazısı (1 sayfa)

Dağıtım:  
ABDULLAH GÜL ÜNİVERSİTESİ  
REKTÖRLÜĞÜNE  
ACIBADEM MEHMET ALİ AYDINLAR  
ÜNİVERSİTESİ REKTÖRLÜĞÜNE  
ADANA ALPARSLAN TÜRKEŞ BİLİM VE  
TEKNOLOJİ ÜNİVERSİTESİ  
REKTÖRLÜĞÜNE  
ADYAMAN ÜNİVERSİTESİ  
REKTÖRLÜĞÜNE  
AFYON KOCATEPE ÜNİVERSİTESİ  
REKTÖRLÜĞÜNE

Doğrulama Kodu :BSLL01BSMK Pin Kodu :58872

Belge Takip Adresi : <https://turkiye.gov.tr/ebd?eK=5767&eD=BSLL01BSMK&eS=304761>

Adres:Namık Kemal Mah. Kampüs Cad. Süleymanpaşa /TEKİRDAĞ  
Telefon:0282 250 00 00 Faks:(282) 250 9912  
e-Posta:halklaileskiler@nku.edu.tr; Elektronik Ağ:http://bhib.nku.edu.tr/

Bilgi için: Taylan Vıraca  
Unvanı: Bilgisayar İşletmeni

Tel No: 1045



**PART A  
NATURAL SCIENCES**

**PART B  
ENGINEERING SCIENCES**

April 2023 Volume:2 Issue:1

ISSN:2822 - 4566

# **JOURNAL OF BALKAN SCIENCE AND TECHNOLOGY**

Journal of Tekirdağ Namık Kemal University Institute of Natural & Applied Sciences

**PART C  
AGRICULTURAL AND FOOD SCIENCES**

**ARCHITECTURAL SCIENCES  
PART D**





**ISSN: 2822-4566**

**International Peer-Reviewed Journal**

**Volume: 2 Number: 1 April 2023**

**© Tekirdağ Namık Kemal University Institute of Natural and Applied Sciences**

**TEKİRDAĞ-2023**



**Volume: 2 Number: 1 April 2023**

**ISSN: 2822-4566**

JBST – Journal of Balkan Science and Technology is a multi-disciplinary, double-blind peer-reviewed, open-access journal international journal published three issue per year (April, August, and December).

**OWNER**

**Assoc. Prof. Dr. Bahar UYMAZ**

Director of Institute of Natural and Applied Sciences On  
Behalf of Tekirdag Namık Kemal University

**MANAGEMENT CENTER**

Tekirdağ Namık Kemal University  
Institute of Natural and Applied Sciences  
Değirmenaltı Campus, 59030, Tekirdağ/TURKEY  
Tel: + (90) 282 250 44 00  
e-mail: [editorialoffice.jbst@nku.edu.tr](mailto:editorialoffice.jbst@nku.edu.tr)  
Web: <http://jbst.nku.edu.tr/>

**COVER DESIGN BY**

**Assist. Dr. Melike ATILKAN**



**EDITOR IN CHIEF**  
**Prof. Dr. Rifat BİRCAN**

**ASSISTANT EDITORS**

**Assist. Dr. Makbule TERLEMEZOĞLU**

Tekirdağ Namık Kemal University

**Assist. Dr. Tuğba ÜSTÜN TOPAL**

Tekirdağ Namık Kemal University

**Assist. Kadir ERTEN**

Tekirdağ Namık Kemal University

**Assist. Güvenç USANMAZ**

Tekirdağ Namık Kemal University

**Assist. Dr. Ozan Süleyman ÜRGÜT**

Tekirdağ Namık Kemal University

**Assist. Dr. Emrullah CULPAN**

Tekirdağ Namık Kemal University

**Assist. Necip Fazıl KARAKURT**

Tekirdağ Namık Kemal University

**FIELD EDITORS**

**Prof. Dr. Havva İLBAĞI**

Tekirdağ Namık Kemal University

**Prof. Dr. Rüya YILMAZ**

Tekirdağ Namık Kemal University

**Prof. Dr. Hafız ALİSOY**

Tekirdağ Namık Kemal University

**Prof. Dr. Metin TUNA**

Tekirdağ Namık Kemal University

**Prof. Dr. Aydın ADILOĞLU**

Tekirdağ Namık Kemal University

**Assoc. Prof. Dr. Özlem KOCAHAN YILMAZ**

Tekirdağ Namık Kemal University

**Assoc. Prof. Dr. Sinan ŞAHİN**

Tekirdağ Namık Kemal University

**Assoc. Prof. Dr. Kenan ÇINAR**

Tekirdağ Namık Kemal University

**Assoc. Prof. Dr. Behiye Banu BİLGİN**

Tekirdağ Namık Kemal University

**Assist. Prof. Dr. Ulviye POLAT**

Tekirdağ Namık Kemal University

**Prof. Dr. Günay YILDIZ TÖRE**

Tekirdağ Namık Kemal University

**Prof. Dr. Cenk ARAL**

Tekirdağ Namık Kemal University

**Prof. Dr. Gökhan UNAKITAN**

Tekirdağ Namık Kemal University

**Prof. Dr. Pelin Gürkan ÜNAL**

Tekirdağ Namık Kemal University

**Assoc. Prof. Dr. Erdiç UZUN**

Tekirdağ Namık Kemal University

**Assoc. Prof. Dr. İbrahim PALABIYIK**

Tekirdağ Namık Kemal University

**Assoc. Prof. Dr. İbrahim İsmet ÖZTÜRK**

Tekirdağ Namık Kemal University

**Assoc. Prof. Dr. Zehra PINAR İZGİ**

Tekirdağ Namık Kemal University

**Assoc. Prof. Dr. Aylin AĞMA OKUR**

Tekirdağ Namık Kemal University

## EDITORIAL BOARD

**Prof. Dr. Tuğba KİPER**

Tekirdağ Namık Kemal University

**Prof. Dr. Cem SEVİK**

Eskişehir Technical University

**Prof. Dr. Muhammet ARICI**

Yıldız Technical University

**Prof. Dr. Boris Ivanov EVSTATIEV**

Ruse Angel Kanchev University

**Prof. Dr. Sotiris K. HADJIKAKOU**

University of Ioannina

**Prof. Dr. Şule TURHAN**

Uludağ University

**Prof. Dr. Aydın ÜNAY**

Adnan Menderes University

**Prof. Dr. Eugenia BEZIRTZOGLU**

Democritus University of Thrace

**Prof. Dr. Mehmet ZENGİN**

Selçuk University

**Prof. Dr. Masroor Ellahi BABAR**

University of Veterinary and Animal Science

**Assoc. Prof. Dr. İsmail YILDIZ**

Van Yüzüncü Yıl University

**Assoc. Prof. Dr. Fevzi HANSU**

Siirt University

**Assoc. Prof. Dr. FÜRÜZAN ASLAN**

Kırklareli University

**Assoc. Prof. Dr. Gonca ÖZÇELİK KAYSERİ**

Ege University

**Assoc. Prof. Dr. Zubair ASLAM**

Faysalabad Agricultural University

**Assist. Prof. Dr. NEDİM ÇETİNKAYA**

Ege University

**Assist. Prof. Dr. Zeynep Banu ÖZGER**

Kahramanmaraş Sütçü İmam University

**Assist. Prof. Dr. Mustafa YILDIRIM**

İstanbul Sağlık ve Teknoloji University

**Assist. Prof. Dr. Anita GRZESKIEWICZ**

Adam Mickiewicz University

**Prof. Dr. Can ÜNAL**

Tekirdağ Namık Kemal University

**Prof. Dr. Bahattin YALÇIN**

Marmara University

**Prof. Dr. Gül E. KREMER**

Iowa State University

**Prof. Dr. Mais SULEYMANOV**

Bakü State University

**Prof. Dr. Jon Bryan BURLEY**

Michigan State University

**Prof. Dr. Yasemin ÖNER**

Uludağ University

**Prof. Dr. Viliana VASILEVA**

Institute of Forage Crops-Pleven

**Prof. Dr. Savvas VASSILIADIS**

University of West Attica

**Prof. Dr. Cemil TÖLÜ**

Çanakkale Onsekiz Mart University

**Assoc. Prof. Dr. Tanju GÜREL**

Tekirdağ Namık Kemal University

**Assoc. Prof. Dr. Ertan ATEŞ**

Tekirdağ Namık Kemal University

**Assoc. Prof. Dr. Krisztina UZUNEANU**

Universitatea Dunarea de Jos Galati

**Assoc. Prof. Dr. Ekaterina ARABSKA**

University of Agribusiness and Rural Development

**Assoc. Prof. Dr. Kostas VLACHONASIOS**

Aristotle University of Thessaloniki

**Assoc. Prof. Dr. Zacharias FRONTİSTİS**

University of Western Macedonia

**Assist. Prof. Dr. Sencer Süreyya KARABEYOĞLU**

Kırklareli University

**Assist. Prof. Dr. Ianut Ştefan IORGU**

National Museum of Natural History Grigore Antipa

**Assist. Prof. Dr. Tuğçe BAŞER**

University of Illionis at Urbana Champaign



## LANGUAGE EDITORS

**Assist. Prof. Dr. Fulya KINCAL**  
Tekirdağ Namık Kemal University

**Teaching Assist. Dr. Suzan DENİZ**  
Tekirdağ Namık Kemal University

**GENERAL MANAGER**  
**Prof. Dr. Rifat BİRCAN**

**LAYOUT EDITOR**  
**Assist. Güvenç USANMAZ**

**REFEREE of the ISSUE**  
**(April 2023)**

**Prof. Dr. Dolunay ŞAKAR**  
Yıldız Technical University

**Prof. Dr. Meryem ODABAŞI KÖPRÜLÜ**  
Ege University

**Prof. Dr. Türker BİLGİN**  
Tekirdağ Namık Kemal University

**Assoc. Prof. Dr. Armağan Fatih KARAMANLI**  
İstinye University

**Assoc. Prof. Dr. Zehra PINAR İZGİ**  
Tekirdağ Namık Kemal University

**Dr. Dilek SALKIM İŞLEK**  
İstanbul University

**Prof. Dr. Esin GÜVEN**  
Erzurum Atatürk University

**Prof. Dr. Tammam SİPAHİ**  
Trakya University

**Prof. Dr. Sırrı KAR**  
Tekirdağ Namık Kemal University

**Assoc. Prof. Dr. Erdoğan ŞEN**  
Tekirdağ Namık Kemal University

**Assist. Prof. Dr. Ufuk GUL**  
Trakya University

**Dr. Mustafa ARDA**  
Trakya University



## CONTENTS

### PART A: NATURAL SCIENCES

**Şimal KÜRÜMOĞLU – Yelda YALÇIN GÜRKAN ..... 1-7**

Degradation Pathway Estimation of Pesticide Molecule by Molecular Modeling

**Japheth CHEMBE - Samuel Abu SOMMA .....8-19**

Stability Analysis of a Mathematical Modeling of Spread and Control of Corona Virus Disease (Covid-19) Incorporating Vaccination Class

**Zafer ŞAKACI – Aylin ER.....20-25**

Principles of Semi-Field Study Design to Obtain Realistic Data about the Effects of Anthropogenic Climate Change on the Biological and Ecological Traits of *Culex pipiens* (L.)

**Şeyma DEMİRKESEN – Cenk ARAL .....26-31**

Melatonin: A Potent Protector of Mitochondria and Cancer

### PART B: ENGINEERING SCIENCES

**Gülizar ALİSOY - Rahima NURALİYEVA - Meltem APAYDIN USTUN - Arif Kıvanc USTUN - Hafız ALİSOY .....32-36**

Modeling of Optimum Control of the Distance Learning Process

**Bahar UYMAZ .....37-47**

Analytical Solution of Bending, Buckling, and Vibration of Functionally Graded Nanobeams based on Nonlocal Elasticity





## Degradation Pathway Estimation of Pesticide Molecule by Molecular Modeling

Şimal KÜRÜMOĞLU<sup>1</sup>, Selim ÖZGÜR<sup>1</sup>, Yelda YALÇIN GÜRKAN<sup>1\*</sup>

<sup>1</sup>Tekirdağ Namık Kemal University, Faculty of Arts and Sciences, Department of Chemistry, 59030, Tekirdağ, Türkiye

### Research Article

### ABSTRACT

#### Keywords:

Azinfos Methyl  
Guthion  
Ach  
AchE  
Gaussian09  
DFT

Received: 07.03.2023

Accepted: 02.04.2023

Published: 30.04.2023

DOI: 10.55848/jbst.2023.24

Azinphos methyl (O,O-Dimethyl S-[(4-oxo-1,2,3-benzotriazin-3(4H)-yl)methyl] phosphorodithioate) is a broad spectrum organophosphate insecticide. Like other pesticides in its class, it owes its insecticidal properties to being an acetylcholinesterase inhibitor. Azinphos methyl is often used as organophosphorus pesticides such as active Guthion, Gusathion (GUS), Gusathion-M, Crysthyron, Cotnion, Cotnion-methyl, Methyltrizotion, Carfene, Bay9027, Bay17147 and R-1852. In the study, the possible reaction pathways between the Azinphos methyl molecule and the OH radical were examined theoretically. The optimized geometries of the molecule were drawn with the Gauss-View 5 program and the lowest energy states were determined using the Gaussian 09 program. By calculating the bond lengths and bond angles of the molecules, geometric structure analysis was performed. The main purpose here is to determine the most likely produced in the reaction between Azinphos methyl and OH radical in aqueous media and gaseous media. The products formed as a result of the reactions of the azinphos methyl molecule with the OH radical were determined and their geometric optimizations were carried out by semi-empirical AM1, Ab initio Hartree Fock HF/6-31G and Functional Density Theory (DFT) methods. COSMO was used as the solving model. Thanks to this method, the area where the reaction takes place between the polarizations on the surface of the molecule and the solvent is determined. Thanks to the dielectric property of water, the reaction medium is stabilized.

### 1. Introduction

Azinphos methyl (O,O-Dimethyl S-[(4-oxo-1,2,3-benzotriazin-3(4H)-yl)methyl] phosphorodithioate) is a broad spectrum acaric acid and mollusc acid organophosphate insecticide [1].

Azinphos suggested that methyl was directly related to the health problems of farmers. Azinphos methyl was phased out over 12 years in the USA, and its use was completely banned on September 30, 2013. Azinphos methyl has been banned in the European Union in 2006 and in Turkey since 2013 [2-4].

Azinphos methyl can enter the body through inhalation, ingestion and skin contact. Azinphos methyl is found in food residues and drinking water, albeit in small amounts. Once absorbed into the body, azinphos methyl may cause neurotoxic effects like other organophosphate insecticides. Azinphos methyl can act as an acetylcholinesterase inhibitor (AChE) in high concentrations, azinphos methyl can be toxic because it functions as an acetylcholinesterase inhibitor. But its toxicity is mostly due to cytochrome p450. In normal conditions, acetylcholine quickly and effectively lowers the neurotransmitter acetylcholine transmitting and limits its biological effect [2-4].

Azinphos methyl is very stable when dissolved in acidic, neutral or slightly alkaline water. However, in an environment above pH 11, it is rapidly hydrolyzed to anthranilic acid, benzamide and other chemicals. Microorganisms in the natural aquatic environment and sunlight can be used to show a faster

degradation of azinphos-methyl. In this way, the half-life can be shortened from a few months to a few days. There are major routes of biodegradation and evaporation under normal conditions. Evaporated Azinphos methyl is exposed to excess UV light and undergoes photodecomposition. If not exposed to bioactivity and UV light, it reaches a half-life of 1 year [2-4].

Azinphos-methyl (AZM) and chlorpyrifos (CPF) are broad-spectrum organophosphate pesticides used for pest control in many parts of the world and have been shown to inhibit cholinesterase activity in the non-target freshwater gastropod *Planorbium corneus*. This study was carried out to determine whether AZM and CPF cause oxidative stress in *P. corneus* and whether pesticides act together more than they do alone, causing increased oxidative stress. For this purpose, non-enzymatic and enzymatic parameters were measured in snail soft tissues acutely exposed to insecticides by single chemical and binary mixed studies. In conclusion, the data shown in this study prove that AZM, CPF and a mixture of both organophosphates cause oxidative stress and oxidative damage in *P. corneus* tissues [5-7].

An agricultural community of farm workers was investigated for changes induced by exposure to agricultural pesticides. A seasonally persistent correlation was found between the detected blood concentration of the insecticide azinphos-methyl and the taxonomic composition of the cheek oral microbiome. In this study, we show in human subjects that exposure to organic phosphate pesticides is associated

<sup>1</sup> Tekirdağ Namık Kemal University, Faculty of Arts and Sciences, Department of Chemistry, 59030, Suleymanpaşa-Tekirdağ, Türkiye  
E-mail address: [yygurkan@nku.edu.tr](mailto:yygurkan@nku.edu.tr)

with large-scale significant changes in the intraoral buccal microbiota composition, with the extinction of all taxa in some individuals. The continuation of this association from spring/summer to winter also indicates that long-term effects on the common microbiota occur. The significant health implications of pesticide-associated microbiological disruptions to these agricultural community members are currently not understood. Future research should index medical and dental records for common and chronic diseases that may be affected by this association between pesticide exposure and microbial change [8-9].

Azinphos-methyl and chlorpyrifos are organophosphorus pesticides that pose a serious threat to the environment, including their harmful effects on humans, and therefore must be removed from the environment. Therefore, in this study, an ultrasound technique was applied for the removal of the above-mentioned hazardous compounds. For this, the effect of influential parameters such as pH, initial pesticide concentration, frequency, electric power and treatment time on the ultrasound degradation of azinphos-methyl and chlorpyrifos was well investigated and clarified. The obtained results showed that azinphos-methyl and chlorpyrifos were degraded effectively and rapidly by ultrasound technique. Two multiple regression-based equations were derived to describe the degradation process of pesticides by ultrasound. The result of this study showed that the polynomial equations satisfactorily describe the behaviour of the present process for various operating conditions [1-10].

The removal of the organophosphorus insecticide azinphos-methyl (AZM) from the water was investigated by the electro-Fenton method, which produces hydroxyl radicals electrocatalytically. The reaction between these radicals and AZM led to the oxidation of carbon dioxide and inorganic ions of AZM, demonstrating complete dissociation from water. It contains aromatic derivatives such as short-chain carboxylic acids and inorganic ions as end products. The identification and quantification of these intermediates have been thoroughly investigated by HPLC, GC-MS and ion chromatography analyses. Based on the identified intermediates, a general oxidation mechanism was proposed. The mineralization ability of the process was also tested using aqueous AZM solutions and its commercial formulation Gusathion M WP 25 (GMWP25) [11].

## 2. Materials and Methods

Gaussian 09W program was used in our studies. Gauss 09 program is the latest version of the Gauss series programs. The program we have used allows us to use state-of-the-art features in electronic structure modelling. The Gaussian 09W program is very comprehensive. We can use Ab initio, semi-experimental and molecular mechanics methods in the program. There are many basic sets and theoretical methods among the Ab initio, semi-experimental and molecular mechanics methods we have used.

Calculations can be made with the Gaussian 09W package program; Ideal geometric optimizations of atoms and molecules can be made. The vibrational frequencies that

depend on the energies of the atoms can be calculated. The energies of atoms and molecules can be calculated. Force constants and dipole moments of atoms and molecules can be calculated. From the results obtained from the calculated IR and Raman spectra of atoms and molecules; Information about many specific properties of atoms and molecules such as electron affinities, ionization energies, NMR, magnetic susceptibility, vibrational intensities, atomic charges, molecular orbitals, reaction energies and thermochemical properties can be obtained. In addition, the stability of the molecular wave function can be examined with the help of the program. The Gaussian 09W program circulates through potential energy levels, showing the transition states and the pathways the reaction will take. These calculations can be done in crystal, solution and gaseous states of molecules [12-13].

The Gauss view 5.0.8 program is a program that we can calculate and transfer the molecules and atoms to the computer environment and prepare the input files [14]. Thanks to the program, he can visualize the molecules that we will calculate. We can ensure that the molecules are ideally positioned [15-16]. It also allows us to make the necessary rotations and positionings to optimize molecules. It presents the results of the molecules to us with certain graphical methods [16-17].

The results we achieved thanks to the program; Normal mode animations based on vibration frequencies, VCD spectra, NMR spectra, Raman spectra, Atomic charges, Electrostatic potential surfaces, molecular orbitals, and optimized molecular structures [18].

## 3. Results and Discussion

In the calculations, the molecular calculations of Azinphos methyl and OH radical, which are in the reactant position, were made by Ab initio Hartree-Fock HF/6-31G(d) and DFT, semi-empirical AM1 methods and they were geometrically optimized. The electronic properties of the optimized molecules were determined.

The conformation states with the lowest energy, that is, the most stable, were determined for each reactant. The Gaussview5 program was used to draw the organic molecules, which are the most stable in conformation.

In the search for a plausible mechanism for the photocatalytic decolourization /degradation reaction of Azin1, DFT Reactivity indices were employed to have information about the most susceptible sites for hydroxyl radical attack. Then the highest values were used to calculate the local softnesses. The calculated local softness  $s^0$  and Fukui functions  $f^0$  are presented in Table 1, Fig. 1 shows the optimized structure of the Azin1 molecule and the numbering system that was used throughout the calculations.

Two main competing reaction pathways shown in Fig. 2 were determined by selecting the specific sites of the Azin1 molecule, based on their softness values being close to that of the •OH radical. These two possible pathways are named the cleavage of the sulfur bond and the cleavage of the C-S bond.

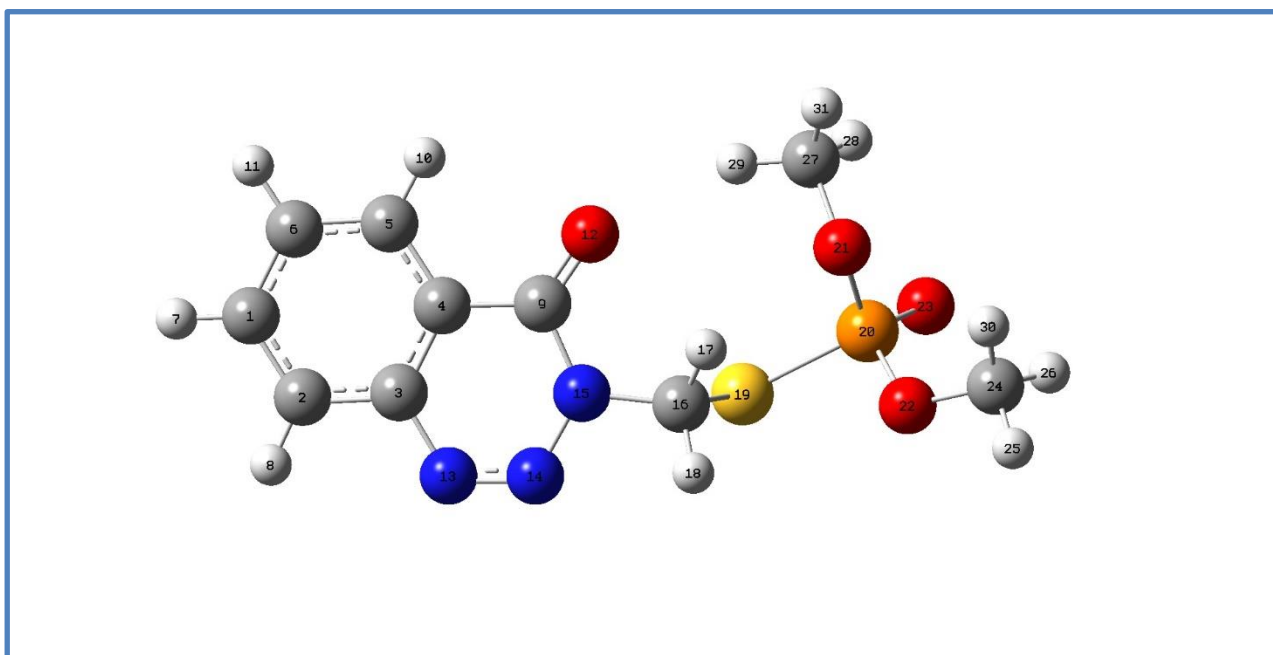


**Fig. 1** Optimized structure of Azin1 and the numbering system (grey, carbon; red, oxygen; blue, nitrogen; white, hydrogen; yellow, sulfur; orange, phosphorus).

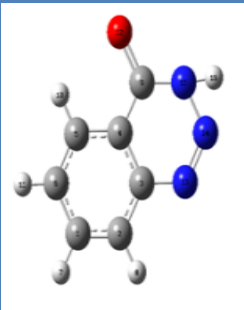
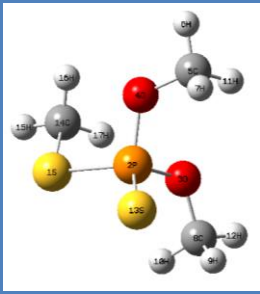
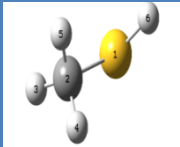
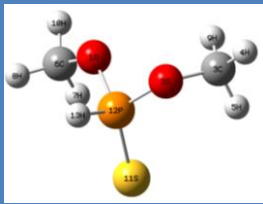
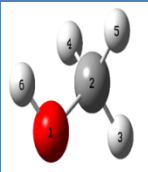
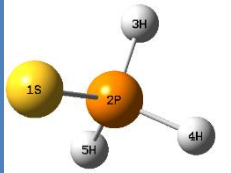
**Table 1.** Chemical Reactivity Descriptors for Azin1 and the •OH radical. Azin1 (S=6.30456).

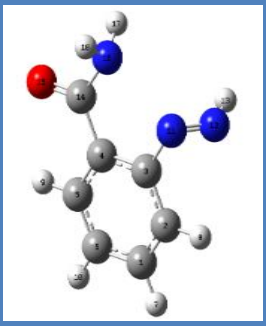
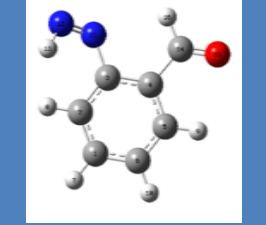
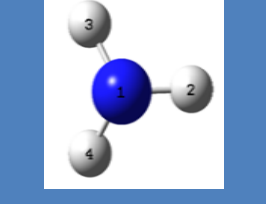
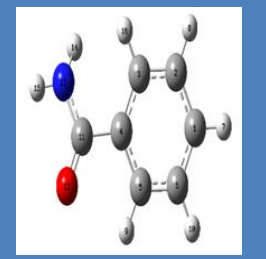
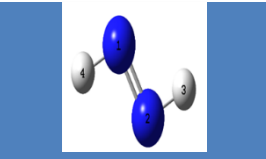
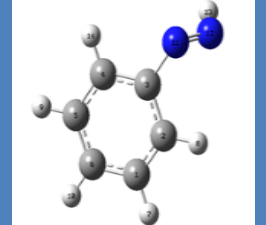
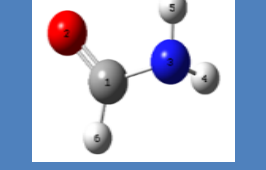
Molecules	$f^0$	$s^0$	$\Delta s^0$
C 16	0.00725	0.05589	3.55623
N 13	0.00685	0.05245	4.36256
N 14	0.07196	0.58780	4.25348
N 15	0.06232	0.48124	4.12590
P 20	0.00645	0.05378	3.99210
S 19	0.00911	0.07055	3.34228
S 32	0.00802	0.06464	3.94908
•OH Radical (S=5.70523)			

The bond angles and bond lengths are given (Table 2). In energy, enthalpy and gibbs free energy values are given.

The fragment with the lowest energy is the most striking (Table 3).

**Table 2.** Components of Azinphos Methyl molecule.

		Bond Lengths (Å°)	DFT	Bond Angles (°)	DFT
	<b>F1</b>	O12-C9	1.22	O12-C9-N15	121.37
		N14-N15	1.36	C9-N15-H16	117.49
		N13-N14	1.27	C9-N15-N14	129.01
		N15-H16	1.01	N15-N14-N13	118.94
		O12-C9	1.22		
		N14-N15	1.36		
		N13-N14	1.27		
N15-H16	1.01				
	<b>F2</b>	S1-C14	1.84	C8-O3-P2	120.24
		S1-P2	2.09	O3-P2-O4	98.57
		P2-O3	1.93	O3-P2-S1	106.76
		P2-O4	1.62	O3-P2-13S	116.02
		P2-S13	1.94	13S-P2-O4	118.72
		O4-C5	1.44	S1-P2-13S	113.33
		O3-C8	1.44	P2-S1-C14	101.51
		P2-O4-C5	119.46		
	<b>F3</b>	C2-S1	1.84	H6-S1-C2	96.92
		S1-H6	1.35		
	<b>F4</b>	H13-P12	1.40	H13-P12-O2	97.05
		O2-P12	1.61	O1-P12-O2	100.64
		O1-P12	1.63	11S-P12-O2	119.11
		11S-P12	1.94	H13-P12-11S	116.07
		O2-C3	1.44	C3-O2-P12	120.15
		O1-C6	1.44	C3-O2-P12	122.20
	<b>F5</b>	C2-O1	1.42	C2-O1-H6	107.67
		H6-O1	0.97		
	<b>F6</b>	H5-P2	1.42	S1-P2-H5	118.09
		H3-P2	1.42	S1-P2-H3	118.09
		H4-P2	1.42	S1-P2-H4	118.09
		S1-P2	1.96	H3-P2-H4	99.63
				H3-P2-H5	99.63

	<b>F7</b>	N12-H13	1.05	H13-N12-N11	111,14
		N12-N11	1.25	N12-N11-C3	120,88
		N11-C3	1.43	C4-C14-O15	119,75
		O15-C14	1.23	O15-C14-N16	122,53
		N16-C14	1.36	C14-N16-H17	117,13
		N16-H17	1.01	C14-N16-H18	121,58
		H16-H18	1.01	H17-N16-H18	121,28
	<b>F8</b>	O15-C14	1.22	C4-C14-O15	122,86
		C3-N11	1.43	H16-C14-O15	121,40
		N11-N12	1.25	C3-N11-N12	120,00
		N12-H13	1.05	N11-N12-H13	111,38
	<b>F9</b>	H3-N1	1.02	H3-N1-H2	105,76
		H4-N1	1.02	H3-N1-H4	105,71
		H2-N1	1.02	H4-N1-H2	105,76
	<b>F10</b>	N13-H14	1.00	H14-N13-C11	119,98
		N13-H15	1.01	H15-N13-C11	114,84
		N13-C11	1.38	H14-N13-H15	116,13
		C11-O38	1.22	N13-C11-O12	121,62
				O12-C11-C4	122,10
				N13-C11-C4	116,27
	<b>F11</b>	H4-N11	1.04	H4-N1-N2	106,1
		N1-N2	1.25	N1-N2-H3	106,1
		N2-H3	1.04		
	<b>F12</b>	H13-N12	1.05	H13-N12-N11	111,48
		N12-N11	1.25	N12-N11-C3	120,23
		N11-C3	1.43	C2-C3-N11	123,31
	<b>F13</b>	H4-N3	1.00	H4-N3-H5	119,00
		H5-N3	1.01	H5-N3-C1	119,18
		N3-C1	1.36	H4-N3-C1	121,81
				N3-C1-O2	125,00

**Table 3.** Energy-Enthalpy-Gibbs Free Energy Results of Compounds.

Compounds	Energy (kcal/mol)	Enthalpy (kcal/mol)	Thermal Free Energy (kcal/mol)
Azin1 gas phase (water phase)	-1202132.925 (-1202142.072)	-1202176.523 (-1202141.479)	-1202132.333 (-1202186.307)
F1 gas phase (water phase)	-319450.270 (-319456.640)	-319449.670 (-319456.050)	-319475.390 (-319481.760)
F2 gas phase (water phase)	-883425.612 (-883431.629)	-883425.020 (-883431.037)	-883457.478 (-883464.028)
F3 gas phase (water phase)	-275255.780 (-275258.270)	-275255.190 (-275257.680)	-275273.230 (-275275.750)
F4 gas phase (water phase)	-608896.889 (-608929.183)	-608896.296 (-608901.645)	-608923.786 (-608902.238)
F5 gas phase (water phase)	-72577.470 (-72580.670)	-72576.870 (-72580.080)	-72593.790 (-72597.010)
F6 gas phase (water phase)	-465172.559 (-465179.860)	-465171.967 (-465196.909)	-465189.557 (-465179.267)
F7 gas phase (water phase)	-320185.650 (-320192.990)	-320185.060 (-320192.390)	-320213.350 (-320220.790)
F8 gas phase (water phase)	-285443.770 (-285449.970)	-285443.180 (-285449.380)	-285469.860 (-285476.090)
F9 gas phase (water phase)	-35460.880 (-35464.740)	-35460.290 (-35464.150)	-35473.990 (-35477.850)
F10 gas phase (water phase)	-251515.340 (-251522.090)	-251514.750 (-251521.500)	-251540.220 (-251547.140)
F11 gas phase (water phase)	-69406.400 (-69409.100)	-69405.810 (-69408.510)	-69421.350 (-69424.050)
F12 gas phase (water phase)	-214341.250 (-214345.970)	-214340.660 (-214345.370)	-214364.300 (-214369.070)
F13 gas phase (water phase)	-106575.870 (-106582.370)	-106575.270 (-106581.780)	-106594.240 (-106600.220)

#### 4. Conclusion

As a result, the decomposition reaction requires energy. OH radicals are used to cleave the Azinphos Methyl molecule. As seen in our trailers, Azinfos Methyl, which is harmful, has been decomposed up to F13 and has become harmless to the environment. We aimed to break Azinfos Methyl into the smallest harmless substances. As can be seen from the results, this fragmentation occurred theoretically. In the computational part of the study, the most reactive sites of the Azin1 molecule for hydroxyl radical attack were determined by the application of the Conceptual Density Functional Theory. The predicted mechanism indicated that the N-N bond cleavage mechanism is a more preferable pathway over the C-S bond cleavage.

#### Declaration

**Author Contribution:** Conceive- S.Ö, Ş.K., Y.Y.G.; Design- S.Ö, Ş.K., Y.Y.G.; Supervision- S.Ö, Ş.K., Y.Y.G.; Experimental Performance, Data Collection and/or Processing S.Ö., Ş.K.; Analysis and/or Interpretation S.Ö.; Literature Review- Y.Y.G.; Writer- S.Ö, Ş.K., Y.Y.G.; Critical Reviews – Y.Y.G.

**Conflict of interests:** The authors have declared no conflicts of interest.

#### Orcid ID

Şimal Kürümoğlu  <https://orcid.org/0000-0001-9456-5456>  
Yelda Yalçın Gürkan  <https://orcid.org/0000-0002-6316-5510>

## References

- [1] (1998). Azinphos-methyl (guthion) risk characterization document. [Online] Available: [https://www.cdpr.ca.gov/docs/risk/rcd/azmrcdre\\_98.pdf](https://www.cdpr.ca.gov/docs/risk/rcd/azmrcdre_98.pdf)
- [2] W. J. Hayes, Pesticides studied in man / Wayland J. Hayes, Jr (no. Accessed from <https://nla.gov.au/nla.cat-vn62073>). Baltimore: Williams & Wilkins, 1982.
- [3] D. Hartley, and H. Kidd, The Agrochemicals Handbook, Update 5. Old Woking, Surrey, UK: Royal Society of Chemistry. Unwin Bros Limited, 1983.
- [4] C. Sine, Farm Chemicals Handbook. Meister Publishing Company, 1991.
- [5] L. C. Cacciatore, S. I. Nemirovsky, N. R. Verrengia Guerrero, and A. C. Cochón, "Azinphos-methyl and chlorpyrifos, alone or in a binary mixture, produce oxidative stress and lipid peroxidation in the freshwater gastropod *Planorbium corneus*," *Aquatic Toxicology*, vol. 167, pp. 12-19, 2015/10/01/ 2015, doi: <https://doi.org/10.1016/j.aquatox.2015.07.009>.
- [6] N. N. Ulusu and B. Tandogan, "Purification and kinetics of sheep kidney cortex glucose-6-phosphate dehydrogenase," *Comparative Biochemistry and Physiology Part B: Biochemistry and Molecular Biology*, vol. 143, no. 2, pp. 249-255, 2006/02/01/ 2006, doi: <https://doi.org/10.1016/j.cbpb.2005.11.018>.
- [7] E. K. Stephensen, J. Sturve, and L. Förlin, "Effects of redox cycling compounds on glutathione content and activity of glutathione-related enzymes in rainbow trout liver," *Comparative Biochemistry and Physiology Part C: Toxicology & Pharmacology*, vol. 133, no. 3, pp. 435-442, 2002/11/01/ 2002, doi: [https://doi.org/10.1016/S1532-0456\(02\)00129-1](https://doi.org/10.1016/S1532-0456(02)00129-1).
- [8] I. B. Stanaway et al., "Human Oral Buccal Microbiomes Are Associated with Farmworker Status and Azinphos-Methyl Agricultural Pesticide Exposure," (in eng), *Appl Environ Microbiol*, vol. 83, no. 2, Jan 15 2017, doi: 10.1128/aem.02149-16.
- [9] U.S. EPA. Air Quality Criteria for Lead (Final Report, 1986). U.S. Environmental Protection Agency, Washington, D.C., EPA/600/8-83/028AF (NTIS PB87142386), 1986.
- [10] S. Agarwal et al., "Degradation of azinphos-methyl and chlorpyrifos from aqueous solutions by ultrasound treatment," *Journal of Molecular Liquids*, vol. 221, pp. 1237-1242, 2016/09/01/ 2016, doi: <https://doi.org/10.1016/j.molliq.2016.04.076>.
- [11] A. Özcan, Y. Şahin, and M. A. Oturan, "Complete removal of the insecticide azinphos-methyl from water by the electro-Fenton method – A kinetic and mechanistic study," *Water Research*, vol. 47, no. 3, pp. 1470-1479, 2013/03/01/ 2013, doi: <https://doi.org/10.1016/j.watres.2012.12.016>.
- [12] J.B. Foresman, and E. Frish, *Exploring Chemistry with Electronic Structure Methods*, Pittsburgh, PA, USA. Gaussian Inc., (1996).
- [13] I. N. Levine, *Quantum Chemistry*. Prentice Hall, 1991.
- [14] I. N. Levine, *Quantum Chemistry*. Prentice Hall, 1983.
- [15] J. P. Lowe, *Quantum Chemistry*. Academic Press, 1993.
- [16] Gaussian 16, Revision B.01, Frisch, M.J., Trucks, G.W., Schlegel, H.B., Scuseria, G.E., Robb, M.A., Cheeseman, J.R.; Scalmani, G.; Barone, V.; Petersson, G.A.; Nakatsuji, H.; Li, X.; Caricato, M.; Marenich, A.V.; Bloino, J., Janesko, B.G., Gomperts, R., Mennucci, B., Hratchian, H.P., Ortiz, J.V., Izmaylov, A.F., Sonnenberg, J.L., Williams-Young, D., Ding, F., Lipparini, F., Egidi, F., Goings, J., Peng, B., Petrone, A., Henderson, T., Ranasinghe, D., Zakrzewski, V.G., Gao, J., Rega, N., Zheng, G., Liang, W., Hada, M., Ehara, M., Toyota, K., Fukuda, R., Hasegawa, J., Ishida, M., Nakajima, T., Honda, Y., Kitao, O., Nakai, H., Vreven, T., Throssell, K., Montgomery Jr., J.A., Peralta, J.E., Ogliaro, F., Bearpark, M.J., Heyd, J.J., Brothers, E.N., Kudin, K.N., Staroverov, V.N., Keith, T.A., Kobayashi, R., Normand, J., Raghavachari, K., Rendell, A.P., Burant, J.C., Iyengar, S.S., Tomasi, J., Cossi, M., Millam, J.M., Klene, M., Adamo, C., Cammi, R., Ochterski, J.W., Martin, R.L., Morokuma, K., Farkas, O., Foresman, J.B., Fox, D.J. Gaussian, Inc., Wallingford CT (2016) GaussView 5.0. Wallingford, E.U.A.
- [17] P. W. Atkins, *Physical chemistry*, 6th ed ed. Oxford: Oxford University Press (in eng), 1998.
- [18] P. W. Atkins and R. S. Friedman, *Molecular Quantum Mechanics*. OUP Oxford, 2011.



License: This article is available under a Creative Commons License (Attribution 4.0 International, as described at <https://creativecommons.org/licenses/by/4.0/>)



## Stability Analysis of a Mathematical Modeling of Spread and Control of Corona Virus Disease (Covid-19) Incorporating Vaccination Class

Japheth CHEMBE<sup>1\*</sup>, Samuel Abu SOMMA<sup>1</sup>

<sup>1</sup> Department of Mathematics, Federal University of Technology Minna, Nigeria.

### Research Article

#### Keywords:

Stability Analysis,  
equilibrium point,  
Corona Virus,  
Sensitivity Analysis,  
Basic Reproduction Number.

Received: 03.01.2023

Accepted: 07.03.2023

Published: 30.04.2023

DOI: 10.55848/jbst.2023.25

### ABSTRACT

In this paper some mathematical models of COVID 19 were extended by incorporating vaccination, social distancing, and proper use of face mask and hand sanitizers for the spread and control of Corona virus (COVID-19). The analysis of the Disease-Free Equilibrium (DFE) and Endemic Equilibrium (EE) points were carried out. The trace -determinant approaches for local stability and Castillo-chaves for global stability were used in the stability and sensitivity analyses. At the stability of the equilibrium points, we find out that the basic reproduction number which implies the (DFE) is locally asymptotically stable, but global asymptotic stability of (EE) exists at . Sensitivity analysis identifies the model's most sensitive parameters; which are responsible for disease transmission and control. Visualization of the effect of the key parameters on the basic reproduction number was carried out. The data visualization demonstrates that vaccination and recovery rate are crucial parameters for eradicating COVID-19 from the population, while contact rate, lack of social distancing, and improper use of facemasks and hand sanitizers are crucial for COVID-19 persistence. The risks of close proximity to infected people should indeed be made known to the general public. The government needs to step up its vaccination efforts.

## 1. Introduction

An unusual Coronavirus Disease 2019 (COVID-19) which is linked to Acute Respiratory Distress Syndrome was declared pandemic on March 11th, 2020, by World Health Organization (WHO). COVID-19 belongs to a new strain of novel coronaviruses known as SARS-CoV-2 [1]. The virus was discovered late December 2019 with patients admitted to hospitals with an initial diagnosis of pneumonia. Patients' illnesses were traced back to a market in Wuhan, Hubei Province, China that sells seafood and wet animals [2]. Because there were so many infected people in the "Huanan Seafood Market," the situation became increasingly dire [3].

A virus with symptoms including pneumonia was reported to the Chinese government, but its exact nature was unknown. Cases from the reported virus rose from 0 to over 40 cases in just 30 days. The virus had a history of killing approximately 770 people in China. They died from what was then called the SARS disease in 2002 and 2003.

Incubation for this virus, which causes respiratory issues, is between two and fourteen days [4]. Its symptoms include ; dry cough, flu, short breath, a runny nose, a sore throat, problems with musculoskeletal joints, diarrhea, and, in rare cases, a loss of sense of smell or taste. The two most common ways for COVID-19 to be transmitted from one individual to another are through respiratory droplet inhalation and skin-to-skin contact. Many people who contract the COVID-19 viral infection will experience moderate to severe respiratory illness,

but will eventually get better without any special treatment. In Africa, Nigeria recorded her first case on February 27, 2020, but as of 13th Nov, 2021 the figure had risen to 213,127 infections with 2960 deaths so far [5]. It is sad to note that most of the mortalities of COVID-19 especially in developing countries are attributed to poor medical facilities and medical personnel.

To effectively reduce the spread of COVID-19, governments have been implementing various control measures such as imposing strict, mandatory lockdowns and encouraging (and in some cases strictly enforcing) other measures such as individuals maintaining a minimum distance between themselves (social distancing), avoiding crowded events, imposing a maximum number of individuals in any gathering (religious and social), and the use of face masks in public [5]. To further help mitigate the spread of COVID-19, contact tracing of suspected infected cases has been stepped up in several countries and detected cases (asymptomatic and symptomatic) are quickly placed in isolation for prompt treatment [8].

As COVID-19 vaccines are being deployed worldwide, we formulate and qualitatively analyze a COVID-19 mathematical model, taking into consideration available therapeutic measures, vaccination of susceptible and treatment of hospitalized/infected individuals. Our proposed model

\* Department of Mathematics, Federal University of Technology Minna, Main Campus, Gidan Kwano, P.M.B 65, Minna, Nigeria.  
E-mail address: japhet.chembe@st.futminna.edu.ng



incorporates some key epidemiological and biological features of COVID-19, including demographic parameters (recruitment/birth and death). The minimum population of Nigeria that must be vaccinated to curb the transmission of COVID 19 was estimated by the herd immunity threshold at 36.638%.

**2. Materials and Methods**

**2.1 The Model Description and Formulation**

In this model, we focus solely on Nigeria human population. The model partitioned the population into six (6) compartments namely "susceptible," "exposed," "quarantine/isolated," "infected," "recovered," and vaccinated. Recruitment into the susceptible class is by birth at the rate  $\Lambda$ . Susceptible individuals who have enough contact with the infected individuals are moved to the exposed class with the infection force. Susceptible individuals can also be vaccinated into the vaccination class at the rate  $v$ . If the vaccine is ineffective (denotes the vaccine inefficacy), those individuals who are vaccinated with the vaccine and have made contact with infected individuals are also moved into the exposed class  $E(t)$  with the force of infection. The exposed individuals are moved into the infected class  $I(t)$  at the rate  $\omega$  or just moved into the quarantine class  $Q(t)$  at rate  $\tau$ . Individuals who are in the quarantine class without showing symptoms after 14 days of incubation are moved to the recovered class  $R(t)$  at the rate  $\sigma_1$  while those that showed symptoms are moved into the infected class  $I(t)$  at the rate  $\sigma_2$ . The infected individuals who after treatment recovered are moved into the recovered class  $R(t)$  at the rate  $\gamma$ . We assume that recovery from Covid-19 does not confer permanent immunity. Thus, the recovered individuals who were not vaccinated can return to the susceptible class at the rate  $\rho$ .

Individuals in each class can die a natural death at the rate  $\mu$ . Those individuals in the infected class have an additional death burden as a result of the infection.

The transition rates from susceptible and vaccinated to exposed is given by the following force of infection.

$$\alpha = \frac{\varepsilon(1-\eta)(1-\xi)}{N(t)}(E+I+Q) \tag{1}$$

Where  $\eta$  is the population that maintains social distancing to prevent the spread of Covid-19 and is denoted by  $0 < \eta \leq 1$  while represents the proportion of the population that makes proper use of face masks and hand sanitizers denoted by  $0 < \xi \leq 1$ . All parameters are positive. Table 2 defines all the variables and parameters used for the formulation of the model (fig 1).

**2.2 Model Equation**

$$\frac{dS(t)}{dt} = \Lambda - \alpha S + \rho R - (\mu + v)S \tag{2}$$

$$\frac{dE(t)}{dt} = \alpha S + \kappa \alpha V - (\omega + \mu + \tau)E \tag{3}$$

$$\frac{dQ(t)}{dt} = \tau E - (\sigma_1 + \sigma_2 + \mu)Q \tag{4}$$

$$\frac{dI(t)}{dt} = \omega E + \sigma_2 Q - (\mu + \delta + \gamma)I \tag{5}$$

$$\frac{dR(t)}{dt} = \gamma I + \sigma_1 Q - (\rho + \mu)R \tag{6}$$

$$\frac{dV(t)}{dt} = vS - \kappa \alpha V - \mu V \tag{7}$$

**Table 1.** Notations and Definition of Variables and Parameters.

Symbol	Description
$S(t)$	Susceptible class at time t
$E(t)$	Exposed class at time t
$I(t)$	Infected class at time t
$Q(t)$	Quarantine class at time t
$R(t)$	Recovered class at time t
$V(t)$	Vaccinated class at time t
$\Lambda$	Recruitment rate into the susceptible class
$\alpha$	Transmission rate of infection
$\sigma_1$	Transition rate to the recovered class after incubation period
$\sigma_2$	Progression rate to the infected class
$\mu$	Per capita natural death rate
$\rho$	Rate of loss of immunity after treatment as time passes by
$v$	Vaccination rate
$\eta$	Rate of social distancing
$\xi$	Rate of use of facemask and hand sanitizers
$\omega$	Progression rate from exposed to infected class
$\tau$	Rate at which exposed individuals are taken into isolation
$\kappa$	Vaccination ineffectiveness (inefficacy)
$\delta$	Death rate due to infection
$\gamma$	Rate of recovery from the infection

**2.3 Existence of Equilibrium Point**

At equilibrium

$$\frac{dS}{dt} = \frac{dE}{dt} = \frac{dI}{dt} = \frac{dQ}{dt} = \frac{dR}{dt} = \frac{dV}{dt} = 0 \tag{8}$$

Let

$$E^* = (S^*, E^*, Q^*, I^*, R^*, V^*) = (S, E, Q, I, R, V) \tag{9}$$

Therefore, the system (2) to (7) become

$$\Lambda + \rho R^* - (\alpha + B_1) S^* = 0 \tag{10}$$

$$\alpha S^* + \kappa \alpha V^* - B_2 E^* = 0 \tag{11}$$

$$\tau E^* - B_3 Q^* = 0 \tag{12}$$

$$\omega E^* + \sigma_2 Q^* - B_4 I^* = 0 \tag{13}$$

$$\gamma I^* + \sigma_1 Q^* - (\rho + \mu) R^* = 0 \tag{14}$$

$$\nu S^* - (\kappa \alpha + \mu) V^* = 0 \tag{15}$$

Where,

$$\left. \begin{aligned} B_1 &= (\mu + \nu), B_2 = (\omega + \mu + \tau), B_3 = (\sigma_1 + \sigma_2 + \mu) \\ B_4 &= (\mu + \delta + \gamma), B_5 = (\rho + \mu) \end{aligned} \right\} \tag{16}$$

**2.4 Disease Free Equilibrium (DFE) State**

Let  $X^0 = (S, E, I, Q, R, V) = (S^0, E^0, I^0, Q^0, R^0, V^0)$  be the DFE point with  $I = 0$

Then, equation (10)-(15) becomes

$$X^0 = (S^0, E^0, I^0, Q^0, R^0, V^0) = \left( \frac{\Lambda}{B_1}, 0, 0, 0, 0, \frac{\nu \Lambda}{\mu B_1} \right) \tag{17}$$

At DFE

$$\left. \begin{aligned} N^0 &= S^0 + E^0 + Q^0 + I^0 + R^0 + V^0 \\ N^0 &= \frac{\Lambda}{\mu} \end{aligned} \right\} \tag{18}$$

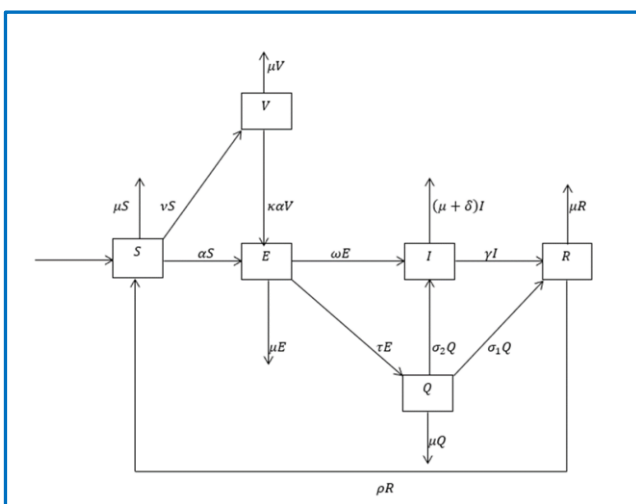


Fig. 1 Schematic Diagram of the model.

**2.5 Basic Reproduction Number  $R_0$**

The potential for the spread of a disease can be estimated using the basic reproduction number  $R_0$ . The basic reproduction number ( $R_0$ ) of an infectious agent, such as the corona virus, is defined as the average amount of secondary infections actually generated by an infectious person in a susceptible host population [9].

Using the basic reproduction number, one can predict how quickly a disease might spread. Reproduction number ( $R_0$ ) is the average number of new infections caused by a single infectious person in a susceptible host population [9]. The corona virus, like many other infectious agents, has a relatively high reproduction number.

A model's basic reproductive number is equal to the largest eigenvalue of  $FV^{-1}$  or the spectral radius of the model. The basic reproduction number  $R_0 = \rho(FV^{-1})$  will be computed using the method of [10], where  $f_i(x)$  is the rate at which infected people emerge in compartment  $i$ ,  $V_i^+(x)$  is the rate at which people move into compartment  $i$  via all mechanisms

**Table 2.** Description of Variables with their Values.

Variables	Description	Values	Source
<b>S(0)</b>	Susceptible class	199,950,894	A9
<b>E(0)</b>	Exposed class	3,550,457	A7
<b>Q(0)</b>	Quarantined class	3,392,457	A5
<b>I(0)</b>	Infected class	212,127	A3
<b>R(0)</b>	Recovered class	205,491	A4
<b>V(0)</b>	Vaccinated class	5,776,679	A8
<b>N(0)</b>	Total Human Population	213,089,105	A1

other than epidemic spread, and  $V_i^-(x)$  is the rate at which people move out of compartment  $i$ .

The disease transmission model consists of the system of equations

$$x_j = f_j(x) = F_j(x) - V_j(x) \tag{19}$$

Where,

$$V_i = V_i^-(x) - V_i^+(x) \tag{20}$$

$$V = \left[ \frac{\partial f_j(X^0)}{\partial x_j} \right] \tag{21}$$

Where  $x_j = E, I, Q$  or  $j=1,2,3$  and  $X^0$  is the Disease Free Equilibrium Point.

Secondary infections are predicted to occur within  $E, I, Q$ , and this is modeled in equations (10) through (15). The occurrence of new infections in each section is detailed in the matrix.

$$f = \begin{pmatrix} \frac{\varepsilon(1-\eta)(1-\xi)(E+I+Q)S}{N} + \frac{\kappa\varepsilon(1-\eta)(1-\xi)(E+I+Q)V}{N} & & \\ & 0 & \\ & & 0 \end{pmatrix} \tag{22}$$

Let  $l_1 = \varepsilon(1-\eta)(1-\xi)$

Equation (22) becomes

$$f = \begin{pmatrix} \frac{l_1}{N}(S + \kappa V)(E + I + Q) \\ 0 \\ 0 \end{pmatrix} \tag{23}$$

At the point where disease-free equilibrium is achieved, the Jacobian matrix F equals;

$$F = \left[ \frac{\partial f_i(X^0)}{\partial x_j} \right], \text{ where } x_j = E, I, Q \text{ for } j=1,2,3 \text{ and } X^0 \text{ is the Disease Free Equilibrium Point.}$$

Jacobian matrix of (233) at the equilibrium point where there is no disease;

$$F = \begin{pmatrix} l_1 \left( \frac{\mu + \nu \kappa}{B_1} \right) & l_1 \left( \frac{\mu + \nu \kappa}{B_1} \right) & l_1 \left( \frac{\mu + \nu \kappa}{B_1} \right) \\ 0 & 0 & 0 \\ 0 & 0 & 0 \end{pmatrix} \tag{24}$$

The following matrix describes the rate at which individuals leave and enter the infective compartment.

$$V_i = V_i^- - V_i^+ = \begin{pmatrix} B_2 E \\ B_4 I - \omega E - \sigma_2 Q \\ B_3 Q - \tau E \end{pmatrix} \tag{25}$$

Where

$$V_i^- = \begin{pmatrix} B_2 E \\ B_4 I \\ B_3 Q \end{pmatrix} \tag{26}$$

The next generation matrix  $FV^{-1}$  is given by

$$FV^{-1} = \begin{pmatrix} l_1(\mu + \nu \kappa) \left[ \frac{B_3 B_4 + \omega B_3 + \tau \sigma_2 + B_4}{B_1 B_2 B_3 B_4} \right] & l_1(\mu + \nu \kappa) \left[ \frac{\sigma_2}{B_1 B_3 B_4} \right] & l_1(\mu + \nu \kappa) \left[ \frac{B_3 + B_4}{B_1 B_3 B_4} \right] \\ 0 & 0 & 0 \\ 0 & 0 & 0 \end{pmatrix} \tag{30}$$

$\rho(FV^{-1})$  is the dominating eigenvalue of the  $(FV^{-1})$  matrix.

The eigenvalue is gotten using  $|FV^{-1} - \lambda I| = 0$

Where;

$$\left( l_1(\mu + \nu \kappa) \left[ \frac{B_3 B_4 + \omega B_3 + \tau \sigma_2 + B_4}{B_1 B_2 B_3 B_4} \right] - \lambda_1 \right) \begin{vmatrix} -\lambda_2 & 0 \\ 0 & -\lambda_3 \end{vmatrix} - \left( l_1(\mu + \nu \kappa) \left[ \frac{\sigma_2}{B_1 B_3 B_4} \right] \right) \begin{vmatrix} 0 & 0 \\ 0 & -\lambda_3 \end{vmatrix} + l_1 \left( l_1(\mu + \nu \kappa) \left[ \frac{B_3 + B_4}{B_1 B_4} \right] \right) \begin{vmatrix} 0 & -\lambda_2 \\ 0 & 0 \end{vmatrix} = 0 \tag{32}$$

And

$$V^+ = \begin{pmatrix} 0 \\ \omega E + \sigma_2 Q \\ \tau E \end{pmatrix} \tag{27}$$

The matrix (25) evaluated at the disease-free equilibrium point is given as;

$$V = \left[ \frac{\partial f_i(X^0)}{\partial x_j} \right] = \begin{pmatrix} B_2 & 0 & 0 \\ -\omega & B_4 & -\sigma_2 \\ -\tau & 0 & B_3 \end{pmatrix} \tag{28}$$

Where  $x_j = E, I, Q$  for  $j=1,2,3$  and  $X^0$  is the Disease Free Equilibrium Point.

The inverse of V is computed using Gauss Jordan method, After carefully solving, we obtain  $V^{-1}$  to be

$$V^{-1} = \begin{pmatrix} \frac{1}{B_2} & 0 & 0 \\ \frac{\omega B_3 + \tau \sigma_2}{B_2 B_3 B_4} & \frac{\sigma_2}{B_3 B_4} & \frac{1}{B_4} \\ \frac{1}{B_2 B_3} & 0 & \frac{1}{B_3} \end{pmatrix} \tag{29}$$

$$\lambda_1 = l_1(\mu + \nu\kappa) \left[ \frac{B_3B_4 + \omega B_3 + \tau\sigma_2 + B_4}{B_1B_2B_3B_4} \right] \tag{33}$$

$$\lambda_1 = l_1(\mu + \nu\kappa) \left[ \frac{B_3B_4 + \omega B_3 + \tau\sigma_2 + B_4}{B_1B_2B_3B_4} \right] \tag{34}$$

Then

$$R_0(\nu) = l_1(\mu + \nu\kappa) \left[ \frac{B_3B_4 + \omega B_3 + \tau\sigma_2 + B_4}{B_1B_2B_3B_4} \right] \tag{35}$$

Where  $B_1 = (\mu + \nu)$

Equation (35) gives the effective reproduction number,  $R_0(\nu)$  when there was vaccine in circulation. In the absence of vaccinations (that is  $\nu = 0$ ) then, the basic reproductive number  $\mathfrak{R}_0$  is given as;

$$\mathfrak{R}_0 = R_0(0) = l_1 \left[ \frac{B_3B_4 + \omega B_3 + \tau\sigma_2 + B_4}{B_2B_3B_4} \right] \tag{36}$$

$\mathfrak{R}_0$  is the basic reproduction number which is the average number of secondary cases arising from one infectious individual in a completely susceptible population.

$$J(E^0) = \begin{vmatrix} -B_1 - \lambda & 0 & 0 & 0 & \rho & 0 \\ 0 & -B_2 - \lambda & 0 & 0 & 0 & 0 \\ 0 & 0 & -B_3 - \lambda & 0 & 0 & 0 \\ 0 & 0 & 0 & -B_4 - \lambda & 0 & 0 \\ 0 & 0 & 0 & 0 & -B_5 - \lambda & 0 \\ 0 & 0 & 0 & 0 & 0 & -\mu - \lambda \end{vmatrix} = 0 \tag{39}$$

$$(-B_1 - \lambda)(-B_2 - \lambda)(-B_3 - \lambda)(-B_4 - \lambda)(-B_5 - \lambda)(-\mu - \lambda) = 0 \tag{40}$$

Either

$$-(B_1 + \lambda_1) = 0 \text{ or } -(B_2 + \lambda_2) = 0 \text{ or } -(B_3 + \lambda_3) = 0 \text{ or } -(B_4 + \lambda_4) = 0 \tag{41}$$

$$-(B_5 + \lambda_5) = 0 \text{ or } -\mu - \lambda_6 = 0 \tag{42}$$

From equation (42)

$$\lambda_1, \lambda_2, \lambda_3, \lambda_4, \lambda_5, \lambda_6 < 0 \tag{43}$$

Hence, the disease free equilibrium point is locally asymptotically stable.

### 3.7 The Disease-Free Equilibrium Analysis

**Theorem 2** Equations (10) to (15) describe a disease free equilibrium that is globally asymptotically stable under the condition that  $R_0 < 1$  holds, but unstable under the state that  $R_0 > 1$ .

**Proof:** Referring to [11], the system of equations (10) to (15) can be written as;

### 2.6 The Model Stability Analysis

**Theorem 1:** The DFE point  $E^0$  of the model is Locally Stable if  $R_0 < 1$

**Proof:** The disease free equilibrium point is said to be locally asymptotically stable, if all the eigenvalues of the Jacobian matrix at DFE are negative or unstable if otherwise.

At DFE, the Jacobian matrix of the underlying equation system is

$$J(E^0) = \begin{pmatrix} -B_1 & 0 & 0 & 0 & \rho & 0 \\ 0 & -B_2 & 0 & 0 & 0 & 0 \\ 0 & \tau & -B_3 & 0 & 0 & 0 \\ 0 & \omega & \sigma_2 & -B_4 & 0 & 0 \\ 0 & 0 & \sigma_1 & \gamma & -B_5 & 0 \\ \nu & 0 & 0 & 0 & 0 & -\mu \end{pmatrix} \tag{37}$$

Reducing equation (37) to upper triangular matrix gives equation whose characteristics equation is;

$$|J(E^0) - \lambda I| = 0 \tag{38}$$

$$\left. \begin{aligned} \frac{dx(t)}{dt} &= F(x, y) \\ \frac{dy(t)}{dt} &= G(x, y) \end{aligned} \right\} \tag{44}$$

Whereas  $x = (S, R, V) \in \mathfrak{R}^3$  represents the various compartments of healthy human beings,  $y = (E, Q, I) \in \mathfrak{R}^3$  represents the various compartments of infected human beings.

Therefore, DFE =  $(x^0, 0)$ , where

$$x^0 = \begin{pmatrix} \frac{\Lambda}{B_1} & 0 & \frac{\nu\Lambda}{\mu B_1} \end{pmatrix} \tag{45}$$

It is paramount to show that,

$$\frac{dx(t)}{dt} = F(x, 0), x^0 \text{ is Globally Asymptotically Stable}$$

(G.A.S.), and

$$G(x, y) = Cy - G(x, y), G(x, y) \geq 0 \text{ for } (x, y) \in \Omega$$

H1: consider the uninfected subsystem,

$$\frac{dx(t)}{dt} = F(x, y) = \begin{pmatrix} \Lambda + \rho R - (\alpha + B_1)S \\ \gamma I + \sigma_1 Q - B_5 R \\ \nu S - (\kappa\alpha + \mu)V \end{pmatrix} \tag{46}$$

When  $y = 0$  that is  $E = Q = I = 0$

Then, equation (46) becomes,

$$F(x, 0) = \begin{pmatrix} \Lambda + \rho R - B_1 S \\ -B_5 R \\ \nu S - \mu V \end{pmatrix} \tag{47}$$

By so doing we obtained

$$S(t) = \frac{(\Lambda + \rho R)}{B_1} + \left( S(0) - \frac{(\Lambda + \rho R)}{B_1} \right) e^{-B_1 t} \tag{48}$$

$$R = R(0) e^{-B_5 t} \tag{49}$$

$$V = \frac{(\nu S)}{\mu} + \left( V(0) - \frac{(\nu S)}{\mu} \right) e^{-\mu t} \tag{50}$$

As  $t \rightarrow \infty, S \rightarrow \frac{\Lambda + \rho R}{B_1}, R \rightarrow 0, V \rightarrow \frac{\nu S}{\mu}$  regardless of the value of  $S(0), R(0)$  and  $V(0)$

Therefore,

$$x_0 = \begin{pmatrix} \frac{\Lambda}{B_1} & 0 & \frac{\nu\Lambda}{\mu B_1} \end{pmatrix} \text{ satisfies global asymptotical stability}$$

H2: consider an infected subsystem

$$y^1 = G(x, y) = \begin{pmatrix} \frac{l_1}{N}(E+I+Q)S + \frac{l_1}{N}\kappa(E+I+Q)V - B_2 E \\ \omega E + \sigma_2 Q - B_4 I \\ \tau E - B_3 Q \end{pmatrix} \tag{51}$$

Such that,

$$G(x, y) = Cy - \hat{G}(x, y) \tag{52}$$

Then,

$$\hat{G}(x, y) = Cy - G(x, y) \tag{53}$$

Where  $C = \frac{\partial G(x, 0)}{\partial t}$  (54)

$$C = \begin{pmatrix} \frac{l_1}{N}S + \frac{l_1}{N}\kappa V - B_2 & \frac{l_1}{N}S + \frac{l_1}{N}\kappa V & \frac{l_1}{N}S + \frac{l_1}{N}\kappa V \\ \omega & \sigma_2 & -B_4 \\ \tau & -B_3 & 0 \end{pmatrix} \tag{55}$$

$$Cy = \begin{pmatrix} \frac{l_1}{N}S + \frac{l_1}{N}\kappa V - B_2 & \frac{l_1}{N}S + \frac{l_1}{N}\kappa V & \frac{l_1}{N}S + \frac{l_1}{N}\kappa V \\ \omega & \sigma_2 & -B_4 \\ \tau & -B_3 & 0 \end{pmatrix} \begin{pmatrix} E \\ Q \\ I \end{pmatrix} \tag{56}$$

$$Cy = \begin{pmatrix} \frac{l_1}{N}(E+I+Q)S + \frac{l_1}{N}\kappa(E+I+Q)V - B_2 E \\ \omega E + \sigma_2 Q - B_4 I \\ \tau E - B_3 Q \end{pmatrix} \tag{57}$$

$$\hat{G}(x, y) = \begin{pmatrix} \frac{I_1}{N}(E+I+Q)S + \frac{I_1}{N}\kappa(E+I+Q)V - B_2 E \\ \omega E + \sigma_2 Q - B_4 I \\ \tau E - B_3 Q \end{pmatrix} - \begin{pmatrix} \frac{I_1}{N}(E+I+Q)S + \frac{I_1}{N}\kappa(E+I+Q)V - B_2 E \\ \omega E + \sigma_2 Q - B_4 I \\ \tau E - B_3 Q \end{pmatrix} \tag{58}$$

$$\hat{G}(x, y) = \begin{pmatrix} \hat{G}_1(x, y) \\ \hat{G}_2(x, y) \\ \hat{G}_3(x, y) \end{pmatrix} = \begin{pmatrix} 0 \\ 0 \\ 0 \end{pmatrix} \tag{59}$$

Which implies that  $\hat{G}(x, y) = 0$  for all  $(x, y) \in \Omega$ . Therefore, the conditions (H1) and (H2) are satisfied. Thus, the global stability of the DFE is obtained. This completes the proof.

Hence, the disease free equilibrium point is globally asymptotically stable when  $R_0 < 1$

**2.8 The Endemic Equilibrium State**

Let  $X^1 = (S, E, Q, I, R, V) = (S^1, E^1, Q^1, I^1, R^1, V^1)$  (60)

Suppose  $I \neq 0$

Then,

$$\left. \begin{aligned} \Lambda + \rho R - (\alpha + B_1)S &= 0 \\ \alpha S + \kappa\alpha V - B_2 E &= 0 \\ \tau E - B_3 Q &= 0 \\ \omega E + \sigma_2 Q - B_4 I &= 0 \\ \gamma I + \sigma_1 Q - B_5 R &= 0 \\ \upsilon S - (\kappa\alpha + \mu)V &= 0 \end{aligned} \right\} \tag{61}$$

Becomes

$$\begin{pmatrix} S^{**} \\ E^{**} \\ Q^{**} \\ I^{**} \\ R^{**} \\ V^{**} \end{pmatrix} = \begin{pmatrix} \frac{K_6 B_2 - K_1 K_6 (K_3 + K_4) + K_1 K_2 K_7}{[B_2 - K_1 (K_3 + K_4)]} \\ \frac{K_2}{[B_2 - K_1 (K_3 + K_4)]} \\ \frac{\tau K_2}{[B_2 B_3 - B_3 K_1 (K_3 + K_4)]} \\ \frac{K_2 K_5}{[B_2 - K_1 (K_3 + K_4)]} \\ \frac{K_1 K_2}{[B_2 - K_1 (K_3 + K_4)]} \\ \frac{K_8 B_2 - K_1 K_8 (K_3 + K_4) + K_1 K_2 K_9}{[B_2 - K_1 (K_3 + K_4)]} \end{pmatrix} \tag{62}$$

Where

$$K_1 = \frac{\omega\gamma B_3 + \tau\sigma_2\gamma - \sigma_1\tau B_4}{B_3 B_4 B_5}$$

$$K_2 = \frac{\alpha\Lambda(\kappa\alpha + \mu) + \alpha\Lambda\kappa\upsilon}{(\alpha + B_1)(\kappa\alpha + \mu)}, K_3 = \frac{\alpha\rho}{(\alpha + B_1)}, K_4 = \frac{\alpha\rho\upsilon\kappa}{(\alpha + B_1)(\kappa\alpha + \mu)}$$

$$K_5 = \left( \frac{\omega B_3 + \sigma_2 \tau}{B_3 B_4} \right)$$

$$K_6 = \frac{\Lambda}{(\alpha + B_1)}, K_7 = \frac{\rho}{(\alpha + B_1)}$$

$$K_8 = \frac{\Lambda \upsilon}{(\alpha + B_1)(\kappa\alpha + \mu)},$$

$$K_9 = \frac{\rho \upsilon}{(\alpha + B_1)(\kappa\alpha + \mu)}$$

respectively

Equation (62) is the Endemic Equilibrium Point (EEP).

Our total population using the endemic equilibrium points is given as;

**2.9 Stability of the Endemic Equilibrium State**

$\mathfrak{R}_0 = R_0(0) = 1.578177354 > 1$ , then the system has an endemic infection because of the introduction of those with secondary infection. Here, we consider the case where  $I \neq 0$ . The Jacobian matrix of the system of equation (10) to (15) at Disease Endemic Equilibrium Point is evaluated. The stability will be determined based on the sign of the eigenvalues of the Jacobian matrix.

$$N^{**} = \frac{B_2(K_6 + K_8) - K_1(K_3 + K_4)(K_6 + K_8) + K_1K_2(K_7 + K_9) + K_2(1 + \tau B_3 + K_5 + K_1)}{B_2 - K_1(K_3 + K_4)} \tag{63}$$

The equation for the endemic equilibrium with the force of infection  $\alpha_0^{**}$  (infection force) is as follows:

$$\alpha_0^{**} = \frac{\varepsilon(1-\eta)(1-\xi)(K_2 + \tau K_2 B_3 + K_2 K_5)}{B_2(K_6 + K_8) - K_1(K_3 + K_4)(K_6 + K_8) + K_1K_2(K_7 + K_9) + K_2(1 + \tau B_3 + K_5) + K_1K_5} \tag{64}$$

$$J = \begin{pmatrix} -\alpha - B_1 & 0 & 0 & 0 & \rho & 0 \\ \alpha & -B_2 & 0 & 0 & 0 & \kappa\alpha \\ 0 & \tau & -B_3 & 0 & 0 & 0 \\ 0 & \omega & \sigma_2 & -B_4 & 0 & 0 \\ 0 & 0 & \sigma_1 & \gamma & -B_5 & 0 \\ \nu & 0 & 0 & 0 & 0 & -\kappa\alpha - \mu \end{pmatrix} \tag{65}$$

Reducing equation (65) to upper triangular matrix gives equation whose characteristics equation is;

$$|J(X^1) - \lambda I| = 0 \tag{66}$$

$$J = \begin{pmatrix} -\alpha_0^{**} - B_1 - \lambda & 0 & 0 & 0 & \rho & 0 \\ 0 & -B_2 - \lambda & 0 & 0 & 0 & \kappa\alpha_0^{**} \\ 0 & 0 & -B_3 - \lambda & 0 & 0 & 0 \\ 0 & 0 & 0 & -B_4 - \lambda & 0 & 0 \\ 0 & 0 & 0 & 0 & -B_5 - \lambda & 0 \\ 0 & 0 & 0 & 0 & 0 & -\kappa\alpha_0^{**} - \mu - \lambda \end{pmatrix} = 0 \tag{67}$$

The determinant gives;

$$(-\alpha_0^{**} - B_1 - \lambda)(-B_2 - \lambda)(-B_3 - \lambda)(-B_4 - \lambda)(-B_5 - \lambda)(-\kappa\alpha_0^{**} - \mu - \lambda) = 0 \tag{68}$$

Equation (68) implies;

$$-\alpha_0^{**} - B_1 - \lambda_1 = 0 \quad \text{or} \quad -B_2 - \lambda_2 = 0 \quad \text{or} \quad -B_3 - \lambda_3 = 0 \quad \text{or} \quad -B_4 - \lambda_4 = 0 \tag{69}$$

$$-B_5 - \lambda_5 = 0 \quad \text{or} \quad -\kappa\alpha_0^{**} - \mu - \lambda_6 = 0$$

Therefore

$$\lambda_1 = -(\alpha_0^{**} + B_1) \quad \text{or} \quad \lambda_2 = -B_2 \quad \text{or} \quad \lambda_3 = -B_3 \quad \text{or} \quad \lambda_4 = -B_4 \quad \text{or} \quad \lambda_5 = -B_5 \quad \text{or} \quad \lambda_6 = -(\kappa\alpha_0^{**} + \mu) \tag{70}$$

From equation

$$\lambda_1, \lambda_2, \lambda_3, \lambda_4, \lambda_5, \lambda_6 < 0 \tag{71}$$

Hence, the disease endemic equilibrium point is asymptotically stable. This means that the disease is prevalent.

$$H_1 = 1 - \frac{B_2 B_3 B_4}{l_1(B_3 B_4 + \omega B_3 + \tau \sigma_2 + B_4)} \tag{73}$$

### 2.10 Covid-19 Vaccine Effectiveness Analysis: Herd Immunity Ratio

For the disease to be prevented, this is the minimum percentage of the population that must be vaccinated [12]. provides an equation for the Herd Immunity Threshold indicated by  $H_1$ .

$$H_1 = 1 - \frac{1}{\mathfrak{R}_0} \tag{72}$$

### 3. Results

The coefficient estimates of model variables and parameters used to conduct the sensitivity analysis and generate the graph display of sensitive constraints against  $R_0$  are provided in Table 3 and 3 respectively.

**3.1 Detailed explanation of all of the parameters and their current values**

**Table 3.** Description of Variables with their Values.

Variables	Description	Values	Source
<b>S(0)</b>	Susceptible class	199,950,894	A9
<b>E(0)</b>	Exposed class	3,550,457	A7
<b>Q(0)</b>	Quarantined class	3,392,457	A5
<b>I(0)</b>	Infected class	212,127	A3
<b>R(0)</b>	Recovered class	205,491	A4
<b>V(0)</b>	Vaccinated class	5,776,679	A8
<b>N(0)</b>	Total Human Population	213,089,105	A1

**Table 4.** Description of Parameters with their Value.

Parameters	Description	Values	Source
$\Lambda$	Recruitment rate into the susceptible class	0.036855	A2
$\mu$	Per capita natural death rate	0.011382	A10
$\delta$	Death rate due to infection	0.013888	A6
$\gamma$	Recovery rate from infection	0.96417	A11
$\nu$	Vaccination rate	0.0456	A15
$\rho$	Rate of loss of immunity after treatment as time passes by	0.00103	A16
$\omega$	Progression rate from exposed to infected class	0.06002	A14
$\tau$	Rate at which exposed individuals are taken into quarantine/isolation	0.9554	A13
$\kappa$	Vaccination ineffectiveness (inefficacy)	0.087	A12
$\eta$	Rate at which people maintain social distancing	0.2	Assumed
$\varepsilon$	Contact rate	1.2	Assumed
$\xi$	Rate at which people make proper use of face masks and hand sanitizers	0.2	Assumed
$\sigma_1$	Progression rate to the recovered class after incubation period	0.937	A18
$\sigma_2$	Progression rate from quarantine to the infected class	0.0628	A17

**3.2 Sensitivity Analysis**

Sensitivity analysis is the study of how the uncertainty in the output of a model can be apportioned to different sources of uncertainty in the model input [12]. The sensitivity analysis in this study follows the procedure outlined in [13]. The normalized forward sensitivity indices with respect to a parameter value Q is defined as

$$\alpha_Q^{R_0} = \frac{\partial R_0}{\partial Q} \times \frac{Q}{R_0} \tag{74}$$

Where

$$Q = \{\varepsilon, \nu, \gamma, \eta, \xi\} \tag{75}$$

Calculating the sensitivity index requires the use of the Maple 16 software as well as the variables found in Table 5.

The results presented in Table 5 demonstrate that the parameters can have either a positive or negative impact on  $R_0$ .  $R_0$  will increase when the parameters are positive, but it will decrease when the parameters are negative. The sensitivity index is highest for the contact rate, followed by the other parameters in descending order.

**3.3 Estimation of the Basic Reproductive Ratio  $R_0$  of COVID-19 Transmission without Vaccination**

From the model equations, we had the basic reproductive ratio of COVID-19 transmission without vaccination as

$$\mathfrak{R}_0 = R_0(0) = l_1 \left[ \frac{B_3 B_4 + \omega B_3 + \tau \sigma_2 + B_4}{B_2 B_3 B_4} \right] \tag{76}$$

Putting the value of the parameters in Table 3.2 into equation (76) we have;

$$\mathfrak{R}_0 = R_0(0) = 1.578177354 > 1 \tag{77}$$

Since  $R_0 > 1$ , the prevalence of Corona Virus is considered an epidemic.

**Table 5.** Parameter sensitivity analysis.

Parameters	Sensitivity index
$\varepsilon$	1.0000000
$\eta$	-0.8002527
$\nu$	-0.2500000
$\gamma$	-0.974460
$\xi$	-0.2500000



### 3.4 Estimation of the Basic Reproductive Ratio $R_0$ of COVID-19 Transmission with Vaccination

From the model equations, we had the basic reproductive ratio of COVID-19 transmission with vaccination as

$$R_0(v) = I_1(\mu + \nu\kappa) \left[ \frac{B_3B_4 + \omega B_2B_3 + \tau\sigma_2B_2 + B_4}{B_1B_2B_3B_4} \right] \quad (78)$$

Putting the value of the parameters in Table 3.2 into equation (78) we have;

$$R_0(v) = 0.42568 < 1 \quad (79)$$

Since the  $R_0(v) < 1$ , it implies that with the proper use of vaccine, the virus can die out naturally if given a clean health bill.

### 3.5 The Herd Immunity Threshold (H1) Estimation

According to the herd immunity hypothesis, infectious diseases that are managed to pass from one individual to another are more likely to have their chains of transmission broken when there are a lot of people in a community who are immune to the disease or have a reduced risk of contracting it. For the purpose of determining the Herd Immunity Threshold H1, this research makes use of the method described in [12].

$H1 = 1 - \frac{1}{\mathfrak{R}_0}$  Where  $\mathfrak{R}_0$  is the Basic Reproduction Number in the absence of vaccination.  
 $= 0.36638$

Therefore, at least 36.638% of the population is going to be vaccinated to control the epidemic.

### 3.7 Graphical Presentation of $R_0$ and Some Parameters of the Model

Some of the parameters that can significantly affect  $R_0$  are shown graphically in Fig 2 through 5.

### 4. Discussions

In this paper, we analysed the sensitivity of the model and studied the existence and stability of both the disease-free and disease-endemic equilibria. Herd immunity was also considered as the sole method of vaccination in our analysis. We compared our stability with that of the existing works and discovered that the local and the global stability of both our work and that of the existing works were locally and globally asymptotically stable at Disease Free Equilibrium point (DFE). All efforts to compare our estimated held immunity threshold

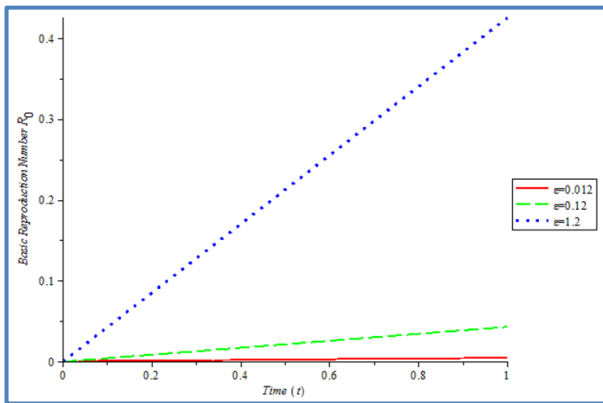


Fig. 2 The Effect of Contact Rates on  $R_0$ .

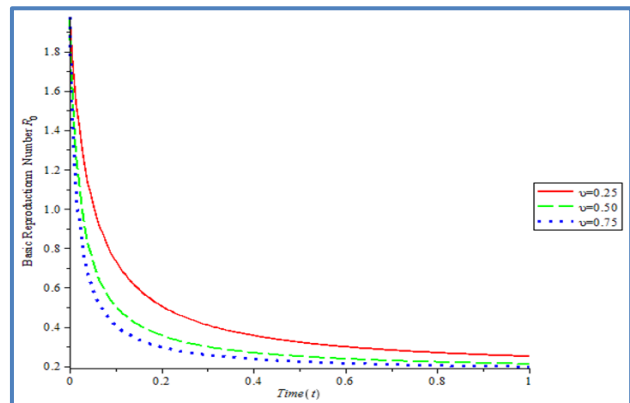


Fig. 3 The Effect of Vaccination Rates on  $R_0$ .

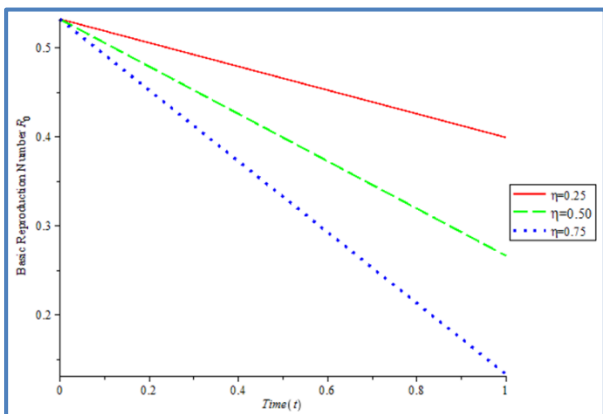


Fig. 4 The Effect of Social Distancing on  $R_0$ .

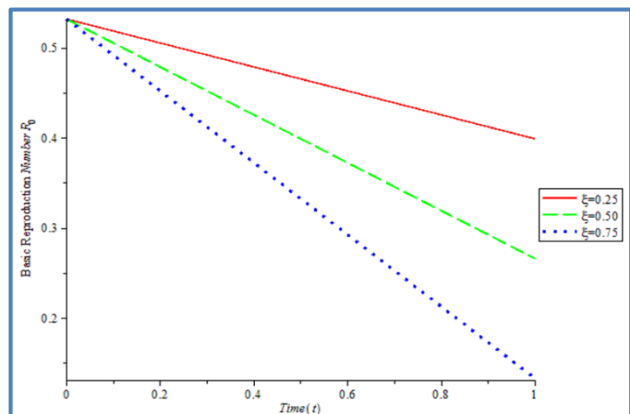


Fig. 5 The Effect of Proper Use of Face Mask on  $R_0$ .

Data in Table 4 allowed us to determine that the basic reproductive number for COVID-19 transmitting without vaccination is  $R_0 = 1.578177354 > 1$ . This suggests an outbreak. This suggestion is in agreement with the work of Pakwan et al. (2021) whose  $R_0 = 1.40995 > 1$  and other literature are considered in this work. COVID-19 transmission with vaccination has a basic reproductive number of  $R_0 = 0.42568$ . The introduction of vaccination into the model has resulted in a drop in the value of  $R_0$ . As a result, increased vaccination will help to prevent the spread of coronavirus.

That is to say, if stakeholders in the country take adequate measures to prevent the disease but if vaccination programs are bolstered generally, the disease will be eradicated for good.

In order to prevent the spread of disease, it is necessary for at least 36.638% of the population to be vaccinated, as determined by the Herd Immunity Threshold that was calculated in this research.

People who have not received vaccinations have a significantly higher risk of contracting diseases from both other people and, more dangerously, from surfaces they come into contact with. If a sufficient number of people are vaccinated through mass vaccination, the disease will be eliminated if it reaches and then transcends the Herd Immunity Threshold level. As a result, 36.638% of the population will have to be vaccinated in order to successfully eradicate the pathogen from the population. If the vaccine used is insufficiently effective or the required coverage cannot be reached, the programme may not be able to exceed the herd immunity threshold; it can, however, disturb the balance of the infection without eliminating it. This change occurs simply because there are now fewer susceptible individuals in the population who can be infected. On the other hand, if the vaccination exercise causes the proportion of immune persons in a population to exceed the Herd Immunity Threshold for a significant length of time, transmission of the COVID-19 disease in that population will gradually come to a halt.

Also, from our simulations, it was found that when the numbers of vaccinated humans are increased, the number of humans that will have attained a level of immunity also increase. If vaccination is done properly, then we are sure to have a lot of COVID-19 immune persons in our system, thereby decreasing the spread of Corona Virus amongst humans.

As shown in Fig. 2, the Basic Reproduction Number  $R_0$  rises as the rate of contact increases over time. This means that those who are susceptible should stay away from infected people to prevent the virus from spreading.

As shown in Fig. 3, as the vaccination rate rises, the Basic Reproduction Number  $R_0$  falls. In other words, if enough people get the vaccinated, the disease could be contained.

As can be seen in Fig. 4, social distance has a negative impact on the  $R_0$ .  $R_0$  decreases as the speed of social distancing increased. This means that susceptible people who abstain from social gatherings have a lower risk of contracting the virus; so, we should practice good social distancing to limit the spread of the disease.

Proper use of face mask has a noticeable impact on the basic reproduction number  $R_0$ , as shown in Fig. 5.  $R_0$  decreases as more people start using face masks correctly. This means that those who are susceptible but who keep using a face mask while around infected people have a better chance of avoiding infection; consequently, we need to keep using face masks correctly to prevent the disease from spreading further.

## 5. Conclusion

In this study, we analysed the Local and Global stabilities of the DFE and calculated the DFE and EE in terms of the infectious force. Since the DFE is consistent everywhere, this implies that the Corona Virus can be contained when  $R_0$  is less than 1. Based on the sensitivity analysis results, it is clear that the contact rate  $R_0$  is the most important factor in raising the  $R_0$ , while the vaccination rate  $v$  is the most important factor in lowering the  $R_0$ . The data visualization shows that eradicating the Corona Virus requires not only a higher vaccination rate, but also a higher recovery rate. Additionally, as shown in Figure 1, the basic reproduction number increases as the amount of contact with infected patients of the Corona Virus grow. Therefore, to lessen the spread of epidemics, infected people should be kept apart from healthy ones. It has also been suggested that the government should invest more in the Corona virus vaccines as well as the distribution of face masks and hand sanitizers to help slow the spread of the disease.

**Authors Contribution:** Conceive – C.J; Design - C.J., S.A.S.; Supervision – S.A.S.; Experimental Performance, Data Collection and/or Processing C.J.; Analysis and/or Interpretation C.J., S.A.S.; Literature Review- C.J; Writer- C.J; Critical Reviews – C.J., S.A.S.

**Acknowledgements:** In closing, the researchers wish to their appreciation to Federal University of Technology, Minna for allowing them to use their facilities and services.

**Conflicts Of Interest:** There are no competing interests to report, as stated by the researchers.

## Orcid-ID

Chembe JAPHETH  <https://orcid.org/0000-0002-0897-5860>

Somma Abu SAMUEL  <https://orcid.org/0000-0002-8354-2010>

## Reference

- [1] World Health Organisation. Coronavirus disease (COVID-19) outbreak. *Emergencies-Diseases*. US Mid report, Nov, 2020.
- [2] H. A. Rothan, and S. N. Byrareddy, "The epidemiology and pathogenesis of coronavirus disease (COVID-19) outbreak". *Journal of autoimmunity*, Vol. 109, May pp. 102 – 123, 2020.
- [3] Aljazeera, *Timeline: How the new coronavirus spread*. Aljazeera and News Agencies, 2020.
- [4] S. A. Lauer, K. H. Grantz, Q. Bi, F. K. Jones, Q. Zheng, H. R. Meredith, and J. Lessler, "The incubation period of coronavirus disease 2019 (COVID-19) from publicly reported confirmed cases: estimation and application."

- Annals of internal medicine*, vol. 172, no. 9, pp. 577-582, 2020.
- [5] Nigeria Centre for Disease Control (NCDC). *COVID-19 Situation Report: Situation Report 1 and Report 58*. NCDC Publication, 2020.
- [6] P. Riyapan, S. E. Shuaib, and A. Intarasit, "Mathematical model of COVID-19 Pandemic: a case study of Bangkok, Thailand". *Computational and Mathematical Methods in Medicine*, Vol. 12, no. 5, pp. 421 – 440, 2021.
- [7] G. O. Sabbih, M. A. Korsah, J. Jeevanandam, and M. K. Danquah, "Biophysical analysis of SARS-CoV-2 transmission and theranostic development via N protein computational characterization." *Biotechnology Progress*, vol. 37, no. 2, pp. 70 - 96, 2021.
- [8] D. Dunford, B. Dale, N. Stylianou, E. Lowther, M. Ahmed, and I. T. A. Dale, *Coronavirus: The world in lockdown in maps and charts*. BBC News. Apr., 2020
- [9] S. Dharmaratne, S. Sudaraka, I. Abeyagunawardena, K. Manchanayake, M. Kothalawala, and W. Gunathunga, "Estimation of the basic reproduction number ( $R_0$ ) for the novel coronavirus disease in Sri Lanka". *Virology Journal*, vol. 17, no. 1, pp. 1-7, 2020.
- [10] O. J. Peter, S. Qureshi, A. Yusuf, M. Al-Shomrani, and A. A. Idowu, "A new mathematical model of COVID-19 Using Real Data from Pakistan". *Results in Physics*, vol. 2, no. 4, pp. 104 – 128, 2021.
- [11] C. Castillo-Chavez, Z. Feng, and W. Huang, "On the computation of  $R_0$  and its role on". *Mathematical approaches for emerging and reemerging infectious diseases: an introduction*, vol. 1, 229. 2002
- [12] K. M. Addo, "An SEIR Mathematical Model for Dog Rabies; Case Study: Bongo District, Ghana" Doctoral dissertation, Kwame Nkrumah University of Science and Technology, 2012.
- [13] S. A. Somma, N. I. Akinwande, P. Gana, O. D. Ogwumu, T. T. Ashezua, and F. Y. Eguda, "Stability and Bifurcation Analysis of a Mathematical Modeling of Measles Incorporating Vitamin a Supplement". *SLU Journal of Science and Technology*, vol. 2 no. 1, pp. 1 - 18, 2021,



License: This article is available under a Creative Commons License ( Attribution 4.0 International, as described at <https://creativecommons.org/licenses/by/4.0/> )



# Principles of Semi-Field Study Design to Obtain Realistic Data about the Effects of Anthropogenic Climate Change on the Biological and Ecological Traits of *Culex pipiens* (L.)

Zafer ŞAKACI\*<sup>1</sup>, Aylin ER<sup>1</sup>

<sup>1</sup> Balıkesir University, Faculty of Science and Literature, Department of Biology, 10100, Çağış-Balıkesir, Türkiye

## Review Article

### Keywords:

Climate change  
Natural conditions  
*Culex pipiens*  
Field data

Received: 05.04.2023

Accepted: 24.04.2023

Published: 30.04.2023

DOI: 10.55848/jbst.2023.26

## ABSTRACT

Mosquitoes, representing an ectothermic metazoan parasite, are hypothesized to be highly affected by concurrent climate change. It is also particularly emphasized that field-based data from the studies conducted under realistically fluctuating natural conditions are needed to perform accurate measurements of the impact of such climate effects. For this purpose, a specific greenhouse unit was established in a highly endemic natural habitat of *Culex pipiens* located on the Tekirdag Namik Kemal University campus. This protocol description-based study was performed in order to reveal a detailed application process of a semi field study unit as well as to underline particular advantages and drawbacks of such units, which were designed for the purpose of obtaining field data, and finally to prompt certain related suggestions. In the preparation of the study documentation, protocols and studies on a sample unit were taken into account in order to base the principles on realistic data.

## 1. Introduction

More than 3500 species of mosquitoes, which constitute the most important arthropod group for human beings as well as animals, have been reported worldwide so far [1]. This importance is due to both the number of agents that they can transmit to the different host groups and the fact that these agents, which can be seen in humans and animals around the world, may cause serious life-threatening diseases [2]. Mosquitoes are common throughout the world; however, species diversity and/or density varies from region to region, and humid tropical/subtropical regions contain  $\frac{3}{4}$  of the known species [3].

Although there is a plethora of studies on the effects of temperature on arthropod life history traits, these have mainly been carried out under laboratory conditions, often applying constant temperature regimes on laboratory colonies. However, it is well known that the laboratory colony or natural population status of the mosquitoes used in the studies, or the territories of the study, can significantly affect the thermal response of insects to varying degrees [4-9]. Furthermore, insects routinely experience variable climatic parameters on a daily, monthly, or seasonal basis in their natural habitats. Various biological and population traits [10, 11] and vector capacities [12-14] are characterized under the constantly variable drivers under the natural circumstances. Therefore, in order to obtain more reliable data on such parameters, it is much more convenient to carry out the relevant studies directly in the natural environment

of insects or in a realistic simulation of their natural habitat [15, 16]. Particular emphasis is placed on the requirement for studies conducted under realistic fluctuating field conditions to accurately measure the impact of climate change on living systems, including vectors, as climate change is predicted to be characterized by variations in temperature values and increased frequency of periodic thermal extremes [14, 17-21].

Although the importance of field data is well known, there are no detailed protocols for obtaining detailed field data on mosquitoes. In particular, the establishment of field simulations is a method that is rarely applied in the world. This is of course also due to the particular challenges of obtaining field data on mosquitoes compared to many other parasites. However, it is now a fundamental necessity to put in place some initiatives in order to reach realistic field data in any case.

In this study, the characteristics of a field simulation complex, which can be used in mosquito studies and the principles of its used protocol, are discussed in some basic aspects. In order to base the analysis and inferences on realistic data, the operation of an existing and actively used sample facility was taken as basis. The sample facility is established in an area containing rather high *C. pipiens* natural population endemically, together with some other mosquito species [22]. In addition to having a population density at the level required for a detailed study in the area, the fact that this species is an ideal model for some ecological studies such as evolutionary

\* Balıkesir University, Faculty of Science and Literature, Department of Biology, 10100 Çağış-Balıkesir, Türkiye  
E-mail address: zafer.sakaci@baun.edu.tr

adaptation [23] also played a role in its selection. In this review, study designs that can be conducted directly under natural conditions in order to obtain field-based data on the life history traits and ecological features of *C. pipiens* in and/or around the greenhouse system, which is designed specifically and established in Tekirdag Namik Kemal University campus are addressed from various aspects.

## 2. Materials and Methods

### 2.1 Principles of the study area selection

The study area is placed in the agricultural research area of the Tekirdag Namik Kemal University campus which is located in the central district of Tekirdag province, in the coastal region of the Marmara Sea, and on the southern part of Eastern Thrace. The site is located in a peri-urban environment and consists of woodlands, fields, greenhouses, and buildings. Trials are conducted in and/or around a greenhouse system (40°59'32.12"N, 27°34'43.93"E) designed as a simulation of natural condition for arthropod research (Fig. 1). The region, which is located in the subtropical zone, is under the influence of "summer arid and hot temperate climate type (Csa)" according to the Köppen-Geiger climate classification [24]. The study area was preferred based on the following features: i) the natural prevalence of *C. pipiens*, which is the most common mosquito species in Tekirdag and almost all regions of Turkey and constitutes the main subject of our study, ii) since the aim of the study was to determine how the natural process proceeds, the mosquitoes to be examined should not have been exposed to special conditions or passed through some special process, and iii) the absence of a clinically important disease outbreak due to active vector dynamic related to the mosquito species belonging to the natural fauna of the region.

### 2.2. Establishment of a purposive greenhouse

The greenhouse system (5 m x 7 m x 2,5 m), which does not have any thermal insulation, artificial lighting, or air conditioning, is established in a wooded part of the study area. The greenhouse is covered with wire mesh and the ceiling is covered with white nylon tarpaulin to prevent the entry of wild animals, direct sunlight, and rain (Fig. 1A).

### 2.3. Recording of climatic parameters

Temperature and humidity values of the study area were recorded hourly by means of dataloggers (TFA Dostmann Klimalogg Pro 30.3039, Germany) placed inside the greenhouse. Dataloggers are positioned in such a way that they do not receive direct sunlight. Rainfall data are recorded daily by rain gauges (TFA Dostmann 47.1008, Germany) placed around the greenhouse. Wind data is obtained from the General Directorate of Meteorology.

### 2.4. Lure of mosquitoes to the vicinity of the study area

It has been reported that CO<sub>2</sub> and various odors emitted by the host are attractive features in mosquitoes' host selection [25]. It has also been emphasized that the addition of bird uropygial gland odorants to CO<sub>2</sub> supplied traps will increase the collection of *Culex* species [26]. Besides, *C. quinquefasciatus* has a specific interest in fecal odorants of poultry [27]. To lure mosquitoes in the vicinity of the study area, ten domestic chickens (*Gallus domesticus*) were constantly maintained in a coop complex (4 m x 5 m x 4 m) covered with wire mesh on three sides, a wall on one side, and a tarpaulin on the ceiling. Feces obtained from chickens were collected in certain areas around the greenhouse. In this way, it is aimed to accelerate the orientation of the mosquitoes existing



**Fig 1.** Study area (A: greenhouse system, B: containers used for the larvae rearing in the greenhouse system).

in the vicinity to the greenhouse environment and to stimulate their feedings in their natural process. Mosquitoes that head to the study area immediately enter the resting mode on the walls or ceilings of the reinforced concrete area in the coop after feeding on the chickens, and these gravid females wait in this mode until they are ready to lay eggs. Chickens are both natural hosts that mosquitoes can feed on, and the presence of chickens, birds, other animals, or humans in an area play as an effective attractant for *C. pipiens*, whose host selectivity is quite flexible [28].

### 2.5. Obtainment of mosquito egg rafts for any trials on larvae

Obtaining egg rafts is a basic requirement for conducting life history traits and population dynamics in the *C. pipiens* mosquito. Accordingly, breeding/laying containers were placed around the greenhouse system for the supply of egg rafts. The egg rafts laid in the containers were collected daily and used for relevant studies performed to determine the larval development process under natural circumstances.

### 2.6. Design of the study targeted to examine the details of life history traits

The main purpose of the experiments, which will investigate the life history characteristics of *C. pipiens*, is to monitor the larval development of the local population from the egg laying to the adult emergence under the local temperature regime. As long as the reproductive dynamics of the natural *C. pipiens* population in the study area continues, it should be aimed to establish trial groups on a monthly basis. The duration of the study should be planned so that at least a one-year cycle is completed. Egg rafts laid directly by mosquitoes obtained from the breeding/laying containers placed in the vicinity of the greenhouse system for the establishment of the trials. Trials should be set up on the day the first instar larvae emerge from these egg rafts. Egg rafts obtained from breeding/laying containers should be taken into egg incubation containers that contain water supplied with fry food. Incubation containers should be followed in the greenhouse until the first stage larvae emerge. A trial group belonging to the relevant month should be established from the larvae emerged in the relevant month. First instar larvae hatching from at least six egg rafts on the same day should be collected in a single pool for each trial group. In total 288 larvae randomly selected from this pool can be divided into 36 clear glass cups (bottom diameter: 6 cm; top diameter: 8 cm; height: 8 cm; water depth 5.5 cm) containing 150 ml of commercial water and eight larvae in each glass. The day on which eight larvae are distributed to the glasses should be marked as the day 0 (starting day). Here, we recommend that the number of larvae to be used should not fall below 200 for each trial to obtain accurate data for the statistical analysis and relevant modellings. Again, it is recommended that the number of larvae to be placed in each glass cup described above should not exceed eight. Because, in a study in which the intraspecific crowding effect was investigated in the larvae of *C. pipiens* mosquitoes, the success of adult emergence in the container containing eight larvae seems ideal among the experimental groups in containers prepared in the same way [29]. Exceeding this number will trigger the larval crowding effect, negatively affecting the main objectives of the experiment. Each cup

should be placed one by one in transparent plastic containers (h: 20 cm; diameter: 20 cm) to prevent the escape of emerging adults (Fig. 1B).

The upper opening of the containers should be covered with gauze and a cotton-plugged hole should be created in the middle of the gauze to collect the emergent adult mosquitoes with a mouth aspirator or any other aspirator types. Water loss due to evaporation during daily checks on glasses should be supplied by adding equal amount of commercial water. Larvae should be fed according to the protocol related to juvenile fish food and feeding should be discontinued from the pupal stage [30]. In order to be able to directly observe the effect of meteorological parameters, special attention should be paid to prevent the larvae from being exposed to nutritional deficiency and crowding in the experimental groups, since it is essential to eliminate other factors.

In the experimental groups, the number of living larvae in the glasses, the number of dead larvae, the number of daily formed pupae, the number of living pupae, the number of dead pupae, the number of emergent males and females and the temperature level in the greenhouse system should be recorded daily. The developmental process of the larvae in the cups should be monitored daily from the first instar larval stage to adult emergence and/or death of the last aquatic form. Relevant examinations must be performed before 18:00 in the evening. All records of larvae, pupae and adult emergence and temperature taken in a 24-hour period from 18:00 to 18:00 for consecutive days should be used as single-day data.

Wing measurements can be taken from randomly selected 30 male and 30 female individuals from the emergent adult collected in a pool. It has been stated that wing length is an indicator of body size in adult mosquitoes [17, 31]. By measuring the wing lengths of the adults, it can be determined to what extent they are affected by the periodic temperature regime exposed during the development. Measurements should be made from the anal lobe to the wing tip, using the same wing (left wing in this study) for each individual [32]. Species identification of mosquitoes used throughout the study was performed under a stereomicroscope using specific identification keys based on the morphological characteristics of different developmental stages [33-35].

In the study designed such a way described above, the development time of the larva until the pupae, the development time of the emergent males and females, the survival rate and wing length, the number of deaths in the larvae and pupae, the daily ambient temperature values experienced during development (daily maximum, minimum and average temperatures, and daily temperature) were taken as indicators to measure the effects of natural circumstances to the development process of *C. pipiens* aquatic forms.

### 2.7. Design of experiments to monitor propagation characteristics and population dynamics

In this study, it has been aimed to determine the monthly reproductive characteristics and population dynamics of *C. pipiens* under the fluctuating natural conditions. In this direction, breeding containers were placed at the different distances in the vicinity of the greenhouse system, some of



**Fig 2.** The localities of breeding containers placed in the study area

which were outdoors and some were indoors. The number of containers and their site may vary according to the conditions of the area where the study is performed [36]. The containers were placed in different foci with different characteristics at some extent; one plastic and one tire container were placed side by side in each focus (Fig. 2). It has been aimed to reveal four facts in the selection of the type and location of the containers, namely the following: i) how far from the feeding focus (chicken house) do mosquitoes lay eggs? ii) is there a difference of interest in tire and plastic containers in the selection of the laying site? iii) do indoor and outdoor preferences change in egg laying? and iv) how does the monthly course change in respect of all these preferences?

It is recommended that this study be conducted for at least one year to clearly demonstrate monthly and seasonal propagation characteristics and population dynamics. Egg rafts in all containers should be counted every day and collected by recording the container codes and other relevant records. Photographs of the rafts should be taken under a stereomicroscope to determine egg numbers per raft. Then, the rafts should be taken into glass cups supplied with fry food one by one and kept until the larvae hatch. The hatching times should be noted by counting the larvae when they emerge.

A wooden board is mounted on top of the breeding containers to prevent them from overflowing by rain and being exposed to direct sunlight. In addition, each container is protected with wire to prevent animals from getting inside and drinking water. Six liters of distilled water up to six cm high was put into rectangular plastic containers (25 cm x 38 cm; h: 27 cm). Six liters of distilled water was poured into the tire (outer diameter: 47 cm, inner diameter: 38 cm, length: 47 cm, width: 25

cm) with a depth of six cm. In order to lure mosquitoes to the water bodies placed in the containers, the attraction technique with straw infusion was used as described in the related study [37].

### 3. Conclusion

Considering the evaluations made on the unit used as a model, it is understood that the following parameters should be considered in fieldwork simulations: i) since *C. pipiens* prefers to lay eggs in containers at the shaded foci for most of the year, rearing containers used in the studies should be kept out of direct sunlight, ii) The instructions for the use of the devices used in the measurement of meteorological parameters should be fully complied with, e.g., at least three rain gauges should be used considering possible local differences, and the average value should be used as ambient data, iii) thermometers must be placed in such a way that they do not receive direct sunlight; this will result in highly erroneous temperature readings being recorded and the related error will manifest itself especially with abnormal increases in temperature difference between day and night, iv) natural mosquito breeding areas in the selected locality should be determined and whether they will affect the study should be evaluated, v) it should definitely be taken into account that larval crowding and feeding deficiencies can result in very crucial problems in larval development, and vi) it should be known that the presence of animal hosts, which are kept in accordance with natural conditions, is one of the most important factors in attracting mosquitoes to a certain area.

When the designs of field research described in this study were evaluated together, the following aspects have been determined: i) the number of egg rafts laid by *C. pipiens* on a daily basis under the circumstances of realistic natural conditions in a year; ii) whether the number of eggs per egg raft changed on a monthly basis; iii) the embryonal development time and the performance of larva hatching from egg rafts

conceived on a monthly basis; and iv) the development time and performance from first instar larvae to adult emergence revealed successfully on a monthly basis. For this purpose, field-based data on *C. pipiens* life history traits and ecology were accurately obtained using the described study area design and the performed study protocols in this document.

**Authors Contribution:** Conceive- Z.S., A.E.; Design- Z.S., A.E.; Supervision- A.E.; Literature Review- Z.S., A.E.; Writer- Z.S., A.E.; Critical Reviews- Z.S., A.E.

**Conflicts Of Interest:** The authors have declared no conflicts of interest.

### Orcid-ID

Zafer ŞAKACI  <https://orcid.org/0000-0002-6736-3792>

Aylin ER  <https://orcid.org/0000-0002-8108-8950>

### Reference

- [1] M.J. Lehane, "The biology of blood-sucking in insects", Cambridge University Press, pp. 336, 2005.
- [2] R.W. Merritt, R.H. Dadd, and E.D. Walker, "Feeding behavior, natural food, and nutritional relationships of larval mosquitoes", Annual review of entomology, vol. 37, pp. 349-374, 1992.
- [3] N. Becker, D. Petrić, M. Zgomba, C. Boase, M. Madon, C. Dalh, and A. Kaiser, "Mosquitoes and Their Control", vol. 2, Berlin, Germany: Springer Verlag, pp. 577, 2010.
- [4] K. Bergant, and S. Trdan, "How reliable are thermal constants for insect development when estimated from laboratory experiments?", Entomologia experimentalis et applicata, vol. 120, pp. 251-256, 2006.
- [5] H. Delatte, G. Gimonneau, A. Triboire, and D. Fontenille, "Influence of temperature on immature development, survival, longevity, fecundity, and gonotrophic cycles of *Aedes albopictus*, vector of chikungunya and dengue in the Indian Ocean", Journal of medical entomology, vol. 46, pp. 33-41, 2009.
- [6] A.S. Vorhees, E.M. Gray, and T.J. Bradley, "Thermal resistance and performance correlate with climate in populations of a widespread mosquito", Physiological and Biochemical Zoology, vol. 86, pp. 73-81, 2013.
- [7] A.T. Ciota, A.C. Matarachiero, A.M. Kilpatrick, and L.D. Kramer, "The effect of temperature on life history traits of *Culex* mosquitoes", Journal of medical entomology, vol. 51, pp. 55-62, 2014.
- [8] J.E. Ruybal, L.D. Kramer, and A.M. Kilpatrick, "Geographic variation in the response of *Culex pipiens* life history traits to temperature", Parasites & vectors, vol. 9, pp. 1-9, 2016.
- [9] E.N. Field, J.J. Shepard, M.E. Clifton, K.J. Price, B.J. Witmier, K. Johnson, ... and R.C. Smith, "Semi-field and surveillance data define the natural diapause timeline for *Culex pipiens* across the United States", Communications Biology, vol. 5, pp. 1300, 2022.
- [10] C. Williams, "Insect thermal baggage", Nature Climate Change, vol. 6, pp. 543-544, 2016.
- [11] M.E. Dillon, and J.D. Lozier, "Adaptation to the abiotic environment in insects: the influence of variability on ecophysiology and evolutionary genomics", Current opinion in insect science, vol. 36, pp. 131-139, 2019.
- [12] L. Lambrechts, K.P. Paaijmans, T. Fansiri, L.B. Carrington, L.D. Kramer, M.B. Thomas, and T.W. Scott, "Impact of daily temperature fluctuations on dengue virus transmission by *Aedes aegypti*", Proceedings of the National Academy of Sciences, vol. 108, pp. 7460-7465, 2011.
- [13] C.C. Murdock, M.V. Evans, T.D. McClanahan, K.L. Miazgovicz, and B. Tesla, "Fine-scale variation in microclimate across an urban landscape shapes variation in mosquito population dynamics and the potential of *Aedes albopictus* to transmit arboviral disease", PLoS neglected tropical diseases, vol. 11, pp. e0005640, 2017.
- [14] B.L. McGregor, J.L. Kenney, and C.R. Connelly, "The effect of fluctuating incubation temperatures on West Nile virus infection in *Culex* mosquitoes", Viruses, vol. 13, pp. 1822, 2021.
- [15] B.W. Alto, K. Wiggins, B. Eastmond, S. Ortiz, K. Zirbel, and L.P. Lounibos, "Diurnal temperature range and chikungunya virus infection in invasive mosquito vectors", Journal of Medical Entomology, vol. 55, pp. 217-224, 2018.
- [16] V. Kellermann, S.L. Chown, M.F. Schou, I. Aitkenhead, C. Janion-Scheepers, A. Clemson, ... and C.M. Sgrò, "Comparing thermal performance curves across traits: how consistent are they?", Journal of Experimental Biology, vol. 222, pp. jeb193433, 2019.
- [17] J.R. Schneider, D.D. Chadee, A. Mori, J. Romero-Severson, and D.W. Severson, "Heritability and adaptive phenotypic plasticity of adult body size in the mosquito *Aedes aegypti* with implications for dengue vector competence", Infection, Genetics and Evolution, vol. 11, pp. 11-16, 2011.
- [18] K.P. Paaijmans, R.L. Heinig, R.A. Seliga, J.I. Blanford, S. Blanford, C.C. Murdock, and M.B. Thomas, "Temperature variation makes ectotherms more sensitive to climate change", Global change biology, vol. 19, pp. 2373-2380, 2013.
- [19] H. Colinet, B.J. Sinclair, P. Vernon, and D. Renault, "Insects in fluctuating thermal environments", Annual review of entomology, vol. 60, pp. 123-140, 2015.
- [20] J.G. Kingsolver, and H.A. Woods, "Beyond thermal performance curves: modeling time-dependent effects of thermal stress on ectotherm growth rates", The American Naturalist, vol. 187, pp. 283-294, 2016.
- [21] J.G. Kingsolver, and L.B. Buckley, "Quantifying thermal extremes and biological variation to predict evolutionary responses to changing climate", Philosophical Transactions of the Royal Society B: Biological Sciences, vol. 372, pp. 20160147, 2017.
- [22] Y. Akbay, "Tekirdağ'da, *Culex* spp.'nin Aylık Üreme Karakteristiklerinin Belirlenmesi", Yüksek Lisans Tezi, Namık Kemal Üniversitesi Fen Bilimleri Enstitüsü, Tekirdağ, 2016.
- [23] E.M. Gray, "Thermal acclimation in a complex life cycle: the effects of larval and adult thermal conditions on metabolic rate and heat resistance in *Culex pipiens* (Diptera: Culicidae)", Journal of Insect Physiology, vol. 59, pp. 1001-1007, 2013.
- [24] <https://tr.climate-data.org/asya/tuerkiye/tekirdag/tekirdag-764513/> (Accessed 01 Apr. 2023).



- [25] W. Takken, "The role of olfaction in host-seeking of mosquitoes: a review", *International Journal of Tropical Insect Science*, vol. 12, pp. 287-295, 1991.
- [26] C.B. Russell, and F.F. Hunter, "Attraction of *Culex pipiens/restuans* (Diptera: Culicidae) mosquitoes to bird uropygial gland odors at two elevations in the Niagara region of Ontario", *Journal of medical entomology*, vol. 42, pp. 301-305, 2005.
- [27] M.F. Cooperband, J.S. McElfresh, J.G. Millar, and R.T. Carde, "Attraction of female *Culex quinquefasciatus* Say (Diptera: Culicidae) to odors from chicken feces", *Journal of Insect Physiology*, vol. 54, pp. 1184-1192, 2008.
- [28] A. Merdivenci "Türkiye Sivrisinekleri (Yurdumuzda varlığı bilinen sivrisineklerin biyo-morfolojisi, biyo-ekolojisi, yayılışı ve sağlık önemleri)", Türkiye, İstanbul: İstanbul Üniversitesi Cerrahpaşa Tıp Fakültesi Yayınları, pp. 354, 1984.
- [29] B. Seymen "Culex pipiens (Diptera: Culicidae) türü sivrisineklerin larvalarında tür içi kalabalık etkisinin araştırılması", Yüksek lisans tezi, Namık Kemal Üniversitesi Fen Bilimleri Enstitüsü, Tekirdağ, 2018.
- [30] E. Kauffman, A. Payne, M.A. Franke, M.A. Schmid, E. Harris, and L.D. Kramer, "Rearing of *Culex* spp. and *Aedes* spp. mosquitoes", *Bio-protocol*, vol. 7, pp. e2542-e2542, 2017.
- [31] R.S. Nasci, "Relationship between adult mosquito (Diptera: Culicidae) body size and parity in field populations", *Environmental Entomology*, vol. 15, pp. 874-876, 1986.
- [32] A. Aryan, M.A. Anderson, J.K. Biedler, Y. Qi, J.M. Overcash, A.N. Naumenko, ... and Z. Tu, "Nix alone is sufficient to convert female *Aedes aegypti* into fertile males and myo-sex is needed for male flight", *Proceedings of the National Academy of Sciences*, vol. 117, pp. 17702-17709, 2020.
- [33] G.C. Rossi, and R.E. Harbach, "Phytotelmatomyia, a new neotropical subgenus of *Culex* (Diptera: Culicidae)", *Zootaxa*, vol. 1879, pp. 1-17, 2008.
- [34] R.E. Harbach, "Culex pipiens: species versus species complex—taxonomic history and perspective", *Journal of the American Mosquito Control Association*, vol. 28, pp. 10-23, 2012.
- [35] R.C. Wilkerson, Y.M. Linton, and D. Strickman, "Mosquitoes of the World (Vol. 1)", Johns Hopkins University Press, pp. 599, 2021.
- [36] Y. Akbay, E. Ipek, G. Akyıldız, Z. Şakacı, Ş. Talay, S.Z. Ahrabi, ... and S. Kar, "The Monthly Oviposition Characteristics of the Mosquito Species *Anopheles maculipennis sensu stricto*, *Anopheles claviger*, and *Culiseta longiareolata* Observed at Some Artificial Containers under Natural Circumstances in a Selected Area of Thrace, Türkiye", *Journal of Balkan Science and Technology*, vol. 1, pp. 81-86, 2022.
- [37] D.A. Ewing, B.V. Purse, C.A. Cobbold, S.M. Schäfer, and S.M. White, "Uncovering mechanisms behind mosquito seasonality by integrating mathematical models and daily empirical population data: *Culex pipiens* in the UK", *Parasites & vectors*, vol. 12, pp. 1-19, 2019.



License: This article is available under a Creative Commons License ( Attribution 4.0 International, as described at <https://creativecommons.org/licenses/by/4.0/>)



## Melatonin: A Potent Protector of Mitochondria and Cancer

Şeyma DEMİRKESEN<sup>1\*</sup>, Cenk ARAL<sup>1</sup>

<sup>1</sup>Tekirdağ Namik Kemal University, Faculty of Arts and Sciences, Department of Molecular Biology and Genetics, 59030 Suleymanpasa Tekirdağ, Türkiye

### Review Article

#### Keywords:

Melatonin  
Mitochondria  
Cancer

Received: 27.02.2023

Accepted: 13.04.2023

Published: 30.04.2023

DOI: 10.55848/jbst.2023.27

### ABSTRACT

In the mitochondrial electron transport pathway (ET-pathway) electrons are transferred from reduced substrates to oxygen which is coupled to the phosphorylation of ADP to ATP. The electron transfer pathway leads to electron leakage, mitochondria, which is the most important source of free radicals in cells. When mitochondria are damaged by oxidation, they cannot keep up with the cell's energy needs. This determines the cell to produce more free radicals. Both mechanisms, namely faulty ATP generation and elevated oxygen radicals, may promote mitochondrial-dependent apoptosis. Melatonin's high concentrations and diverse antioxidant activities provide substantial protection to organelles which are exposed to a large number of free radicals. It has been shown that melatonin reduces oxidative stress and stress-induced mitochondrial dysfunction both in vitro and in vivo. Moreover, melatonin is protective against a number of illnesses in which excessive free radical production is the primary cause of the disease. Several diseases are characterized by mitochondrial damage caused by oxidative stress. Consequently, melatonin has gained recognition as a potential therapeutic agent for treating cancer and other mitochondrial dysfunctions in cancer cells.

### 1. Introduction: Mitochondria generate ROS

In eukaryotic cells, mitochondria are essential organelles that provide the energy source adenosine triphosphate (ATP), which powers the majority of a cell's biological functions. During the synthesis of ATP, electron transporters transfer electrons to oxygen, where they bond to produce water [1]. Membrane-bound electron transfer pathway consists of sets of electron carriers distributed across four enzyme complexes, namely complex I, complex II, complex III, and complex IV [2]. Across the inner mitochondrial membrane, a proton gradient is formed by the process of electron transport. Complex V (ATP synthase) then uses this proton gradient to create ATP. The other components of the mitochondrial electron transfer pathway are tricarboxylic acid (TCA) cycle, mitochondrial matrix dehydrogenases, and the carriers involved in metabolite transport across the mitochondrial membrane. As a result, the mitochondria are responsible for the synthesis of a wide variety of chemicals, such as amino acids, nucleotides, and reactive oxygen species (ROS) [3]. Complex IV generates water as the last product of the respiratory chain by a four-electron reduction of molecular oxygen (O<sub>2</sub>). The transfer of electrons from one carrier to the next in the ET pathway is not a perfect process; some electrons are lost in translation and end up interacting with nearby ground-state oxygen molecules, which results in the production of ROS [4]. Some of these are the superoxide anion radical (O<sub>2</sub><sup>-</sup>), the hydroxyl radical (·OH), the hydroperoxyl radical (HOO·), the peroxy radical (ROO·), and the alkoxy radical (RO) [5].

The cell's natural antioxidative defense mechanism typically decomposes free radicals and neutralizes their peroxidation products. When these metabolites build up out of control, free radicals trigger chain reactions that damage proteins, lipids, and DNA. Since mitochondria play a crucial role in ROS production, they have been the major target, causing injury to the mitochondrial respiratory system and an increase in free radical creation. Increased cellular oxidative stress is a contributing factor to the development of illnesses including diabetes [6], cardiovascular disease [7], neurodegenerative disease, and cancer [8] under these conditions. However, cells have evolved defense mechanisms to fight the oxidative stress caused by ROS. Due to this, the main defense is to use different types of antioxidants, such as small antioxidant molecules like melatonin. It is well acknowledged that melatonin serves as a crucial regulator of mitochondrial integrity and function and protects cells from oxidative damage [9]. This has also been shown in several in vivo and in vitro studies [8,10].

### 2. The Origins of Melatonin and Its Diverse Roles

Melatonin is thought to have evolved for the first time with the task to get rid of harmful O<sub>2</sub> derivatives made by photosynthetic bacteria during photosynthesis [11,12]. The fact that the structure of melatonin in cyanobacteria is the same as the structure of melatonin in mammals today is an important sign that its chemical structure has not changed [13]. Therefore,

\* Tekirdağ Namik Kemal University, Faculty of Arts and Sciences, Department of Molecular Biology and Genetics, 59030 Suleymanpasa Tekirdağ, Türkiye  
E-mail address: seymayildrm@gmail.com.tr

the original property of being an antioxidant was kept and helped by evolution and other properties. Melatonin, which was first isolated and described by Lerner et al in 1958, is synthesized by the pineal gland and released into circulation [14]. Melatonin production also occurs in lymphocytes [15], the skin [16], the gastrointestinal tract [17], the thymus, various areas of the eye, and bone marrow, also it is involved in paracrine and autocrine signaling. Therefore, the pineal glands' melatonin release is connected to the circadian rhythm and synced with the light-dark cycle. In mammals, unlike other species, its production is restricted to darkness. It is a crucial physiological ingredient that signals circadian time and synchronizes several activities in the body [18].

Among the many physiological processes that melatonin regulates are those related to sleep [19], immunity [20], and seasonal control of reproduction [21]. It has been demonstrated that the pharmacological dosages of melatonin decrease tumor development and have therapeutic efficacy in several forms of cancer, including breast cancer, prostate cancer, and melanoma [22]. Melatonin membrane receptors belong to the G-protein coupled receptor families (MT1, MT2) and the quinone reductase enzyme family (MT3), making them molecularly separate [23]. Activation of MT1 receptors by melatonin is typically reliant on the inhibition of cAMP, leading to an increase in cytosolic calcium, while binding to MT2 receptors inhibits cAMP and cGMP [24]. MT1 receptors are involved in reproductive and metabolic processes, while MT2 receptors play a role in the circadian rhythm and dopamine release from the retina [25]. Similarly, the binding location in the nucleus has been found and described for RZR/ROR $\alpha$  and RZR $\beta$  orphan receptors [26]. The interaction of melatonin with these receptors contributes to some of its genomic effects. Some of the melatonin's effects do not involve its receptors at all. Melatonin interacts with cytosolic proteins, including calmodulin, which regulates the cytoskeleton and nuclear receptors, and it functions as a direct scavenger of free radicals [27].

### 3. Melatonin and Mitochondria: Melatonin is a Mitochondria-Targeted Antioxidant

When examining the interaction between melatonin and mitochondria, three features of melatonin that are crucial to mitochondrial homeostasis come to the forefront. The first is that mitochondria create significant quantities of ROS and that melatonin is a potent ROS-scavenging antioxidant; the second is that melatonin is highly produced in mitochondria and the apoptotic signals associated with mitochondria are extremely strong. Thirdly, the circadian rhythm significantly affects mitochondrial structure and function [28,29]. Within a decade after the discovery of indole as potent free radical destroyer and passive antioxidant, it was shown that melatonin prevents ROS damage at the mitochondrial level [30]. The seizure-inducing fatal characteristics of cyanide, a complex IV inhibitor, were reversed by the injection of melatonin in mice, as shown by Yamamoto and Yang. Melatonin also counteracts the neurotoxic effects of 6-hydroxydopamine (6-OHDA) [31], and 1-methyl-4-phenyl-1,2,3,6 tetrahydropyridine (MPTP) [32]-mediated malfunction of mitochondrial Complex I. In addition, research on rats revealed that it increased complex I and IV activities and repaired mitochondrial damage simultaneously [33].

Oxygen is necessary for aerobic organisms and increases the amount of ATP produced by glucose oxidation. Even though oxygen is a biradical, it is one of the primary causes of ROS production [34]. This is especially significant in mitochondria, where electrons leak each time during electron transport, resulting in oxygen reduction and the generation of one of the most critical ROS, superoxide anion [35].

Melatonin is also known as an indirect antioxidant because it can increase the activity of several antioxidant enzymes, such as superoxide dismutase and glutathione peroxidase, and decrease the activity of pro-oxidant enzymes. As a result, this plays a significant role in the antioxidant system, helping to maintain mitochondrial homeostasis, cutting down on ROS formation, and enhancing ET-pathway activity. Due to the antioxidant action of melatonin, lipids are protected, lipid peroxidation is reduced, and membrane fluidity is maintained, therefore preventing oxidative degradation [36]. The antioxidant activity of melatonin depends on the redox cascade pathway, and this scavenger cascade ensures that melatonin works very effectively in removing free radicals and as an antioxidant. It is also known that melatonin enhances the enzymatic or non-enzymatic cellular defense mechanism by modulating the intracellular redox signaling system and protecting critical proteins in the redox pathway from oxidation, such as Trx1 [37]. Melatonin's scavenger activity does not require a receptor, according to *in vitro* studies, but certain antioxidant effects may be receptor-mediated. Melatonin's protective impact as an oncostatic agent or in the neurological system may be attributed to this quality [38].

Melatonin can affect mitochondrial bioenergetic parameters by regulating the oxygen flux and the mitochondrial membrane potential. *In vitro* experiments with normal mitochondria have also shown that mitochondrial function is protected against ROS-induced oxidative damage and oxygen consumption is reduced in the presence of ADP, which leads to a decrease in membrane potential and inhibition of O<sub>2</sub><sup>•-</sup> and H<sub>2</sub>O<sub>2</sub> [39]. Melatonin is also known to cause a decrease in membrane potential and ATP production by increasing the gene expression of uncoupling proteins (UCPs), which play an important role in the modulation of mitochondrial membrane potential. Melatonin may counterbalance the decreased ATP generation caused by the activation of UCPs by decreasing electron leakage and increasing electron flow through the membrane bound electron carriers [40].

### 4. Melatonin, Mitochondria, And Cancer

Mitochondrial damage greatly contributes to the dysregulation of cellular metabolism by directing glucose breakdown from the aerobic to the anaerobic pathway. Dysregulation of mitochondrial activity, defined by Krebs cycle abnormalities, has been linked to the overproduction of ROS, which may contribute to oncogenic signaling and tumor growth by irreversibly modifying DNA and oxidizing proteins. Otto Warburg hypothesized that even if there is no change in oxygen circumstances, metabolic alterations may play a role in the switch from oxidative phosphorylation to glycolysis, resulting in cancer. This phenomenon is known as the Warburg effect or aerobic glycolysis [41].

Although it is known that the conversion of glucose to lactate via glycolysis in anaerobic conditions is inefficient when it comes to ATP generation compared to oxidative respiration, tumor cells must make the conversion of glucose to glucose-6-phosphate efficient. Based on positron emission tomography (PET) examinations conducted for this purpose, it has been shown that the glucose absorption of cancer cells is directly correlated with their aggressiveness. In addition to revealing the significance of metabolic research in cancer, these findings will boost the efficacy of targeted treatments as a consequence of a comprehensive analysis of the function of mitochondria in cancer. Research into MDA-MB231 cells undergoing metabolic reprogramming to a glycolytic phenotype has shown a strong correlation between mitochondrial and cell membrane morphology and energy consumption in cancer [42].

Many researches in recent years have proven the anti-cancer impact of melatonin on cancer cells, and its usage is expanding. According to research, increasing melatonin levels at night aid in the control of homeostatic balance. Melatonin's behavior varies depending on cell type or circumstance [43]. Melatonin has this oncostatic impact through receptor-dependent or receptor-independent mechanisms, as shown [44]. MT-1 and MT-2 receptors are G-protein coupled receptors that are involved in the downstream pathway. In this process, it is claimed that the decrease in linoleic acid intake and therefore the anti-proliferative impact of melatonin are implicated in the mechanism of action due to the suppression of cAMP [45].

Apoptosis, also known as programmed cell death, is the most essential mechanism for balancing cell growth and death. There are two key extrinsic and intrinsic pathways in apoptosis. While death receptors and caspases play a role in the extrinsic apoptotic process, Bid (tBid), which is released into the mitochondria upon Caspase activation, initiates the internal apoptotic pathway. The intrinsic apoptotic pathway is a mitochondrial-mediated pathway that is activated by factors like DNA damage, chemotherapy, and radiation therapy. This pathway involves bax-bak, a member of the pro-apoptotic bcl-2 family, and the apoptotic process starts when molecules like cytochrome c are released. Therefore, getting bax/bak to work is a very important part of treating cancer [46].

Melatonin is known to have both pro-apoptotic and anti-apoptotic properties. It prevents apoptosis from occurring in normal cells while encouraging it in cancer cells. However, this double effect remained a topic of discussion. In addition, melatonin may start apoptosis by stimulating the cytosolic cascade and triggering the release of cytochrome c or an increase in antiapoptotic proteins.

The effects of melatonin on cancer cell growth and apoptosis are the result of a number of research and processes. It has been shown that melatonin inhibits ERK and Akt when they are activated by reactive oxygen species (ROS), resulting in suppression of cyclin D1, Bcl-2, and up-regulation of bax in cancer cells. It also induces apoptosis by inhibiting the expression of the p53 negative regulator MDM2, increasing caspase-3 and caspase-9 activity [47].

Under hypoxic circumstances, it is known that cancer cells acquire resistance to TRAIL-mediated death, which is another method of action. Melatonin therapy inhibits hypoxic

conditions for bax release via modulating mitochondrial membrane potential and promoting apoptotic cell death by removing TRAIL-mediated apoptosis resistance in cancer cells [48]. In addition, it has been shown in HepG-2 cancer cells that melatonin decreases proliferation by arresting the cell cycle in the G2/M phase [49]. Melatonin has a function in early apoptosis by increasing the production of AIF via TGF-1, and in late apoptosis by reducing the bcl-2/bax ratio through caspase-7 and caspase-9 [50].

In recent years, the use of melatonin to enhance the therapeutic efficacy of anti-cancer drugs has increased. Studies have shown that the combination of melatonin and pterostilbene promotes PARP activation in colorectal cancer cells [51] and inhibits ERK phosphorylation and induces HSP-27 dephosphorylation when combined with cisplatin [52].

In addition, the millimolar concentration of melatonin lowered the S-phase population in colon cancer cells while decreasing the G2/M transition in osteosarcoma and leukemia cells without affecting cell survival. All of these findings demonstrate that the apoptotic effect varies based on the metabolic and differentiation levels of cancer cells [53, 54].

## 5. Conclusion

Mitochondria plays a crucial role in maintaining cellular equilibrium, including calcium balance and apoptosis, while providing essential functions such as supplying cells with chemical energy and power. The mitochondrial dysfunction caused by oxidative stress has led to the development of mitochondrial-targeted antioxidant systems. Melatonin, which is also produced by mitochondria, is one of these compounds. Diverse investigations have shown that it may reduce the harm that may arise from an increase in mitochondrial ROS production or an excessive increase in ROS. It has been demonstrated that melatonin is particularly powerful in combating oxidative stress; thus, its absorption or production by mitochondria makes it the most important participant when ROS levels rise.

Melatonin's oncostatic effects in malignancies with the Warburg effect may be explained by its capacity to regulate glucose metabolism by transferring it primarily from the cytosol to the mitochondria. However, although there are studies that hypothetically explain its ability to change this situation, it is believed to have an effect with basically the same mechanism as anti-cancer agents. The use of melatonin should be explored if the impact of melatonin is significant at the mitochondrial level, if mitochondrial dysfunctions are improved, or if the energy mechanism works better for no apparent reason.

Blockade of glycolysis metabolism is presently one of the most significant targets in anticancer investigations. Melatonin should be regarded as significant in this context due to its capacity to alter mitochondrial processes. Melatonin may also make apoptotic processes stronger because it controls the mitochondrial respiratory chain with mitochondrial apoptotic effectors and is involved in calcium release.

This degree of interdependence between mitochondria and melatonin may allow the impact to be apparent in several cell types, including tumor cells. Depending on the kind and stage of cancer, it may exhibit varied mitochondrial features,

such as improving the efficiency of chemotherapy or minimizing its negative side effects while opposing cell growth, apoptosis, or chemotherapy resistance. As a result, when evaluated together, melatonin acts as a versatile molecule in reducing ROS levels, improving mitochondrial energy mechanisms, and its effects on tumor cells, as well as its mechanism of action should be studied in depth, either alone or in combination with other agents in a variety of cancer types.

### Declaration

**Author Contribution:** Conceive – Ş.D., C.A.; Design - Ş.D., C.A.; Supervision - Ş.D., C.A.; Experimental Performance, Data Collection and/or Processing Ş.D., C.A.; Analysis and/or Interpretation Ş.D., C.A.; Literature Review- Ş.D.; Writer- Ş.D.; Critical Reviews – Ş.D., C.A.

**Conflict of interests:** The author(s) declare no conflict of interest and this study has received no financial support.

### Orcid-ID

Şeyma DEMİRKESEN  <https://orcid.org/0000-0002-9945-2554>

Cenk ARAL  <https://orcid.org/0000-0002-6044-1372>

### References

- [1] M. Cedikova et al., “Mitochondria in White, Brown, and Beige Adipocytes,” *Stem Cells Int*, vol. 2016, 2016, doi: 10.1155/2016/6067349 .
- [2] G. Lenaz and M. L. Genova, “Structure and Organization of Mitochondrial Respiratory Complexes: A New Understanding of an Old Subject,” <https://home.liebertpub.com/ars>, vol. 12, no. 8, pp. 961–1008, Mar. 2010, doi: 10.1089/ARS.2009.2704.
- [3] D. C. Wallace, “Mitochondria and cancer,” *Nat Rev Cancer*, vol. 12, no. 10, pp. 685–698, Oct. 2012, doi: 10.1038/NRC3365.
- [4] B. Halliwell, “Free radicals, proteins and DNA: oxidative damage versus redox regulation,” *Biochem Soc Trans*, vol. 24, no. 4, pp. 1023–1027, Nov. 1996, doi: 10.1042/BST0241023.
- [5] I. Fridovich, “Oxygen: how do we stand it?,” *Med Princ Pract*, vol. 22, no. 2, pp. 131–137, 2013, doi: 10.1159/000339212.
- [6] M. Rafieian-Kopaei, B. Baharvand-Ahmadi, M. Bahmani, P. Tajeddini, and N. Naghdi, “An ethno-medicinal study of medicinal plants used for the treatment of diabetes *Journal of Nephropathology* \*Corresponding author: ARTICLE INFO,” *J Nephropathol*, vol. 5, no. 1, pp. 44–50, 2015, doi: 10.15171/jnp.2016.08.
- [7] M. Sadeghi et al., “Cheese consumption in relation to cardiovascular risk factors among Iranian adults- IHHP Study,” *Nutr Res Pract*, vol. 8, no. 3, p. 336, 2014, doi: 10.4162/NRP.2014.8.3.336.
- [8] M. Martín et al., “Melatonin-induced increased activity of the respiratory chain complexes I and IV can prevent mitochondrial damage induced by ruthenium red in vivo,” *J Pineal Res*, vol. 28, no. 4, pp. 242–248, 2000, doi: 10.1034/J.1600-079X.2000.280407.X.
- [9] J. Leon, D. Acuña-Castroviejo, R. M. Sainz, J. C. Mayo, D. X. Tan, and R. J. Reiter, “Melatonin and mitochondrial function,” *Life Sci*, vol. 75, no. 7, pp. 765–790, Jul. 2004, doi: 10.1016/J.LFS.2004.03.003.
- [10] M. J. Jou et al., “Melatonin protects against common deletion of mitochondrial DNA-augmented mitochondrial oxidative stress and apoptosis,” *J Pineal Res*, vol. 43, no. 4, pp. 389–403, Nov. 2007, doi: 10.1111/J.1600-079X.2007.00490.X.
- [11] L. C. Manchester et al., “Melatonin: an ancient molecule that makes oxygen metabolically tolerable,” *J Pineal Res*, vol. 59, no. 4, pp. 403–419, Nov. 2015, doi: 10.1111/JPI.12267.
- [12] G. Noctor, S. Veljovic-Jovanovic, and C. H. Foyer, “Peroxide processing in photosynthesis: antioxidant coupling and redox signalling,” 2000, doi: 10.1098/rstb.2000.0707.
- [13] T. H. Champney, A. P. Holtorf, R. W. Steger, and R. J. Reiter, “Concurrent determination of enzymatic activities and substrate concentrations in the melatonin synthetic pathway within the same rat pineal gland,” *J Neurosci Res*, vol. 11, no. 1, pp. 59–66, 1984, doi: 10.1002/JNR.490110107.
- [14] T. J. Agric, F. Hanci, M. Çingi, H. Akinci, and O. İd, “Influence of L-Tryptophan and Melatonin on Germination of Onion and Leek Seeds at Different Temperatures,” *Turkish Journal of Agricultural Research*, vol. 6, no. 2, pp. 214–221, Jun. 2019, doi: 10.19159/TUTAD.559617.
- [15] A. Carrillo-Vico et al., “Evidence of melatonin synthesis by human lymphocytes and its physiological significance: possible role as intracrine, autocrine, and/or paracrine substance,” *The FASEB Journal*, vol. 18, no. 3, pp. 537–539, 2004, Accessed: Feb. 20, 2023. [Online]. Available: [https://www.academia.edu/3219395/Evidence\\_of\\_melatonin\\_synthesis\\_by\\_human\\_lymphocytes\\_and\\_its\\_physiological\\_significance\\_possible\\_role\\_as\\_intracrine\\_a\\_utocrine\\_and\\_or\\_paracrine\\_substance](https://www.academia.edu/3219395/Evidence_of_melatonin_synthesis_by_human_lymphocytes_and_its_physiological_significance_possible_role_as_intracrine_a_utocrine_and_or_paracrine_substance)
- [16] A. Slominski et al., “On the role of melatonin in skin physiology and pathology,” *Endocrine*, vol. 27, no. 2, pp. 137–147, 2005, doi: 10.1385/ENDO:27:2:137.
- [17] G. A. Bubenik, “Gastrointestinal melatonin: localization, function, and clinical relevance,” *Dig Dis Sci*, vol. 47, no. 10, pp. 2336–2348, Oct. 2002, doi: 10.1023/A:1020107915919.
- [18] R. J. Reiter, “Melatonin: The chemical expression of darkness,” *Mol Cell Endocrinol*, vol. 79, no. 1–3, pp. C153–C158, Aug. 1991, doi: 10.1016/0303-7207(91)90087-9.
- [19] R. Wurtman, I. Z.-T. Lancet, and undefined 1995, “Improvement of sleep quality by melatonin,” [thelancet.com](https://www.thelancet.com), Accessed: Feb. 20, 2023. [Online].

- Available:  
[https://www.thelancet.com/journals/lancet/article/PIIS0140-6736\(95\)92509-0/fulltext](https://www.thelancet.com/journals/lancet/article/PIIS0140-6736(95)92509-0/fulltext)
- [20] V. Srinivasan, G. J. M. Maestroni, D. P. Cardinali, A. I. Esquifino, S. R. Pandi Perumal, and S. C. Miller, "Melatonin, immune function and aging," *Immunity and Ageing*, vol. 2, Nov. 2005, doi: 10.1186/1742-4933-2-17.
- [21] V. Srinivasan, W. D. Spence, S. R. Pandi-Perumal, R. Zakharia, K. P. Bhatnagar, and A. Brzezinski, "Melatonin and human reproduction: Shedding light on the darkness hormone," *Gynecological Endocrinology*, vol. 25, no. 12, pp. 779–785, Dec. 2009, doi: 10.3109/09513590903159649.
- [22] V. Srinivasan, D. Warren Spence, S. R. Pandi-Perumal, I. Trakht, and D. P. Cardinali, "Therapeutic actions of melatonin in cancer: possible mechanisms," *journals.sagepub.com*, vol. 7, no. 3, pp. 189–203, Sep. 2008, doi: 10.1177/1534735408322846.
- [23] M. L. Dubocovich and M. Markowska, "Functional MT 1 and MT 2 Melatonin Receptors in Mammals elatonin, dubbed the hormone of darkness, is known to regulate a wide variety of physiological processes in mammals.," *Endocrine*, vol. 27, no. 2, pp. 101–110, 2005.
- [24] L. Brydon et al., "Dual Signaling of Human Mella Melatonin Receptors via G i2 , G i3 , and G q/11 Proteins," *Molecular Endocrinology*, vol. 13, pp. 2025–2038, 1999, Accessed: Feb. 20, 2023. [Online]. Available: <https://academic.oup.com/mend/article/13/12/2025/2747797>
- [25] M. L. Dubocovich and M. Markowska, "Functional MT1 and MT2 melatonin receptors in mammals," *Endocrine*, vol. 27, no. 2, pp. 101–110, 2005, doi: 10.1385/ENDO:27:2:101.
- [26] I. Wiesenberg, ... M. M.-R. neurology, and undefined 1998, "The potential role of the transcription factor RZR/ROR as a mediator of nuclear melatonin signaling," *content.iospress.com*, Accessed: Feb. 20, 2023. [Online]. Available: <https://content.iospress.com/articles/restorative-neurology-and-neuroscience/rnn00030>
- [27] M. Macías et al., "Calreticulin–melatonin: An unexpected relationship," *Wiley Online Library*, vol. 270, no. 5, pp. 832–840, Mar. 2003, doi: 10.1046/j.1432-1033.2003.03430.x.
- [28] S. Proietti, A. Cucina, M. Minini, and M. Bizzarri, "Melatonin, mitochondria, and the cancer cell," *Cell Mol Life Sci*, vol. 74, no. 21, pp. 4015–4025, Nov. 2017, doi: 10.1007/S00018-017-2612-Z.
- [29] D. X. Tan, L. C. Manchester, L. Qin, and R. J. Reiter, "Melatonin: A Mitochondrial Targeting Molecule Involving Mitochondrial Protection and Dynamics," *Int J Mol Sci*, vol. 17, no. 12, Dec. 2016, doi: 10.3390/IJMS17122124.
- [30] M. Valko, H. Morris, and M. Cronin, "Metals, toxicity and oxidative stress," *Curr Med Chem*, vol. 12, no. 10, pp. 1161–1208, Apr. 2005, doi: 10.2174/0929867053764635.
- [31] F. DABBENI-SALA, S. Santo, D. FRANCESCHINI, S. D. SKAPER, and A. pietro GIUSTI, "Melatonin protects against 6-OHDA-induced neurotoxicity in rats: a role for mitochondrial complex I activity," *The FASEB Journal*, vol. 15, no. 1, pp. 164–170, Jan. 2001, doi: 10.1096/FJ.00-0129COM.
- [32] E. Absi, A. Ayala, A. Machado, and J. Parrado, "Protective effect of melatonin against the 1-methyl-4-phenylpyridinium-induced inhibition of Complex I of the mitochondrial respiratory chain," *J Pineal Res*, vol. 29, no. 1, pp. 40–47, Aug. 2000, doi: 10.1034/J.1600-079X.2000.290106.X.
- [33] M. Martín et al., "Melatonin-induced increased activity of the respiratory chain complexes I and IV can prevent mitochondrial damage induced by ruthenium red in vivo," *J Pineal Res*, vol. 28, no. 4, pp. 242–248, 2000, doi: 10.1034/J.1600-079X.2000.280407.X.
- [34] "Reactive Species and Antioxidants. Redox Biology Is a Fundamental Theme of Aerobic Life on JSTOR." <https://www.jstor.org/stable/20205747> (accessed Feb. 20, 2023).
- [35] R. J. Reiter, D. X. Tan, and A. Galano, "Melatonin: Exceeding Expectations", doi: 10.1152/physiol.00011.2014.
- [36] J. J. García et al., "Protective effects of melatonin in reducing oxidative stress and in preserving the fluidity of biological membranes: a review," *J Pineal Res*, vol. 56, no. 3, pp. 225–237, Apr. 2014, doi: 10.1111/JPI.12128.
- [37] A. Rodriguez-Garcia et al., "Thioredoxin 1 modulates apoptosis induced by bioactive compounds in prostate cancer cells," *Redox Biol*, vol. 12, p. 634, Aug. 2017, doi: 10.1016/J.REDOX.2017.03.025.
- [38] N. Watson, T. Diamandis, C. Gonzales-Portillo, S. Reyes, and C. v. Borlongan, "Melatonin as an Antioxidant for Stroke Neuroprotection," *Cell Transplant*, vol. 25, no. 5, pp. 883–891, 2016, doi: 10.3727/096368915X689749.
- [39] A. López et al., "Melatonin protects the mitochondria from oxidative damage reducing oxygen consumption, membrane potential, and superoxide anion production," *J Pineal Res*, vol. 46, no. 2, pp. 188–198, Mar. 2009, doi: 10.1111/J.1600-079X.2008.00647.X.
- [40] D. X. Tan, L. C. Manchester, L. Qin, and R. J. Reiter, "Melatonin: A Mitochondrial Targeting Molecule Involving Mitochondrial Protection and Dynamics," *Int J Mol Sci*, vol. 17, no. 12, Dec. 2016, doi: 10.3390/IJMS17122124.
- [41] O. Warburg and S. Minami, "Versuche an Überlebendem Carcinom-gewebe," *Klin Wochenschr*,

- vol. 2, no. 17, pp. 776–777, Apr. 1923, doi: 10.1007/BF01712130.
- [42] I. Vega-Naredo et al., “Mitochondrial metabolism directs stemness and differentiation in P19 embryonal carcinoma stem cells,” *Cell Death Differ*, vol. 21, no. 10, p. 1560, Oct. 2014, doi: 10.1038/CDD.2014.66.
- [43] Y. Li et al., “Melatonin for the prevention and treatment of cancer,” *Oncotarget*, vol. 8, no. 24, pp. 39896–39921, 2017, doi: 10.18632/oncotarget.16379.
- [44] G. Nikolaev, R. Robeva, and R. Konakchieva, “Membrane Melatonin Receptors Activated Cell Signaling in Physiology and Disease,” *International Journal of Molecular Sciences 2022*, Vol. 23, Page 471, vol. 23, no. 1, p. 471, Dec. 2021, doi: 10.3390/IJMS23010471.
- [45] S. L. Deming et al., “Melatonin pathway genes and breast cancer risk among Chinese women,” *Breast Cancer Res Treat*, vol. 132, no. 2, pp. 693–699, Apr. 2012, doi: 10.1007/S10549-011-1884-5.
- [46] S. Thomas et al., “Targeting the Bcl-2 Family for Cancer Therapy,” *Expert Opin Ther Targets*, vol. 17, no. 1, p. 61, Jan. 2013, doi: 10.1517/14728222.2013.733001.
- [47] J. Song et al., “Downregulation of AKT and MDM2, Melatonin Induces Apoptosis in AGS and MGC803 Cells,” *Anat Rec*, vol. 302, no. 9, pp. 1544–1551, Sep. 2019, doi: 10.1002/AR.24101.
- [48] Y. J. Lee, J. H. Lee, J. H. Moon, and S. Y. Park, “Overcoming Hypoxic-Resistance of Tumor Cells to TRAIL-Induced Apoptosis through Melatonin,” *International Journal of Molecular Sciences 2014*, Vol. 15, Pages 11941-11956, vol. 15, no. 7, pp. 11941–11956, Jul. 2014, doi: 10.3390/IJMS150711941.
- [49] J. Martín-Renedo, J. L. Mauriz, F. Jorquera, O. Ruiz-Andrés, P. González, and J. González-Gallego, “Melatonin induces cell cycle arrest and apoptosis in hepatocarcinoma HepG2 cell line,” *J Pineal Res*, vol. 45, no. 4, pp. 532–540, Nov. 2008, doi: 10.1111/J.1600-079X.2008.00641.X.
- [50] “Evidence for a biphasic apoptotic pathway induced by melatonin in MCF-7 breast cancer cells.” <https://sci-hub.ru/10.1111/j.1600-079X.2008.00645.x> (accessed Feb. 20, 2023).
- [51] J. Hoon Jung et al., “NEDD9 Inhibition by miR-25-5p Activation Is Critically Involved in Co-Treatment of Melatonin-and Pterostilbene-Induced Apoptosis in Colorectal Cancer Cells,” 2019, doi: 10.3390/cancers11111684.
- [52] J. H. Kim, S. J. Jeong, B. Kim, S. M. Yun, D. Y. Choi, and S. H. Kim, “Melatonin synergistically enhances cisplatin-induced apoptosis via the dephosphorylation of ERK/p90 ribosomal S6 kinase/heat shock protein 27 in SK-OV-3 cells,” *J Pineal Res*, vol. 52, no. 2, pp. 244–252, Mar. 2012, doi: 10.1111/J.1600-079X.2011.00935.X.
- [53] Y. Hong et al., “Melatonin treatment induces interplay of apoptosis, autophagy, and senescence in human colorectal cancer cells,” *J Pineal Res*, vol. 56, no. 3, pp. 264–274, Apr. 2014, doi: 10.1111/JPI.12119.
- [54] L. Liu, Y. Xu, and R. J. Reiter, “Melatonin inhibits the proliferation of human osteosarcoma cell line MG-63,” *Bone*, vol. 55, no. 2, pp. 432–438, Aug. 2013, doi: 10.1016/J.BONE.2013.02.021.



License: This article is available under a Creative Commons License ( Attribution 4.0 International, as described at <https://creativecommons.org/licenses/by/4.0/>)



## Modeling of Optimum Control of the Distance Learning Process

Gülizar ALİSOY<sup>1</sup>, Rahima NURALİYEVA<sup>2</sup>, Meltem APAYDIN USTUN<sup>3</sup>, Arif Kıvanc USTUN<sup>3</sup>, Hafiz ALİSOY<sup>3\*</sup>

<sup>1</sup> Tekirdağ Namık Kemal University, Faculty of Arts and Sciences, Department of Mathematics, 59030, Tekirdağ, Türkiye

<sup>2</sup> Azerbaijan State Oil and Industry University, Baku, Azerbaijan

<sup>3</sup> Tekirdağ Namık Kemal University, Faculty of Engineering, Department of Electrical and Electronics, 59860, Corlu-Tekirdağ, Türkiye

### Research Article

#### Keywords:

Optimal control  
Control vector  
Forgetting coefficient  
Residual knowledge coefficient  
Learning intensity

Received: 05.03.2023

Accepted: 25.04.2023

Published: 30.04.2023

DOI: 10.55848/jbst.2023.28

### ABSTRACT

In this study, based on the use of the principle of modal control, the solution to the problem of modeling the optimal control of the process of distance learning is considered. It is assumed that the process of distance learning is described by a finite-difference equation that contains the main parameters of the learning process (the degree of knowledge, the coefficients of forgetting, and residual knowledge). Based on the results obtained, a scheme for modeling the optimal system of the distance learning process in MATLAB/Simulink is proposed.

## 1. Introduction

Solving complex management problems in the educational system is currently almost impossible without preliminary modeling of learning processes. Control problems as well as methods of mathematical modeling of learning processes have been studied in numerous works [1-4]. In these works, some aspects of the optimal management of educational processes in the university are considered. In particular, the development of an optimal curriculum begins with the creation of a model for managing the processes of interest. Generally, the parameters of the learning process are the degree of knowledge, the coefficients of forgetting, and residual knowledge. In those problems, simulation modeling methods are applied using the principle of a system approach of control theory [5-7]. Therefore, the development of mathematical models for solving problems of analysis and synthesis of the learning process is crucial.

The organization of the distance learning process, including a set of organizational and methodological measures and the object of learning (or control), will be called a system. The management (organization) system is optimal when it has the best quality of the distance learning process in terms of its parameters, the degree of knowledge, the coefficients of forgetting, and residual knowledge, under given conditions and restrictions. The quality of such systems can be assessed by some optimality criterion  $J$ , considering the current level of

knowledge  $x(n)$  (state) and effort cost (or management) for training  $g(n)$  for some finite time interval  $[0, N]$ .

Commonly, a finite-difference equation of the process of distance learning is known as a non-linear vector [8,9]. Restrictions on the control and state of the system are set. It is required to find a control vector (control algorithm) that transfers the control object from the initial state to the final state, keeps it in this final state, or changes it by the input signal while providing an extreme value of the optimality criterion [10,11]. The simulation is considered complete if the control algorithm is found as a function of the vector of state variables under known restrictions on the components of the control vector. The task of modeling an optimal system is to develop a system or control algorithm that minimizes some optimality criterion, considering the constraints on the control and state.

## 2. Materials and Methods

### 2.1 Statement of the problem

Here, we study linear and discrete dynamical systems. Let us consider the application of the Z-transform for solving the problems of the analysis of such one-dimensional stationary systems.

Let the process of distance learning of higher mathematics in the engineering discipline be described by an ordinary linear difference equation of the first order:

\* Tekirdağ Namık Kemal University, Faculty of Engineering, Department of Electrical and Electronics, 59860 Corlu-Tekirdağ, Türkiye  
E-mail address: halisoy@nku.edu.tr



$$x(n + 1) - (1 - a)x(n) = g(n), \tag{1}$$

where  $x \in [0,1]$  is the degree of knowledge of elements of mathematics,  $a \in [0,1]$  is the forgetting coefficient,  $g \in [0,1]$  is the control of the learning process, and  $g(n) = \mu(n) + b$ , where  $\mu(n) \in [0,1]$  is the learning intensity, and  $b \in [0,1]$  is the coefficient of residual knowledge,  $n \in [0, N]$  is the current learning time. After applying transformations to equation (1), we obtain the equation in deviations as

$$x^*(n) = x(n) - q, \tag{2}$$

where  $q$  is the desired level of knowledge. Note that equation (2) is valid for any  $n$ , including  $n + 1$ . Analyzing this expression, it is easy to see that in the limit  $q = 1$  and as  $n \rightarrow \infty, x^* \rightarrow 0$ .

However, such a requirement on the average can never be achieved. Optimal management (or organization of learning) can only provide the best approximation in some sense to the desired level.

Considering these, the finite-difference equation of the learning process in (2) can be written in the following form:

$$x^*(n + 1) - (1 - a)x^*(n) = g(n) - aq. \tag{3}$$

It should be noted that the right side of equation (3) represents the optimal control of the learning process, i.e.,  $g^*(n) = g(n) - aq$ . In addition, if we consider the equation in (3), the control of the learning process  $g(n)$  is determined, respectively, through the intensity of learning  $\mu(n)$  and the coefficient of residual knowledge  $b$ . We then obtain

$$x^*(n + 1) - (1 - a)x^*(n) = \mu(n) + b - aq. \tag{4}$$

For further analysis, we require that the control delivers a minimum quadratic error with minimum training intensity. To solve this problem, we will use the method of variational calculus [5-9].

According to the principle of variation, the problem of finding the extreme values of a function in the presence of constraints in the form of equalities is solved by the method of indefinite Lagrange multipliers. In this case, the optimality criterion can be written as follows:

$$J_c = \sum_n^N F_c[x(n), g(n)], \tag{5}$$

Where

$$F_c[x(n), g(n)] = \frac{1}{2}[x^2(n) + g^2(n)] + \lambda(n + 1)[x(n + 1) - (1 - a)x(n) - g(n)].$$

As a result of the expansion of the function,  $F_c$  in a Taylor series and limited to the first terms of the expansion, we will have [9]

$$F_c^*(n) = \frac{1}{2}[x^{*2}(n) + g^{*2}(n)] + \lambda^*(n + 1)[x^*(n + 1) - (1 - a)x^*(n) - g^*(n)], \tag{6}$$

and

$$F_c^*(n - 1) = \frac{1}{2}[x^{*2}(n - 1) + g^{*2}(n - 1)] + \lambda^*(n)[x^*(n) - (1 - a)x^*(n - 1) - g^*(n - 1)]. \tag{7}$$

Next, we define the discrete Euler-Lagrange equation for which the case under consideration has the form

$$\frac{\partial F_c^*(n)}{\partial x^*(n)} + \frac{\partial F_c^*(n-1)}{\partial x^*(n)} = \frac{1}{2}2x^*(n) - (1 - a)\lambda^*(n + 1) + \lambda^*(n) = 0,$$

or

$$x^*(n) - (1 - a)\lambda^*(n + 1) + \lambda^*(n) = 0. \tag{8}$$

In the next step, we obtain the process equation under optimum conditions. To do this, by differentiating expression (4) with respect to the Lagrange multiplier, we obtain

$$\frac{\partial F_c^*(n)}{\partial \lambda^*(n+1)} = x^*(n + 1) - (1 - a)x^*(n) - g^*(n) = 0 \tag{9}$$

We also define the optimal control as follows:

$$\frac{\partial F_c^*(n)}{\partial g^*(n)} = g^*(n) - \lambda^*(n + 1) = 0,$$

where

$$g^*(n) = \lambda^*(n + 1). \tag{10}$$

Equation (8) means that to determine the optimal control, it is necessary to know the law of change in the Lagrange multiplier,  $\lambda^*(n + 1)$ . Based on the joint solution of two first-order difference equations (equations (6) and (7)) and considering the equation in (8), we can determine the Lagrange multiplier,  $\lambda^*(n + 1)$ . Since  $x(0)$  and  $x(N)$  are given, these values determine the boundary conditions for solving equations (6) and (7). The system of two difference equations has the form:

$$\begin{cases} (1 - a)\lambda^*(n + 1) - \lambda^*(n) - x^*(n) = 0, \\ x^*(n + 1) - \lambda^*(n + 1) - (1 - a)x^*(n) = 0, \end{cases} \tag{11}$$

under boundary conditions  $x^*(0)$  and  $x^*(N)$ .

### 2.2. Solution of the equations of the optimal system by the z-transformation method

We solve equations (11) by the z-transform method. Let's introduce the new notation:  $x^* = x$ ,  $\lambda^* = y$ . Then, equations (11) can be written as follows:

$$\begin{cases} (1 - a)y(n + 1) - y(n) - x(n) = 0, \\ x(n + 1) - y(n + 1) - (1 - a)x(n) = 0. \end{cases} \tag{12}$$

We apply z-transform to the equations in (12) using the time domain shift theorem:

$$\begin{cases} (1-a)[zY(z) - y(0)] - Y(z) = X(z), \\ zX(z) - x(0) - (1-a)X(z) = [zY(z) - y(0)]. \end{cases} \quad (13)$$

Given that  $x(0) = 1$ , we express (13) in its matrix form as:

$$\begin{bmatrix} 1 & (1+az-z) \\ (z+a-1) & -z \end{bmatrix} \begin{bmatrix} X(z) \\ Y(z) \end{bmatrix} = \begin{bmatrix} (a-1)y_0 \\ 1-y_0 \end{bmatrix}. \quad (14)$$

Solving the matrix equation for X and Y, respectively, we will have

$$X(z) = \frac{(1-a)z + y_0 - 1}{(1-a)z^2 - (a^2 - 2a + 3)z + 1 - a}, \quad (15a)$$

and

$$Y(z) = \frac{(a-1)y_0z + (a^2 - 2a + 2)y_0 - 1}{(1-a)z^2 - (a^2 - 2a + 3)z + 1 - a} \quad (15b)$$

Further, to simplify the analysis, let's assume that the forgetting coefficient  $a=0.4$ . Then, based on equations (15a) and (15b), we will have:

$$X(z) = \frac{0.6z + y_0 - 1}{0.6z^2 - 2.36z + 0.6} \quad (16a)$$

and

$$Y(z) = \frac{y_0z - 2.67y_0 + 1.67}{z^2 - 3.933z + 1}. \quad (16b)$$

To obtain the originals (inverse transformations), we first decompose the equation (16a) and (16b) into the sum of the simplest terms as

$$X(z) = \frac{0.6z}{0.6z^2 - 2.36z + 0.6} + \frac{y_0 - 1}{0.6z^2 - 2.36z + 0.6}, \quad (17a)$$

and

$$Y(z) = \frac{y_0z}{z^2 - 3.933z + 1} - \frac{2.67y_0 - 1.67}{z^2 - 3.933z + 1}. \quad (17b)$$

First, the denominators of all expansion terms must be linear in the form of  $+p_i$ , where  $p_i$  is a real non-positive root of the denominator of the equations (17a) or (17b). Thus, having performed the inverse z-transformation for the equations (17a) and (17b), we obtain the original function for them in the following form, respectively:

$$x^*(n) = 1.081 * 3.66^n - 0.0807 * 0.2732^n + (y_0 - 1) * 0.4921 * (3.66^n - 0.2732^n), \quad (18a)$$

$$y^*(n) = y_0 * (1.0807 * 3.66^n - 0.0807 * 0.2732^n) - (2.67y_0 - 1) * 0.2953 * (3.66^n - 0.2732^n). \quad (18b)$$

Based on the equations above, to solve the problem, we need to determine the initial condition and the law of optimal

control. Let, for concreteness, the final error  $x(N) = x(10) = 0$ . Under these assumptions, using equation (18a), we can find the initial value of  $y_0$ . Thus, we will have

$$x_{i|N=10}^*(n) = 1.081 * 3.66^{10} - 0.0807 * 0.2732^{10} + (y_0 - 1) * 0.4921 * 3.66^{10} = 0. \quad (19)$$

Further, from the equation in (19) for the initial value  $y_0$ , we obtain

$$y_0 = \lambda^*(0) = -1.1967$$

Substituting this initial value into (18a), we find the optimal trajectory as

$$X^*(n) = 0.2732^n \quad (20)$$

As shown above, the optimal control is then described by the relation

$$g^*(n) = \lambda^*(n + 1),$$

where,  $\lambda^*(n + 1)$  satisfies equation (18b), which is valid for any  $n$ , including  $n + 1$ . Therefore, substituting it into (18b), we obtain

$$y_0 = \lambda^*(0) = -1.1967,$$

and after performing simple arithmetic transformations, we get

$$y^*(n) = \lambda^*(n) = -1.1967 * 0.2732^n.$$

Further in this expression, replacing  $n$  with  $n + 1$ , we will have

$$\lambda^*(n + 1) = -1.1967 * 0.2732^{n+1} = -0.3269 * 0.2732^n.$$

The resulting expression allows us to have the control law for the distance learning system in a closed form:

$$g^*(n) = \lambda^*(n + 1) = -0.3269 * 0.2732^n,$$

or

$$g^*(n) = -0.3269 * x^*(n) = -C * x^*(n), \quad (21)$$

where  $C = 0.3269$ .

Thus, the task of modeling optimal control has been solved.

### 3. Results & Discussion

For clarity of the obtained results of the task, Fig. 1 shows the simulation scheme of the optimal system in MATLAB/Simulink. Based on this scheme, the change in the intensity of learning, as well as the change in the degree of knowledge, for the optimal system are shown in Fig. 2 and Fig. 3, respectively.

In MATLAB/Simulink, the change curve of the degree of information determined for the simulation circuit with the same parameters as the optimum system but not optimal is shown in Figure 4.

Comparison of the results shows that by increasing the intensity of training (management), the degree of knowledge of the elements of the discipline increases from 0.16 (in the original non-optimal system) to ~ 0.46 (in the optimal system).

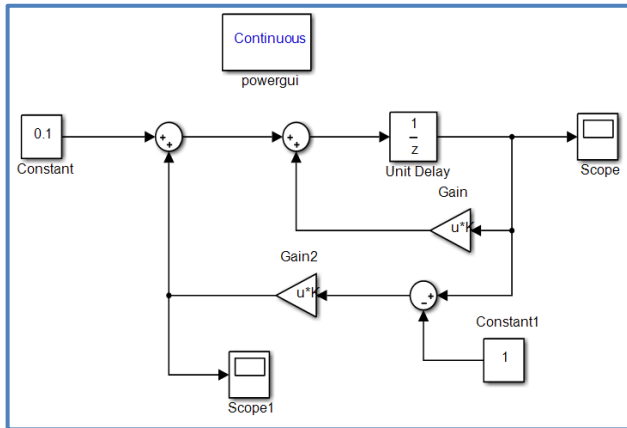


Fig 1. Optimal System Modeling Scheme.

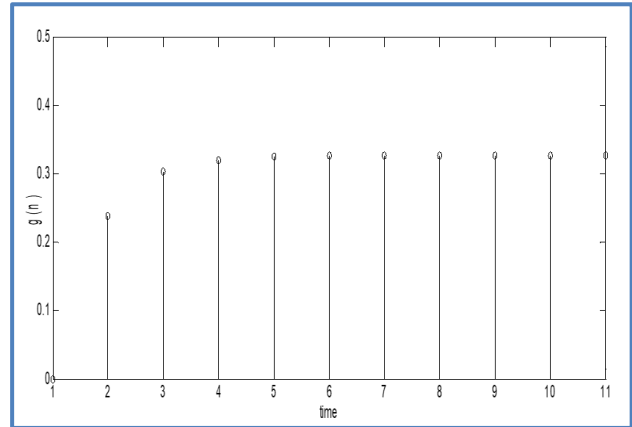


Fig 2. Changing the intensity of the learning (management).

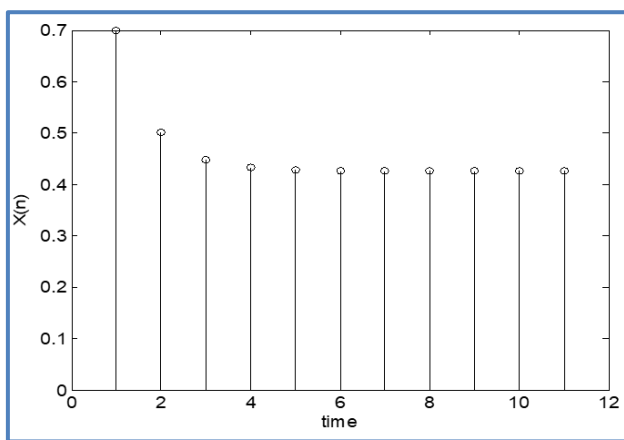


Fig 3. Changing the degree of knowledge (state) in the optimal system.

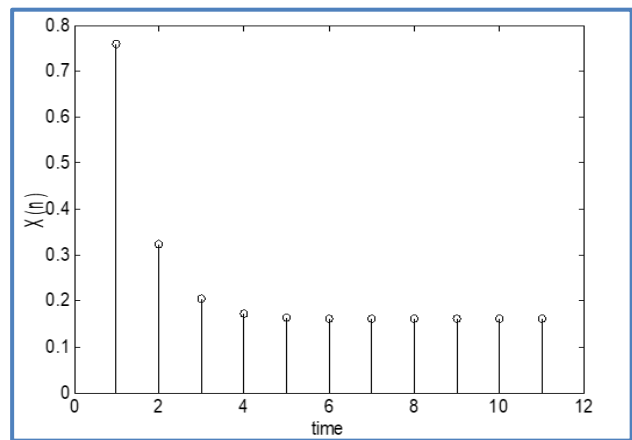


Fig 4. Changing the degree of knowledge in a non-optimal system.

#### 4. Conclusion

In this paper, the problem of modelling the optimal control system for distance learning is formulated. Using the method of indefinite Lagrange multipliers, a system of finite-difference equations for determining the law of optimal control is obtained and its solution is found using the Z-transform.

Under the proposed optimal system, the implementations performed in MATLAB/Simulink show the advantage of the optimal system over the non-optimal one.

**Authors Contribution:** Conceive – G.T.A., H.A.; Design - M.A.Ü., R.N.; Supervision – H.A.; Experimental Performance, Data Collection and/or Processing – A.K.Ü., M.A.Ü., R.N.; Analysis and/or Interpretation – G.T.A., H.A.; Literature Review – R.N.; Writer - M.A.Ü., A.K.Ü., R.N.; Critical Reviews – G.T.A., H

**Conflicts Of Interest:** The authors have declared no conflicts of interest.

#### Orcid-ID

Gülizar ALİSOY [ID https://orcid.org/0000-0003-2114-6669](https://orcid.org/0000-0003-2114-6669)  
Rahima NURALİYEVA [ID https://orcid.org/0000-0001-5939-1403](https://orcid.org/0000-0001-5939-1403)

Meltem APAYDIN USTUN [ID https://orcid.org/0000-0001-9225-9455](https://orcid.org/0000-0001-9225-9455)  
Arif KIVANC USTUN [ID https://orcid.org/0000-0002-9336-7930](https://orcid.org/0000-0002-9336-7930)  
Hafiz ALİSOY [ID https://orcid.org/0000-0003-4374-9559](https://orcid.org/0000-0003-4374-9559)

#### Reference

- [1] Talizina N.F. Managing the process of learning. Moscow State University Publishing House. – 1975, 342 c.
- [2] Leontyev L.P., Gohman O.G. Problems of management of educational processes: Mathematical models. - Riga, 1984. – 239 c.
- [3] R. S. Sutton and A. G. Barto, Reinforcement Learning: An Introduction, MIT Press, Cambridge, MA, USA, 1998.
- [4] Mayer R.B. Cybernetic pedagogy: Simulation of the learning process. - Eyes: GGPI, 2013. – 138 c.
- [5] Pontryagin, L.S.; Boltyanskii, V.G.; Gamkrelidze, R.V.; Mishchenko, E.F. Pontryagin Selected Works: The Mathematical Theory of Optimal Process; Gordon and Breach Science Publishers: NY, USA, 1985; Volume 4, p. 360.

- [6] Pivneva S. V. Modeling of discrete optimization problems / S. V. Pivneva, M. A. Trifonov // Vector of Science. - No. 3 (13), 2010. - pp. 31-34. (in Russian)
- [7] Porter B., Grossley R. Modal Control. Theory and Applications. London: Taylor and Francis, 1972.
- [8] Volgin L.N. Optimal discrete control of dynamical systems. M. Science, 1986, 240p (in Russian)
- [9] Dumachev VN Fundamentals of control theory. 2015, 383p (in Russian)
- [10] Vasiliev E.M., Gusev K.Yu. Modal control of non-stationary systems // Bulletin of the Voronezh State

Technical University. 2008. V. 4. No. 8. pp. 46-54. (in Russian)

- [11] Makkapati, V.R.; Dor, M.; Tsiotras, P. Trajectory desensitization in optimal control problems. In Proceedings of the IEEE Conference on Decision and Control, Miami, FL, USA, 17–19 December 2018; pp. 2478–2483



License: This article is available under a Creative Commons License ( Attribution 4.0 International, as described at <https://creativecommons.org/licenses/by/4.0/> )



# Analytical Solution of Bending, Buckling, and Vibration of Functionally Graded Nanobeams based on Nonlocal Elasticity

Bahar UYMAZ<sup>\*</sup>

<sup>1</sup>Tekirdağ Namık Kemal University, Faculty of Engineering, Department of Mechanical Engineering, 59860, Corlu-Tekirdağ, Türkiye

## Research Article

### Keywords:

Nonlocal elasticity  
Functionally graded nanobeam  
Bending  
Buckling  
Free vibration

Received:25.03.2023

Accepted:29.04.2023

Published:30.04.2023

DOI: 10.55848/jbst.2023.29

## ABSTRACT

Navier solution presented for bending, buckling, and free vibration of simply supported functionally graded nanobeams based on generalized shear deformation theory. The results are obtained for parabolic shear deformation theory corresponding to Reddy beam theory using nonlocal differential constitutive equations which were formulated by Eringen [1,2,3]. The material properties of the functionally graded nanobeam vary through the thickness direction according to a simple power law. Effects of the nonlocal parameter, different material composition and length-to-thickness ratio on the maximum deflection, critical buckling load, and natural frequencies of the nanobeam are investigated. The results show that the scale effects, material composition, and dimensional changes are affected by considered parameters. Nonlocal elasticity theory predicts softening material behavior compared to classical elasticity theory because it takes into account the effects of long-range interactions between material particles. As a result of this, the maximum deflections, critical buckling loads, and natural frequencies obtained by the classical theory are higher than obtained by the nonlocal theory in all considered conditions.

## 1. Introduction

Classical elasticity assumes that the stress at a point depends only on the local deformation of the material. However, nonlocal elasticity accepts that the stress at a point also depends on the deformation of neighboring points, which are weighted according to a nonlocal kernel function unlike classical elasticity [1,2,3]. The non-local approach is particularly useful for modeling materials with non-local effects, such as nanomaterials and biological tissues, where the interactions between particles are not limited to the immediate vicinity of a point, but can also be an effective approach for wave propagation, fracture behavior, and stability of structures. Nonlocal elasticity has been applied in a variety of fields, including materials mechanics, structural engineering, and biomechanics, although its formulation is more complex than classical elasticity and requires numerical techniques to solve governing equations.

There are many presented analytical solutions on the mechanical behavior of nanobeams such as bending, buckling, and vibration based on Euler-Bernoulli beam theory and Timoshenko beam theory, which in the framework of nonlocal constitutive relation proposed by Eringen. Reddy [4] presented an analytical solution of bending, buckling, and vibration of nanobeams using various beam theories including the Euler-Bernoulli, Timoshenko, Reddy, and Levinson beam theories based on the nonlocal elasticity. Thai [5] proposed a nonlocal shear deformation theory for bending, buckling, and vibration of nanobeams using the nonlocal differential constitutive

relations of Eringen. According to the theory, shear strains and consequently shear stresses vary quadratically through the thickness. The Euler-Bernoulli, Timoshenko, Reddy, Levinson, and Aydogdu beam theories are used as a special case by Aydogdu [6] on bending, buckling, and vibration of nanobeams. Ghannadpour et al. [7] investigated bending, buckling, and vibration based on nonlocal Euler-Bernoulli beam theory using Ritz method. Wang et al. [8] concerned with the bending problem of micro- and nanobeams based on the Eringen nonlocal elasticity theory and Timoshenko beam theory. Lu et al. [9] used nonlocal Euler-Bernoulli beam theory for vibration analysis of nanobeams.

Li et al. [10] considered the free vibration of nonlocal Euler and Timoshenko beams. It was provided a novel explanation for the stiffening phenomenon of nonlocal cantilever beams, clarified the effects of local and nonlocal boundary conditions on the free vibration, and revealed the effects of different constitutive relations for nonlocal Timoshenko beams. Wang et al. [11] concerned with the free vibration problem for micro/nanobeams modeled after Eringen's nonlocal elasticity theory and Timoshenko beam theory.

Thai and Vo [12] used a sinusoidal shear deformation beam theory which is capable of capturing both small-scale effect and transverse shear deformation effects of nanobeams, and does not require shear correction factors for the bending,

<sup>\*</sup> Tekirdağ Namık Kemal University, Faculty of Engineering, Department of Mechanical Engineering, 59860, Corlu-Tekirdağ, Türkiye  
E-mail address: buymaz@nku.edu.tr

buckling, and vibration of nanobeams. Eltaher et al. [13] used an efficient finite element model for dynamic characteristics analysis of a nonlocal Euler–Bernoulli nanobeam. Roque et al. [14] used the nonlocal elasticity theory of Eringen to study bending, buckling, and free vibration of Timoshenko nanobeams. A meshless method was presented to obtain numerical solutions.

Functionally graded materials (FGMs) are a class of engineered materials that are designed to have spatial variations in their composition and/or microstructure to achieve specific mechanical, thermal, electrical, or other properties. Unlike traditional materials, which have uniform properties throughout their volume, FGMs exhibit a gradual or abrupt transition in their properties along one or more directions [15]. The concept of FGM was first developed by Japanese researchers in the 1980s as materials capable of withstanding the extreme temperature changes were encountered in aerospace applications but has since found a wide range of applications in fields such as aerospace, energy, biomedical engineering, and materials science. While FGMs can be designed to exhibit a variety of property gradients, such as variations in composition, porosity, grain size, and fiber orientation, the composition gradient is the most common type of gradient. The composition gradient involves a gradual change in the type or concentration of one or more constituents of the material as in the example of a metal-ceramic FGM which has a gradient in the concentration of ceramic particles increasing from one end of the material to the other.

Although the design and fabrication of FGMs can be challenging and require advanced materials processing techniques, they have a wide range of potential application areas due to their several advantages over traditional homogeneous materials, such as improved fracture resistance, reduced stress concentration, and enhanced thermal shock resistance. FGM structures which can be designed and optimized for specific applications by tailoring their composition and properties have a wide range of applications such as aircraft and spacecraft components, missile components, armor plating, dental implants, prosthetics, bone grafts, fuel cells and batteries, heat sinks and heat exchangers, bridges, buildings, and other civil engineering structures.

There are many studies in the literature dealing with bending, buckling, and free vibration of functionally graded beams [16-29]. With this, bending, buckling, and free vibration are important mechanical behaviors that need to be analyzed in order to design and optimize functionally graded nanobeam structures for various nano applications. Eltaher et al. [30] presented a free vibration analysis of functionally graded size-dependent nanobeams using a finite element method based on nonlocal Euler-Bernoulli beam theory. Simsek and Yurtcu [31] investigated static bending under uniformly distributed load and buckling analysis of functionally graded nanobeams based on nonlocal Timoshenko beam theory that first-order shear deformation theory. Buckling results and vibration results of

functionally graded nanobeams based on Reddy theory were presented by Rahmani and Jandaghian [32] and Ebrahimi and Barati [33], respectively. Explicit analytical equations for the vibration of a bidirectional functionally graded nonlocal nanobeam are presented by Nazmul et al. [34].

However, it is seen that the effect of Poisson ratio was not taken into account in these studies on functionally graded nanobeams. However, the Poisson ratio is a measure of the deformation of a material in response to an applied force. It is defined as the ratio of the lateral strain to the longitudinal strain in a material when it is stretched or compressed. In other words, it is a measure of how much a material will shrink or expand perpendicular to the direction of an applied force. The value of Poisson's ratio is an important factor in determining the mechanical behavior of materials under stress, as it affects their elastic modulus, shear modulus, and other mechanical properties. It becomes even more important to consider the effect of Poisson ratio in functionally graded materials where mechanical properties such as elastic modulus, density, and Poisson ratio vary across thickness. The static bending, the buckling, and the free vibration of the functionally graded nanobeam with the effect of Poisson's ratio taken into account is the subject of this paper. In this study, the generalized shear deformation theory with the shape function corresponding to the Reddy theory is used based on the nonlocal elasticity theory. The material properties of the functionally graded nanobeam assumed to vary in the thickness direction. The Navier-type solution is used for simply-supported boundary conditions, and exact formulas are proposed for the maximum deflections, the critical buckling load, and the natural frequencies. The effects of the nonlocal parameter  $((e_0a)^2)$ , the material composition ( $p$  index), and the length-to-thickness ratio ( $L/h$ ) on the static, the stability and free vibration responses of the functionally graded nanobeam are discussed.

## 2. Theoretical formulations

### 2.1 Nonlocal elasticity theory

According to nonlocal elasticity theory, different from the classical elasticity theory, the stress field at a point  $x$  in an elastic continuum not only depends on the strain field at the same point but also on strains at all other points of the body. As a result of this, in classical elasticity theory, the behavior of a material is described purely in terms of its local properties, such as its stiffness and strength. However, in nonlocal elasticity theory, the behavior of a material is also affected by the material's microstructure, such as the size and shape of its particles. Nonlocal elasticity theory introduces a length scale parameter known as the nonlocal parameter, which is related to the material's microstructure. The presence of this length scale parameter causes the stress and strain in a material to be more distributed over a larger area, which leads to a reduction in the overall stiffness of the material. This effect is particularly pronounced in materials with a high surface area-to-volume ratio, such as nanomaterials. Therefore, nonlocal elasticity theory predicts that the material will be less stiff and less resistant to deformation than classical elasticity theory. In other

words, the material will exhibit a softer response to external loads.

The nonlocal stress tensor  $\sigma$  at point  $\mathbf{x}$  is defined as follows:

$$\sigma(\mathbf{x}) = \int_{\mathcal{V}} \alpha(|\mathbf{x}' - \mathbf{x}|, \tau) \mathbf{t}(\mathbf{x}') d\mathcal{V}(\mathbf{x}') \quad (1)$$

$$\mathbf{t}(\mathbf{x}) = \mathbf{C}(\mathbf{x}) : \boldsymbol{\varepsilon}(\mathbf{x}) \quad (2)$$

where  $\mathbf{t}(\mathbf{x}')$  is the classical, macroscopic stress tensor at point  $\mathbf{x}$ ,  $\alpha(|\mathbf{x}' - \mathbf{x}|, \tau)$  is the Kernel function and  $\tau$  is the material constant which depends on a constant appropriate to each material ( $e_0$ ), internal characteristic ( $a$ ) such as lattice parameter, granular distance and external characteristic length ( $l$ ) such as crack length, wavelength. With the reduced and simplified differential form of Eq. (1) and using Eq. (2) the relationship between classical, macroscopic stress tensor  $\mathbf{t}$  and nonlocal stress tensor  $\sigma$  is given by Laplacian operator  $\nabla$  as follows:

$$(1 - \tau^2 l^2 \nabla^2) \sigma = \mathbf{C}(\mathbf{x}) : \boldsymbol{\varepsilon}(\mathbf{x}) \quad \tau = \frac{e_0 a}{l} \quad (3)$$

It is seen that when the internal characteristic length  $a$  is zero, nonlocal elasticity corresponds to classical elasticity.

**2.2 Governing equations of functionally graded nanobeams**

The considered functionally graded nanobeam is a straight prismatic beam with length  $L$  along the  $x$ -axis and thickness  $h$  along the  $z$ -axis. The governing equations in terms of reduced stiffness coefficients, including Poisson's ratio effects, are as follows:

$$(1 - (e_0 a)^2 \frac{d^2}{dx^2}) \sigma_x = Q_{11} \varepsilon_x$$

$$(1 - (e_0 a)^2 \frac{d^2}{dx^2}) \tau_{xz} = Q_{55} \gamma_{xz} \quad (4)$$

Where  $Q_{ij}$  are the reduced stiffness coefficients defined according to FGMs as follows:

$$Q_{11} = \frac{E(z)}{1 - \nu(z)^2}, \quad Q_{55} = \frac{E(z)}{2(1 + \nu(z))} \quad (5)$$

The displacement model of the beam defined according to the generalized shear deformation theory, as the axial displacement defined at any point,  $w_1$  and the vertical displacement  $w_3$  are as follows:

$$w_1 = u(x; t) - z \frac{\partial w}{\partial x} + f(z) u_1(x; t)$$

$$w_2 = 0$$

$$w_3 = w(x; t) \quad (6)$$

where  $u$  and  $w$  are the displacement components of a point on the mid-plane of the beam along the  $x$ - and  $z$ - axis, respectively. And  $f(z)$  is the transverse shear shape function which determines the distribution of the transverse shear strains and stresses throughout the beam thickness. Frequently used shape functions and derivatives along with their corresponding theories are given in Table 1 and illustrated in Fig.1.

**Table 1.** The mostly used transverse shape functions and derivatives along with their corresponding theories.

Shape function	Derivative of shape function	Corresponding theory
$f(z) = 0$	$\frac{df}{dz} = 0$	Euler-Bernoulli beam theory (EBT)
$f(z) = z$	$\frac{df}{dz} = 1$	Timoshenko beam theory (TBT)
$f(z) = z \left( 1 - \frac{4z^2}{3h^2} \right)$	$\frac{df}{dz} = 1 - \frac{4z^2}{h^2}$	Reddy beam theory (RBT)
$f(z) = z 3 \frac{-2(z/h)^2}{\ln 3}$	$\frac{df}{dz} = 3 \frac{-2(z/h)^2}{\ln 3} \left( 1 - \frac{4z^2}{h^2} \right)$	Aydogdu beam theory (ABT)

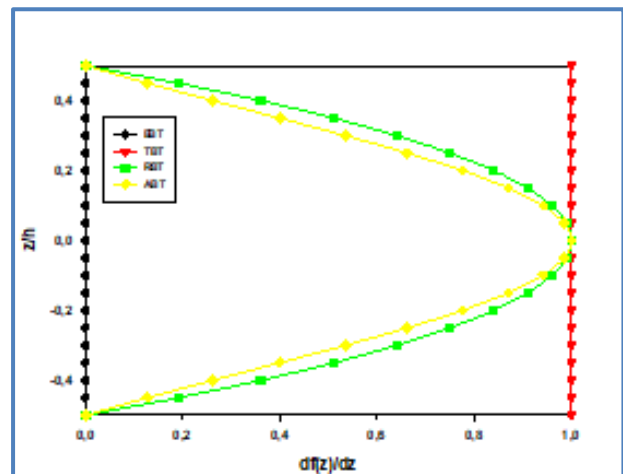
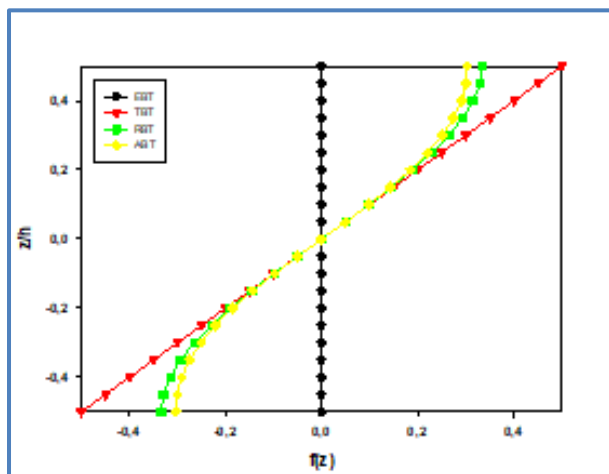


**Fig 1.** Variation of the frequently used (a) transverse shape functions and (b) derivatives along with their corresponding theories throughout the thickness coordinate.

The strain components in terms of the displacement components are as follows:

$$\begin{aligned} \epsilon_x &= \frac{\partial u}{\partial x} - z \frac{\partial^2 w}{\partial x^2} + f(z) \frac{\partial u_1}{\partial x} \\ \gamma_{xz} &= \frac{df}{dz} u_1 \end{aligned} \quad (7)$$

The internal force and moment resultants are as follows:

$$\begin{aligned} (N_x^c, M_x^c) &= \int_{-h/2}^{h/2} \sigma_x(1, z) dz \\ M_x^{sd} &= \int_{-h/2}^{h/2} \sigma_x f(z) dz \\ Q_x^{sd} &= \int_{-h/2}^{h/2} \tau_{xz} \left( \frac{df}{dz} \right) dz \end{aligned} \quad (8)$$

The constitutive relations are as follows:

$$\begin{aligned} \begin{Bmatrix} N_x^c \\ M_x^c \\ M_x^{sd} \end{Bmatrix} &= \begin{bmatrix} A_{11} & B_{11} & E_{11} \\ B_{11} & D_{11} & F_{11} \\ E_{11} & F_{11} & H_{11} \end{bmatrix} \begin{Bmatrix} u_{,x} \\ -w_{,xx} \\ u_{1,x} \end{Bmatrix} \\ \{Q_x^{sd}\} &= [A_{55}] \{u_1\} \end{aligned} \quad (9)$$

The extensional, coupling, bending, and transverse shear rigidities are as follows:

$$\begin{aligned} (A_{11}, B_{11}, D_{11}) &= \int_{-h/2}^{h/2} Q_{11}(1, z, z^2) dz \\ (E_{11}, F_{11}, H_{11}) &= \int_{-h/2}^{h/2} Q_{11}f(z)(1, z, f(z)) dz \\ A_{55} &= \int_{-h/2}^{h/2} Q_{55} \left( \frac{df}{dz} \right)^2 dz \end{aligned} \quad (10)$$

The governing equations of nanobeam obtained using principle of virtual work are as follows:

$$\begin{aligned} \frac{\partial N_x^c}{\partial x} &= (1 - (e_0 a)^2 \frac{\partial^2}{\partial x^2}) \left( \rho_0 \frac{\partial^2 u}{\partial t^2} - \rho_1 \frac{\partial^3 w}{\partial x \partial t^2} + \rho_{01} \frac{\partial^2 u_1}{\partial t^2} \right) \\ \frac{\partial^2 M_x^c}{\partial x^2} &= (1 - (e_0 a)^2 \frac{\partial^2}{\partial x^2}) \left( \rho_0 \frac{\partial^2 w}{\partial t^2} + \rho_1 \frac{\partial^3 u}{\partial x \partial t^2} - \right. \\ &\quad \left. \rho_2 \frac{\partial^4 w}{\partial x^2 \partial t^2} + \rho_{11} \frac{\partial^3 u_1}{\partial x \partial t^2} - N_x^e \frac{\partial^2 w}{\partial x^2} - q(x; t) \right) \\ \frac{\partial M_x^{sd}}{\partial x} - Q_x^{sd} &= (1 - (e_0 a)^2 \frac{\partial^2}{\partial x^2}) \left( \rho_{01} \frac{\partial^2 u}{\partial t^2} - \rho_{11} \frac{\partial^3 w}{\partial x \partial t^2} + \right. \\ &\quad \left. \rho_{02} \frac{\partial^2 u_1}{\partial t^2} \right) \end{aligned} \quad (11)$$

Where inertia terms are as follows:

$$\begin{aligned} \rho_i &= \int_{-h/2}^{h/2} \rho(z) z^i dz \quad (i=0,1,2) \\ \rho_{jm} &= \int_{-h/2}^{h/2} \rho(z) z^j f_j^m dz \quad (j=0,1 ; m=1,2) \end{aligned} \quad (12)$$

Where  $\rho$  is the mass per unit volume.

### 2.3. Functionally graded materials

The considered structural element is a straight prismatic functionally graded nanobeam having length  $L$  along the  $x$ -axis and thickness  $h$  along the  $z$ -axis. Effective material properties elasticity modulus ( $E$ ), Poisson ratio ( $\nu$ ) and mass density ( $\rho$ ) are varying in the thickness direction according to a simple power law distribution defined as follows:

$$\begin{aligned} P_{eff} &= V_U P_U + V_L P_L \\ V_U + V_L &= 1 \\ V_U &= \left( \frac{z}{h} + \frac{1}{2} \right)^{p_z} \\ P_{eff} &= \left( \frac{z}{h} + \frac{1}{2} \right)^{p_z} P_U + \left( 1 - \left( \frac{z}{h} + \frac{1}{2} \right)^{p_z} \right) P_L \end{aligned} \quad (13)$$

where  $P_{eff}$  corresponding to the effective material property, the subscript  $U$  and  $L$  corresponding to the material property of the upper and lower surface, respectively. In this study upper surface material ceramic rich and lower surface material metal rich are preferred. Variation of the volume fraction  $V_U$  through the thickness direction of the functionally graded nanobeam is given in Fig.2 where  $V_U$  is the volume fraction of the ceramic; and  $p_z$  is the volume fraction exponent,  $0 \leq p_z < \infty$ . Different value of the volume fraction of  $V_U$  corresponds to different distribution of material composition on functionally graded nanobeam: e.g. if that value is 0, material of the nanobeam is ceramic; if that value is 1, the variation of the volume fraction of the ceramic is linear from lower surface to upper surface. If the ceramic volume ratio is different from 0 and 1, variation of the material composition is nonlinear.

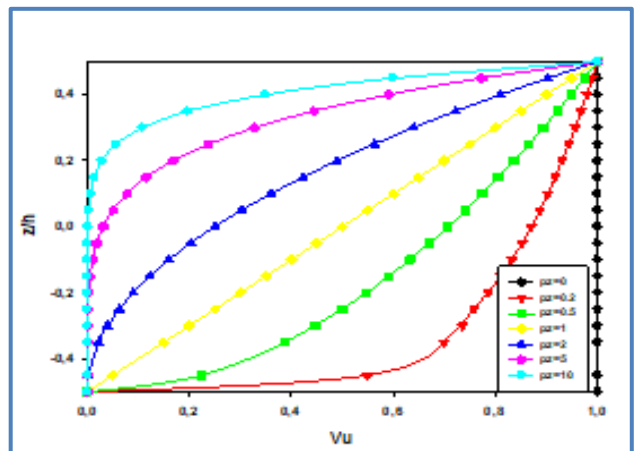


Fig.2. Variation of the volume fraction  $V_U$  (ceramic component) through the thickness direction of the functionally graded nanobeam.



**2.4 Analytical solution for bending, buckling, and free vibration of simply supported functionally graded nanobeam**

In this study Navier method is applied for static bending, buckling, and free vibration problem of functionally graded nanobeam. The sets of boundary conditions of the beam at  $x=0$ ,  $L$  are as follows:

either  $u$  or  $N_x^c = \bar{N}_x$   
 either  $w$  or  $M_{x,x}^c = \bar{Q}_x$   
 either  $w_x$  or  $M_x^c = \bar{M}_x$   
 either  $u_1$  or  $M_x^a = \bar{M}_x^a$  (14)

where  $\bar{N}_x$ ,  $\bar{Q}_x$ ,  $\bar{M}_x$ ,  $\bar{M}_x^a$  are corresponding to prescribed force and moment resultants acting on the beam boundaries.

The simply supported boundary conditions of nanobeam are as follows:

$N_x^c = w = M_x^c = M_x^a = 0$  (15)

The nanobeam equations given by Eq.(11) are organized as the external force ( $N_x^e$ ) term, and time dependent terms are zero on bending problem. Similarly the equations are organized as the time dependent terms and transverse load ( $q(x;t)$ ) term are zero on buckling problem. Similarly the equations are organized as the external force ( $N_x^e$ ) term and transverse load ( $q(x;t)$ ) term are zero on free vibration problem.

The kinematic components that provide the simply supported boundary condition in the bending and buckling analysis of the nanobeam examined are as follows:

$u(x) = A_m \cos \frac{m\pi x}{L}$   
 $w(x) = C_m \sin \frac{m\pi x}{L}$   
 $Lu_1(x) = D_m \cos \frac{m\pi x}{L}$  (16)

where  $u$  and  $w$  are the displacement components of a point in the midplane in the  $x$  and  $z$  directions; and  $u_1$  is the displacement components showing effects of vertical shear strains in the midplane. For bending analysis, the transverse load that provides the simply supported boundary condition is defined in the Fourier series form as follows:

$q(x) = \sum_{m=1}^M Q_m \sin \frac{m\pi x}{L}$   
 $Q_m = \frac{2}{L} \int_0^L q(x) \sin \frac{m\pi x}{L} dx$  (17)

Considered two types of loading that one of uniformly distributed load and one of point load condition in bending analysis are defined as follows:

Uniformly distributed load;

$q(x) = q_0, Q_m = \frac{4q_0}{m\pi} (-1)^{m-1}, (m = 1,3,5, \dots),$   
 $Q_m = 0 (m = 2,4,6, \dots)$  (18)

Point load applied to point  $x_0$  from  $x=0$  to  $L$ :

$q(x) = q_0, Q_m = \frac{2q_0}{L} \sin \frac{m\pi x_0}{L}, (m = 1,2,3, \dots)$  (19)

Firstly by substituting of the expansions Eq.(16) and Eq.(17) into Eq.(11) and then by applying non-dimensionalization procedure, max deflection is obtained.

For buckling analysis, the external in-plane uniaxial compression load is defined as follows:

$N_x^e = -N_0$  (20)

Firstly by substituting of the Eq.(16) and Eq.(20) into Eq.(11) and then by applying non-dimensionalization procedure critical buckling load is obtained.

The kinematic components that provide the simply supported boundary condition in the free vibration analysis of the nanobeam examined in the  $xz$ -plane are as follows:

$u(x) = A_m \cos \frac{m\pi x}{L} \sin \omega t$   
 $w(x) = C_m \sin \frac{m\pi x}{L} \sin \omega t$   
 $Lu_1(x) = D_m \cos \frac{m\pi x}{L} \sin \omega t$  (21)

Firstly by substituting of the Eq.(21) into Eq.(11) and then by applying non-dimensionalization procedure an eigenvalue problem in matrix form is obtained as follows:

$[K_{ij} - \Omega^2 M_{ij}] \begin{Bmatrix} A_m \\ C_m \\ D_m \end{Bmatrix} = \{0\}$  (22)

where  $\Omega$  is the frequency parameter corresponding to  $\rho_c \omega^2$  and  $\rho_c$  represent mass density of ceramic component of the functionally graded material. The solution of the eigenvalue problem given by Eq.(22) gives the natural frequencies of the nanobeam.

**3. Numerical results**

The static bending, axial buckling, and free vibration analyses are carried out for functionally graded nanobeams whose material properties vary through the thickness direction according to a simple power rule. The solutions are obtained by the Navier method and hence for the simply supported boundary condition. The material properties considered in this study are given in Table 2.

Non-dimensionalization terms are used in the study as follows:

Uniformly distributed load;

$$\bar{w} = \frac{100E_c D_0}{q_0 L^4} w \quad \left( D_0 = \frac{E_c h^3}{12(1-\nu_c^2)} \right) \quad (23)$$

**Table 2.** Mechanical properties of component materials of functionally graded material which are considered in the study.

Component Material	Elasticity Modulus (GPa)	Poisson Ratio	Mass Density (kg/m <sup>3</sup> )
SUS304 (Metal)	201.04	0.3262	8166
Si <sub>3</sub> N <sub>4</sub> (Ceramic)	348.43	0.2400	2370

Point load applied to point x0 from x=0 to L:

$$\bar{w} = \frac{D_0}{q_0 L^3} w \quad (24)$$

Critical buckling load:

$$\bar{N} = \frac{N_0 L^2}{D_0} \quad (25)$$

Natural frequency parameter:

$$\Delta = \omega L^2 \sqrt{\frac{\rho_c}{D_0}} \quad (26)$$

The thickness (h) of functionally graded nanobeam is 1 nm. Effects of the nonlocal parameter ((e<sub>0a</sub>)<sup>2</sup>), different material composition (p<sub>z</sub>) and the beam geometry (length-to-thickness) on the bending, buckling, and vibration are investigated.

The comparison results for bending, buckling, and vibration are given in Table 3-7. The results obtained in this study are quite self-consistent among themselves. In addition, although a good agreement is observed in the comparison results, it is also seen that there are some differences between them. Although both of the generalized shear deformation theory and the Reddy theory are higher-order beam theories that take into account the effect of transverse shear deformation, which is neglected in classical beam theories. In this study, in-plane displacement components are also taken into account, leading to some differences between the results. However, the effect of Poisson's ratio on the mechanical behavior of beams is particularly significant in cases where the beam is subjected to out-of-plane deformation such as bending. In such cases, the beam experiences both tensile and compressive stresses along its length, as well as shear stresses across its cross-section. Poisson's ratio plays a crucial role in determining the deformation of the beam under these complex loading conditions. As it is seen in comparison results, considering the Poisson ratio in case of axial stress also affects the results. Because when the effect of Poisson's ratio is taken into account, the material exhibits a more rigid behavior. As a result, in the

results obtained by considering the Poisson ratio, the bending deformation takes smaller values, while the critical buckling load and natural frequencies take larger values.

**Table 3.** Comparison of non-dimensional maximum center deflection of nanobeam under uniformly distributed load, (ν=0.3,  $\bar{w} = \frac{100EI}{q_0 L^4} w$ , q<sub>0</sub>=1 ).

(e <sub>0a</sub> ) <sup>2</sup>	L/h=10			L/h=100		
	Ref. [5]	Present (without ν)	Present (with ν)	Ref. [5]	Present (without ν)	Present (with ν)
0	1.3346	1.3059	1.1913	1.3024	1.2735	1.1589
1	1.4622	1.4347	1.3088	1.4274	1.3992	1.2733
2	1.5898	1.5636	1.4264	1.5525	1.5249	1.3877
3	1.7174	1.6925	1.5440	1.6775	1.6506	1.5021
4	1.8450	1.8214	1.6616	1.8025	1.7763	1.6165

**Table 4.** Comparison of non-dimensional maximum center deflection of nanobeam under point load at center, (ν=0.3,  $\bar{w} = \frac{100EI}{q_0 L^3} w$ , q<sub>0</sub>=1).

(e <sub>0a</sub> ) <sup>2</sup>	L/h=10			L/h=100		
	Ref. [4]	Present (without ν)	Present (with ν)	Ref. [4]	Present (without ν)	Present (with ν)
0	1.9878	2.0513	1.8713	1.9449	2.0005	1.8205
1	2.1564	2.2537	2.0560	2.1115	2.1979	2.0002
2	2.3250	2.4562	2.2406	2.2782	2.3954	2.1798
3	2.4936	2.6586	2.4253	2.4448	2.5928	2.3595
4	2.6623	2.8611	2.6100	2.6115	2.7903	2.5392

**Table 5.** Comparison of non-dimensional critical buckling load under uniaxial compression load, (ν=0.3,  $\bar{N} = \frac{N_0 L^2}{EI}$  ).

(e <sub>0a</sub> ) <sup>2</sup>	L/h=10			L/h=100		
	Ref. [4]	Present (without ν)	Present (with ν)	Ref. [4]	Present (without ν)	Present (with ν)
0	9.6228	9.6226	10.5483	9.8671	9.8670	10.8425
1	8.7583	8.7582	9.6007	8.9807	8.9806	9.8686
2	8.0364	8.0363	8.8093	8.2405	8.2404	9.0551
3	7.4245	7.4244	8.1385	7.6130	7.6129	8.3656
4	6.8991	6.8990	7.5626	7.0743	7.0742	7.7736

**Table 6.** Comparison of non-dimensional fundamental frequencies, (ν=0.3,  $\Delta = \omega L^2 \sqrt{\frac{\rho}{EI}}$ ).

(e <sub>0a</sub> ) <sup>2</sup>	L/h=10			L/h=100		
	Ref. [5]	Present (without ν)	Present (with ν)	Ref. [5]	Present (without ν)	Present (with ν)
0	9.7075	9.7071	10.1634	9.8679	9.8679	10.3442
1	9.2612	9.2608	9.6961	9.4143	9.4142	9.8687
2	8.8714	8.8709	9.2879	9.0180	9.0179	9.4532
3	8.5269	8.5265	8.9273	8.6678	8.6677	9.0861
4	8.2197	8.2193	8.6057	8.3555	8.3554	8.7588

**Table 7.** Comparison of first three non-dimensional fundamental frequencies, ( $L/h=5, \nu=0.3, \Delta = \omega L^2 \sqrt{\frac{\rho}{EI}}$ ).

Modes	$(e_0a)^2$	Ref. [5]	Present (without $\nu$ )	Present (with $\nu$ )
1	0	9.2745	9.2690	9.6740
	1	8.8482	8.8429	9.2293
	2	8.4757	8.4706	8.8407
	3	8.1466	8.1417	8.4975
	4	7.8530	7.8484	8.1913
2	0	32.1847	31.9441	33.0538
	1	27.2519	27.0481	27.9878
	2	24.0589	23.8790	24.7086
	3	21.7765	21.6137	22.3646
	4	20.0407	19.8908	20.5818
3	0	61.5746	59.8105	61.3641
	1	44.8095	43.5257	44.6563
	2	36.9531	35.8943	36.8267
	3	32.1645	31.2430	32.0545
	4	28.8569	28.0301	28.7582

Table 8 and Table 9 show that the results of bending analysis of functionally graded nanobeam under uniformly

distributed load and point load respectively. In all considered conditions in terms of material composition or geometry, maximum deflection increased with increasing nonlocal parameter value. This result confirms the nonlocal elasticity behavior of the considered material. The volume ratio exponent  $p_z$  determines the rate of change of the ceramic volume fraction from the lower surface to the upper surface; and as the  $p_z$  value increases, the ceramic volume ratio decreases, and the metal volume ratio increases. As a result, it can be said that the maximum deflection increases with increasing  $p_z$  value and therefore with increasing metal volume ratio. From the geometric point of view, the maximum deflection value decreases with the increase of  $L/h$  value; that is, the decrease in nanobeam thickness, in both loading conditions. However, in terms of all parameters examined, the beam with at least  $L/h=50$  ratio is affected by all variation amounts.

According to the buckling results given in Table 10, the critical buckling load decreases as the  $p_z$  value and the nonlocal parameter value increase, so the material becomes softer. And, as the value of  $L/h$  increases, it increases; that is, the strength of the material against buckling increases.

The free vibration results for first three natural frequencies are presented in Table 11-Table 13. The natural frequencies decrease as the  $p_z$  value and the nonlocal parameter value increase, but increase as the  $L/h$  value increases, similar to the buckling results. However, unlike the buckling results, vibration frequencies are less affected by the change of parameters. It can be thought that the reason for this is not an applied external force.

**Table 8.** Non-dimensional maximum center deflection under uniformly distributed load.

L/h	$(e_0a)^2$	Volume fraction exponent $p_z$						
		0	0.2	0.5	1	2	5	10
10	0	1.3063	1.4217	1.5418	1.6552	1.7496	1.8455	1.9260
	1	1.4352	1.5620	1.6940	1.8186	1.9223	2.0276	2.1160
	2	1.5641	1.7023	1.8461	1.9820	2.0949	2.2098	2.3061
	3	1.6930	1.8427	1.9983	2.1453	2.2676	2.3919	2.4962
	4	1.8220	1.9830	2.1505	2.3087	2.4403	2.5741	2.6863
20	0	1.2815	1.3949	1.5126	1.6227	1.7126	1.8031	1.8816
	1	1.4079	1.5326	1.6619	1.7829	1.8816	1.9810	2.0673
	2	1.5344	1.6703	1.8111	1.9431	2.0507	2.1590	2.2530
	3	1.6609	1.8080	1.9604	2.1032	2.2197	2.3370	2.4387
	4	1.7874	1.9457	2.1097	2.2634	2.3887	2.5149	2.6244
50	0	1.2745	1.3875	1.5044	1.6136	1.7023	1.7912	1.8691
	1	1.4003	1.5244	1.6529	1.7729	1.8703	1.9680	2.0536
	2	1.5261	1.6613	1.8013	1.9322	2.0383	2.1448	2.2381
	3	1.6519	1.7983	1.9498	2.0914	2.2063	2.3216	2.4226
	4	1.7777	1.9352	2.0983	2.2507	2.3743	2.4983	2.6070

**Table 9.** Non-dimensional maximum deflection under point load at center.

L/h	$(e_0a)^2$	Volume fraction exponent $p_z$						
		0	0.2	0.5	1	2	5	10
10	0	2.0519	2.2332	2.4219	2.6001	2.7482	2.8989	3.0253
	1	2.2544	2.4536	2.6609	2.8567	3.0195	3.1850	3.3239
	2	2.4569	2.6740	2.8999	3.1133	3.2907	3.4712	3.6225
	3	2.6594	2.8945	3.1390	3.3699	3.5620	3.7573	3.9211
	4	2.8620	3.1149	3.3780	3.6265	3.8332	4.0434	4.2197
20	0	2.0129	2.1912	2.3760	2.5490	2.6902	2.8323	2.9556
	1	2.2116	2.4075	2.6105	2.8006	2.9557	3.1118	3.2473
	2	2.4103	2.6237	2.8450	3.0522	3.2212	3.3914	3.5390
	3	2.6090	2.8400	3.0795	3.3038	3.4867	3.6709	3.8307
	4	2.8076	3.0563	3.3140	3.5553	3.7523	3.9505	4.1224
50	0	2.0020	2.1794	2.3631	2.5347	2.6739	2.8136	2.9360
	1	2.1996	2.3945	2.5963	2.7849	2.9378	3.0913	3.2258
	2	2.3972	2.6096	2.8296	3.0351	3.2018	3.3690	3.5156
	3	2.5948	2.8247	3.0628	3.2852	3.4657	3.6467	3.8054
	4	2.7924	3.0399	3.2960	3.5354	3.7296	3.9244	4.0952

**Table 10.** Non-dimensional critical buckling load under uniaxial compression load.

L/h	$(e_0a)^2$	Volume fraction exponent $p_z$						
		0	0.2	0.5	1	2	5	10
10	0	9.6197	8.8387	8.1502	7.5916	7.1823	6.8090	6.5245
	1	8.7556	8.0447	7.4180	6.9097	6.5371	6.1973	5.9384
	2	8.0339	7.3816	6.8066	6.3401	5.9983	5.6865	5.4489
	3	7.4221	6.8195	6.2883	5.8573	5.5415	5.2535	5.0340
	4	6.8969	6.3369	5.8433	5.4429	5.1494	4.8817	4.6778
20	0	9.8058	9.0081	8.3076	7.7436	7.3373	6.9692	6.6785
	1	8.9250	8.1989	7.5614	7.0480	6.6782	6.3431	6.0785
	2	98.1893	7.5231	6.9381	6.4671	6.1277	5.8203	5.5775
	3	7.5657	6.9502	6.4098	5.9746	5.6611	5.3771	5.1528
	4	7.0303	6.4584	5.9562	5.5518	5.2605	4.9966	4.7872
50	0	9.8593	9.0568	8.3528	7.7873	7.3819	7.0154	6.7229
	1	8.9736	8.2432	7.6025	7.0878	6.7188	6.3852	6.1190
	2	8.2339	7.5638	6.9758	6.5036	6.1650	5.8589	5.6146
	3	7.6069	6.9878	6.4446	6.0083	5.6955	5.4127	5.1871
	4	7.0686	6.4933	5.9886	5.5832	5.2925	5.0297	4.8200

**Table 11.** Non-dimensional fundamental natural frequency parameter.

L/h	$(e_0 a)^2$	Volume fraction exponent $p_z$						
		0	0.2	0.5	1	2	5	10
10	0	9.7056	7.8369	6.6273	5.7806	5.1701	4.6857	4.4533
	1	9.2594	7.4766	6.3227	5.5149	4.9324	4.4703	4.2486
	2	8.8696	7.1618	6.0565	5.2827	4.7247	4.2821	4.0697
	3	8.5252	6.8837	5.8213	5.0776	4.5413	4.1158	3.9117
	4	8.2181	6.6357	5.6116	4.8947	4.3777	3.9675	3.7707
20	0	9.8277	7.9370	6.7131	5.8571	5.2414	4.7536	4.5178
	1	9.3759	7.5721	6.4045	5.5878	5.0004	4.5351	4.3101
	2	8.9811	7.2533	6.1348	5.3526	4.7899	4.3442	4.1286
	3	8.6324	6.9717	5.8966	5.1448	4.6039	4.1755	3.9683
	4	8.3214	6.7205	5.6842	4.9594	4.4380	4.0250	3.8253
50	0	9.8628	7.9658	6.7378	5.8791	5.2620	4.7732	4.5364
	1	9.4094	7.5996	6.4280	5.6089	5.0201	4.5538	4.3279
	2	9.0133	7.2797	6.1574	5.3727	4.8087	4.3621	4.1457
	3	8.6633	6.9970	5.9183	5.1641	4.6220	4.1927	3.9847
	4	8.3511	6.7449	5.7051	4.9781	4.4555	4.0416	3.8411

**Table 12.** Non-dimensional second natural frequency parameter.

L/h	$(e_0 a)^2$	Volume fraction exponent $p_z$						
		0	0.2	0.5	1	2	5	10
10	0	37.0562	29.9004	25.2717	22.0217	19.6578	17.7734	16.8925
	1	31.3767	25.3177	21.3984	18.6465	16.6449	15.0493	14.3034
	2	27.7004	22.3513	18.8912	16.4618	14.6947	13.2861	12.6276
	3	25.0726	20.2309	17.0991	14.9001	13.3007	12.0257	11.4296
	4	23.0740	18.6183	15.7361	13.7124	12.2405	11.0671	10.5186
20	0	38.8226	31.3476	26.5095	23.1227	20.6804	18.7430	17.8133
	1	32.8724	26.5431	22.4464	19.5788	17.5108	15.8703	15.0831
	2	29.0208	23.4331	19.8165	17.2848	15.4591	14.0108	13.3159
	3	26.2677	21.2101	17.9366	15.6451	13.9926	12.6817	12.0526
	4	24.1739	19.5194	16.5068	14.3980	12.8772	11.6708	11.0919
50	0	39.3708	31.7973	26.8946	23.4662	21.0008	19.0481	18.1030
	1	33.3365	26.9238	22.7726	19.8696	17.7821	16.1286	15.3284
	2	29.4307	23.7692	20.1044	17.5416	15.6986	14.2389	13.5325
	3	26.6387	21.5143	18.1972	15.8775	14.2094	12.8881	12.2487
	4	24.5153	19.7994	16.7466	14.6119	13.0767	11.8608	11.2723

**Table 13.** Non-dimensional third natural frequency parameter.

L/h	$(e_0a)^2$	Volume fraction exponent $p_z$						
		0	0.2	0.5	1	2	5	10
10	0	77.8803	62.7809	53.0270	46.1532	41.0983	37.0424	35.2069
	1	56.6756	45.6874	38.5891	33.5869	29.9083	29.9567	25.6210
	2	46.7387	37.6770	31.8233	27.6981	24.6645	22.2304	21.1289
	3	40.6820	32.7946	27.6995	24.1088	21.4683	19.3497	18.3909
	4	36.4986	29.4222	24.8510	21.6297	19.2607	17.3599	16.4997
20	0	85.6191	69.1127	58.4315	50.9444	45.5245	41.2156	39.1720
	1	62.3073	50.2952	42.5222	37.0736	33.1294	29.9937	28.5065
	2	51.3830	41.4769	35.0668	30.5735	27.3208	24.7349	23.5085
	3	44.7245	36.1021	30.5226	26.6116	23.7804	21.5296	20.4621
	4	40.1253	32.3896	27.3839	23.8750	21.3350	19.3157	18.3579
50	0	88.2852	71.2985	60.3027	52.6114	47.0768	42.6913	40.5734
	1	64.2475	51.8858	43.8839	38.2868	34.2590	31.0676	29.5263
	2	52.9830	42.7887	36.1897	31.5739	28.2524	25.6205	24.3495
	3	46.1172	37.2439	31.5001	27.4824	24.5913	22.3005	21.1942
	4	41.3748	33.4140	28.2608	24.6563	22.0625	20.0073	19.0147

#### 4. Conclusion

The aim of the study is to show that the nonlocal theory of elasticity is an effective tool for predicting the mechanical behavior of functionally graded nanobeams. The incorporation of nonlocal effects into models of bending, buckling, and vibration can provide valuable insights into the behavior of these structures and can aid in the design of advanced nanomaterials and devices. The material properties of functionally graded nanobeam were considered varying according to simple power law along the thickness direction. Effect of the nonlocal parameter  $((e_0a)^2)$ , variation of volume fraction exponent ( $p_z$ ), and the geometrical parameters of nanobeam (length -to-thickness) on the bending under two types of loading conditions, buckling under uniaxial compression loading condition and free vibration were researched. The results show that this study is worthy of conduct, and especially in cases where the L/h value is below 50, the nonlocal parameter and the material volume fraction affect all the results more.

**Authors Contribution:** Conceive – B.U.; Design - B.U.; Supervision – B.U.; Experimental Performance, Data Collection and/or Processing – B.U.; Analysis and/or Interpretation – B.U.; Literature Review – B.U.; Writer - B.U.; Critical Reviews – B.U.

**Conflicts Of Interest:** The authors have declared no conflicts of interest.

#### Orcid-ID

Bahar UYMAZ  <https://orcid.org/0000-0002-0036-0730>

#### Reference

- [1] Talizina N.F. Managing the process of learning. Moscow State University Publishing House. – 1975, 342 c.
- [2] Leontyev L.P., Gohman O.G. Problems of management of educational processes: Mathematical models. - Riga, 1984. – 239 c.
- [3] R. S. Sutton and A. G. Barto, Reinforcement Learning: An Introduction, MIT Press, Cambridge, MA, USA, 1998.
- [4] Mayer R.B. Cybernetic pedagogy: Simulation of the learning process. - Eyes: GGPI, 2013. – 138 c.
- [5] Pontryagin, L.S.; Boltyanskii, V.G.; Gamkrelidze, R.V.; Mishchenko, E.F. Pontryagin Selected Works: The Mathematical Theory of Optimal Process; Gordon and Breach Science Publishers: NY, USA, 1985; Volume 4, p. 360.
- [6] Pivneva S. V. Modeling of discrete optimization problems / S. V. Pivneva, M. A. Trifonov // Vector of Science. - No. 3 (13), 2010. - pp. 31-34. (in Russian)
- [7] Porter B., Grossley R. Modal Control. Theory and Applications. London: Taylor and Francis, 1972.
- [8] Volgin L.N. Optimal discrete control of dynamical systems. M. Science, 1986, 240p (in Russian)
- [9] Dumachev VN Fundamentals of control theory. 2015, 383p (in Russian)
- [10] Vasiliev E.M., Gusev K.Yu. Modal control of non-stationary systems // Bulletin of the Voronezh State Technical University. 2008. V. 4. No. 8. pp. 46-54. (in Russian)
- [11] Makkapati, V.R.; Dor, M.; Tsiotras, P. Trajectory desensitization in optimal control problems. In Proceedings of

the IEEE Conference on Decision and Control, Miami, FL, USA, 17–19 December 2018; pp. 2478–2483.



License: This article is available under a Creative Commons License (Attribution 4.0 International, as described at <https://creativecommons.org/licenses/by/4.0/> )



T.C.  
TEKİRDAĞ NAMIK KEMAL ÜNİVERSİTESİ REKTÖRLÜĞÜ  
Fen Bilimleri Enstitüsü Müdürlüğü

Sayı : E-96396750-824.02.03-304310  
Konu : Fen Bilimleri Enstitüsü JBST -2023 Nisan  
Sayısı

26.05.2023

GENEL SEKRETERLİĞE  
(Basın ve Halkla İlişkiler Birimi)

Enstitümüz tarafından 2023 yılı nisan ayı itibariyle 2. Cilt 1. Sayısı yayımlanan Journal of Balkan Science and Technology (The Journal of Tekirdağ Namık Kemal University Institute of Natural & Applied Sciences), çok disiplinli uluslararası hakemli dergi niteliğinde bir dergi olup, Part A: Natural Sciences, Part B:Engineering Sciences, Part C: Agricultural and Food Sciences ve Part D: Architectural Sciences olmak üzere dört kısımdan oluşmaktadır ve yazım dili İngilizce'dir. JBST doğa bilimleri, mühendislik bilimleri, ziraat ve gıda bilimleri, mimarlık bilimleri alanlarında ulusal ve uluslararası düzeyde akademik bilgi birikimine katkı sağlayacak makaleleri kabul etmektedir. Açık kaynak yayın politikasını benimseyen JBST ilk sayıdan itibaren hakemlik sürecini yürütmekte olup <http://jbst.nku.edu.tr> adresi üzerinden hizmet vermektedir. Nisan, Ağustos ve Aralık ayları olmak üzere yılda 3 (üç) kez yayımlanacak olan JBST, Editörler Kurulu ve Yayın Kurulu kararıyla "özel sayı" olarak da yayımlanabilecektir. JBST dergisinde makale gönderme, değerlendirme ve yayımlanma aşamalarında ücret talep edilmemekte olup, yazarlara telif ücreti de ödenmemektedir. Derginin 2023 Ağustos sayısı için makale kabulü devam etmektedir. Akademisyenler dergiyi <http://jbst.nku.edu.tr> adresinden inceleyebilir ve yayımlanmasını istedikleri makalelerini <http://jbst.nku.edu.tr/JournalofBalkanScienceandTechnology/0/s/17710/23847> linki üzerinden gönderebilir ve soruları için [rifatbircan.jbst@nku.edu.tr](mailto:rifatbircan.jbst@nku.edu.tr) mail adresi üzerinden Baş Editör Prof. Dr. Rıfat BİRCAN'a [editorialoffice.jbst@nku.edu.tr](mailto:editorialoffice.jbst@nku.edu.tr) mail adresi üzerinden editör ofisine ulaşabilmektedirler.

Enstitümüz Journal of Balkan Science and Technology (The Journal of Tekirdağ Namık Kemal University Institute of Natural & Applied Sciences) dergisinin 2. Cilt 1. Sayısı ekte sunulmuştur.

Söz konusu makale çağrımızın tüm üniversitelerdeki akademik personele duyurulmasının sağlanması hususunda gereğini bilgilerinize arz ederim.

Doç. Dr. Bahar UYMAZ  
Müdür V.

Ek: 2. Cilt 1. Sayı (54 sayfa)

Bu belge, güvenli elektronik imza ile imzalanmıştır.

Doğrulama Kodu :BS4L07P5TT Pin Kodu :60082

Belge Takip Adresi : <https://turkiye.gov.tr/ebd?eK=5767&eD=BS4L07P5TT&eS=304310>

Adres:Namık Kemal Mah. Kampüs Cad. Süleymanpaşa / TEKİRDAĞ

Telefon:(282) 250 4400 Faks:(282) 250 9930

e-Posta:fbe@nku.edu.tr Elektronik Ağ:http://fbe.nku.edu.tr/

Bilgi için: Çiğdem Koçkaya

Unvanı: Bilgisayar İşletmeni

